University of Cape Town

A Nonlinear Adaptive Filter for Improved Operation and Protection of Power Systems

R. M. Naidoo

Thesis submitted to the

University of Cape Town

in complete fulfillment of the requirement for the award of the degree of

Doctor of Philosophy

In the

Department of Electrical Engineering

Supervised By

Prof. P. Pillay

Part-time Professor, Department of Electrical Engineering

University of Cape Town

Professor and Hydro-Quebec Senior Chair

Concordia University, Quebec, Canada

May 2008

STUDENT NUMBER: NDXREJ001

Abstract

Amplitude, phase and frequency estimation is critical for real-time power system applications, especially under non-stationary conditions. Non-stationary waveforms pose a problem for conventional methods that are used to track or estimate power system parameters. In recent decades, many adaptive techniques and algorithms have been developed and applied to solve this problem. However, these methods suffer poor performance under conditions of harmonics, noise and frequency deviations. This thesis presents the application of a nonlinear adaptive filter to selected areas in power systems. The filter has demonstrated excellent performance against conventional methods in biomedical applications. The algorithm is robust in structure and highly immune to noise. Applications in this thesis include (1) sag detection, (2) symmetrical component estimation, (3) phase and frequency estimation, (4) sag analysis and (5) distributed generation synchronisation and protection. The applications were chosen such that the amplitude, phase and frequency tracking ability are thoroughly tested. Practical considerations such as the effect of power system harmonics, noise, frequency changes, and load changes are taken into account during implementation of this technique. This thesis assesses the performance of the algorithm against conventional methods through simulations, laboratory experiments and field testing.

Declaration

The thesis is submitted as a requirement for the award of the degree of Doctor of Philosophy in Electrical Engineering at the University of Cape Town. It has not been submitted before at this or any other university. The author hereby confirms that it is based on his own work. The total number of words is less than 80,000.

Signed by candidate

R.M Naidoo

Acknowledgments

My most sincere gratitude goes to my supervisor **Prof. Pragasen Pillay** for his constant support and mentorship. It is through his efforts that I gained exposure to numerous international forums. The long plane trips to South Africa to supervise students does not go unnoticed and we greatly appreciate your effort. I owe a great deal to the numerous scholars, colleagues and friends (at UCT and overseas) who, through their comments, challenges and questions have encouraged and enabled me to put together this work. They include **Dr. Azeem Khan** for his support, motivation and assistance; **Dr. Hugh Douglas** who assisted in many ways in Potsdam; **Dr. Lotten Mthombeni** as well as **Maru** and **Julia Manyage** for their hospitality in Potsdam; **Dr. Ben Sebitosi** for his fruitful discussions and assistance; **Mr Paul Barendse** for his hospitality in Cape Town; and **Mr. Chris Wozniak** for laboratory assistance at UCT. I would also like to thank **Mr Paul Keller** and **Mr Adam Bartylak** of Eskom for assistance with the field data.

I am grateful to my mom (**Thaan**), sisters (**Molly** and **Melini**) and mother-in-law. I wish to make a special dedication to my late dad (**Moonsamy**) for his motivation, humility and allowing me to make my own choices in life. Finally, I wish to say a special thank you to my wife **Annie** and my sons **Kian** and **Roan** for putting up with me having to travel for extended periods in the USA, Cape Town and various conferences to pursue this research.

Contents

List of Figures

List of Tables

Abbreviations

ADALINE	-	Adaptive Linear Combiner
ADC	-	Analogue to Digital Converter
APF	-	Active Power Filter
ATP	-	Alternative Transients Program
AVR	-	Automatic Voltage Regulator
CBEMA	-	Computer and Business Equipment Manufacturers Association
CWT	-	Continuous Wavelet Transform
DFIG	-	Doubly Fed Induction Generator
DFT	-	Discrete Fourier Transform
DPGS	-	Distributed Power Generation System
DSP	-	Digital Signal Processor
DVR	-	Dynamic Voltage Restorer
ECG	-	Electrocardiogram
FA	-	Fourier Algorithm
FACTS	-	Flexible Alternating Current Transmission System
FFT	-	Fast Fourier Transform
FIR	-	Finite Impulse Response
FOC	-	Field Oriented Control
HVDC	-	High Voltage Direct Current
IEC	-	International Electrotechnical Commission
MFP	-	Magnitude Frequency Properties
NRS	-	National Rationalised Standard

PC	-	Personal Computer
PI	-	Proportional Integral
PLL	-	Phase Locked Loop
PFC	-	Power Factor Correction
PR	-	Proportional Resonant
PV	-	Peak Voltage
PWM	-	Pulse Width Modulation
QT	-	Quadratic transform
RMS	-	Root Mean Square
RPC	-	Reactive Power Compensation
ST	-	S Transform
STATCOM	-	Static Compensator
UPS	-	Uninterruptible Power Supply
VSC	-	Voltage Source Converter
WLSE	-	Weighted Least Square Estimation
WRIM	-	Wound Rotor Induction Generator
WVD	-	Wigner-Ville Distribution

Chapter 1

Introduction

The ideal power system consists of sinusoidal voltages and currents at a constant frequency. Power system loads and system faults affect the shape and frequency of the current and voltage waveforms. The deviation of the waveform from a pure sinusoidal can cause maloperation of sensitive equipment, and even downtime. The problem has been aggravated by the increasing use of power-electronic loads. Voltage sags in particular can cause expensive downtime. Voltage sags may be caused by switching operations (associated with a temporary disconnection of supply), the flow of in-rush currents (associated with the starting of motor loads) or the flow of fault currents. It is possible for sags of short duration to cause problems in certain sensitive equipment. The instantaneous detection of sags is a key factor for effective mitigation. The problem becomes one of identification and classification of power system disturbances.

It is generally assumed that the power system network operates in steady state. However, in practice, to achieve this ideal of steady state is nearly impossible. Loads are continually changing and the power system is continually adjusting to these changes. It is important to understand the kinds of power variations that can occur and the problems that can be experienced with sensitive loads. Standards are being developed with a consistent set of definitions in order for measurement equipment to be designed in a consistent manner so that information can be shared between different groups [1]. In the past, measurement equipment has been designed to handle either

disturbances (e.g. disturbance analysers) or steady state variations (e.g. voltage recorders and harmonics monitors). With advances in signal processing capability and the increased hardware performance of instruments, new methods are available that can potentially characterise a large range of power-quality variations. The new challenge involves detecting and characterising all the events in a convenient form so that it can be used to help identify and solve problems.

Deregulation of the electric power industry of South Africa will make the quality of electric power supplied extremely important. Customers with highly sensitive equipment, such as variable speed drives, automated production lines etc. desire higher levels of power quality to ensure the continued operation of their equipment and processes. The possibility of incorporating wind energy into the grid poses power quality problems that need to be addressed.

Commercial pressures and the increasing diversity of generation sources mean that it is now more important than ever to know the dynamic characteristics of a power system. The task of accurately predicting and tracking power system parameters in real-time is difficult. All available mathematical tools and methods need to be considered to improve the estimation accuracy.

This research aims to find improved solutions to power system problems through the use of a new nonlinear adaptive filter. Although the research focuses on the grid system, off-grid applications are considered.

1.1 Categorising Power Quality Phenomena

Current and voltage transducers, which are located at various points in the power system, send proportional signals to measurement and protection equipment. These continuous signals are converted at an appropriate sampling rate into discrete form by the Analogue to Digital Converters (ADC) of microcontrollers or by the Digital

Signal Processors (DSP). The data is then processed at different levels to derive useful information [2].

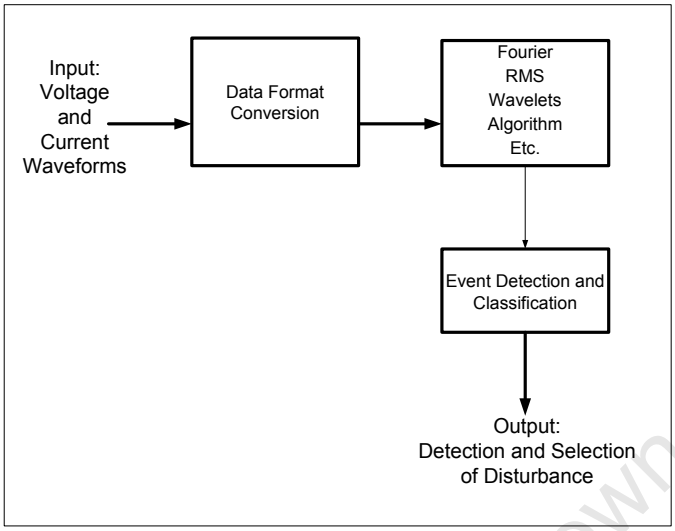

Figure 1-1: Detection and classification flowchart.

Power quality is defined as [3]:

> "Any power problem manifested in voltage, current, or frequency deviations that result in failure, degrading or misoperation of customer equipment."

Power quality phenomena can be categorised in terms of voltage and frequency deviations.

1.1.1 Voltage Deviation

Deviations in voltage from the pure sine wave can be categorised as shown in Figure 1-2. A disturbance is a temporary deviation from the steady state waveform. This deviation can either be a high-frequency (transients) or a low frequency (sags and swells) phenomenon. Waveform distortion is generally discussed in terms of harmonics, which are sinusoidal voltages or currents with frequencies that are integer multiples of the fundamental frequency at which the supply system is designed to operate. Voltage unbalance arises when either or both the magnitudes of the phase voltages and the

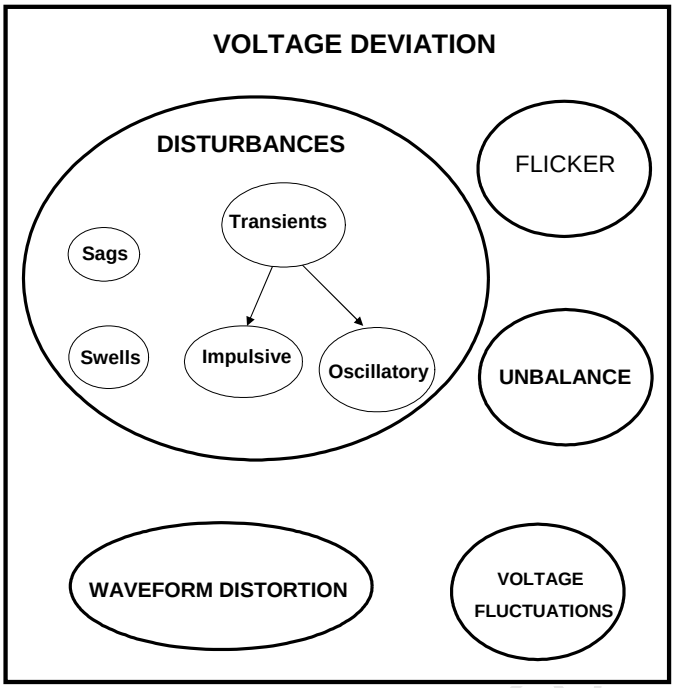

Figure 1-2: Categorising power quality phenomena.

relative phase displacements of the phases are not equal. Voltage fluctuations can be described as a cyclical variation of the voltage envelope or a series of random voltage changes, the magnitude of which does not exceed the range of permissible operational voltage changes (i.e. up to 10%). This phenomenon is characterised by the amplitude of the voltage changes and the rate of repetition. Flicker is the irritation experienced by the human eye when light levels change. The IEEE Standard 100 [4] defines flicker as a luminosity variation or an image disruption caused by lower frequency voltage fluctuations.

1.1.2 Frequency Deviation

Frequency deviation is the amount by which a frequency differs from a prescribed value. For satisfactory operation of the power system, the frequency should remain nearly constant. Relatively close control over the power system frequency ensures a constancy of speed of induction and synchronous motors. A considerable drop in frequency can result in high magnetising currents in induction motors and transformers [5].

1.2 Measurement Criteria [6]-[7]

In [6]-[7], a set of three criteria, i.e. measurement accuracy, dynamic response and real time capability, is proposed as useful tools to evaluate existing measurement techniques and guide the development of new methods.

1.2.1 Measurement Accuracy

The instantaneous amplitude, phase angle, frequency, power and other derived electrical quantities of the fundamental and harmonic components in a non-stationary power disturbance waveform solely characterise the nature or pattern of an electrical fault or power quality event. Hence the accurate measurement of these quantities is of the highest priority. The measuring technique should be able to directly process any signal component in the waveform, regardless of actual signal composition or frequency deviation. It should also possess high measurement accuracy in all service conditions, even when encountering a waveform severely distorted by harmonics, inter-harmonics, frequency deviation, decaying dc offsets and noise.

1.2.2 Dynamic Response

As the time varying attribute of a power disturbance, the above-mentioned electrical quantities may fluctuate in a wide range. The measuring technique should be able to track the changes of these quantities and converge to the actual values as quickly as possible.

1.2.3 Real-Time Capability

Processing manner

It is best for the measuring technique to estimate the instantaneous electrical quantities at only the current instant once a new sample value is obtained, rather than to update all estimates in a window when all sample values in this window are available. The reason is that the latter method, which is termed "block processing"[6]-[7],

cannot reflect the time-varying characteristics of a power disturbance or electrical fault in time. This poses problems for applications that have strict real time requirements, such as protection, control of power electronic device, etc. Furthermore, the block processing method may also result in an incorrect identification of a power disturbance when its duration is longer than the window.

Computational complexity

The measurement technique should ideally have a recursive algorithm that can process data in the time or frequency domain. The recursive algorithm should use only the present and previous sample values and previous outputs rather than their future values. The computational complexity should be independent of sampling frequency, and the coefficients in the recursive algorithm should remain unchanged. A recursive algorithm of the Continuous Wavelet Transform (CWT) was proposed for relay and power quality monitoring. Several recursive algorithms have been published for band pass filtering in image processing and matching the pursuit of which may be valuable for electric power applications. However, these algorithms are based on the block processing method and require future sample values and outputs to update the current output. Hence they cannot satisfy the real-time requirement.

1.3 Monitoring Equipment

Monitoring equipment plays an important role in understanding the impact of poor power quality on the power system. The monitoring equipment assists in characterising the disturbance or steady state condition of the network. Monitoring equipment include:

1.3.1 Disturbance Monitors and Analysers

Disturbance analysers and disturbance monitors form a category of instruments which has been developed specifically for power quality measurements. They are typically capable of measuring a wide variety of system disturbances from transient voltages

to outages, undervoltages or overvoltages of longer duration. Thresholds can be set and the instruments left unattended to record disturbances over a period of time. It is often difficult to determine the characteristics of a disturbance or a transient from the summary information available from conventional disturbance analysers. For instance, an oscillatory transient cannot be effectively described by a peak and a duration. Therefore it is almost imperative to have the waveform capture capability in a disturbance analyser for detailed analysis of a power quality problem. The application of signal processing methods that can reconstruct the signal helps to reduce the memory requirement of disturbance analysers and loggers.

1.3.2 Spectrum Analysers and Harmonic Analysers

Many instruments and on-line monitoring equipment now include the capability to sample waveforms and perform Fast Fourier Transform (FFT) calculations. The capabilities of these instruments can vary in functionality and performance. The user must ensure that the accuracy and information obtained is adequate for an investigation. For harmonic measurements, the following are basic requirements for carrying out an investigation:

- Capability to measure both voltage and current simultaneously so that harmonic power flow information can be obtained.
- Capability to measure both magnitude and phase angle of individual harmonic components (also needed for power flow calculations).
- Synchronisation and a high enough sampling rate for accurate measurement of harmonic components up to at least the 50th harmonic (this requirement is a combination of a high sampling rate and a sampling interval based on the 50/60 Hz fundamental).
- Capability to characterise the statistical nature of harmonic distortion levels (harmonics levels change with changing load conditions and changing system conditions).

Harmonic distortion is a continuous phenomenon. It can be characterised at a point in time by the frequency spectra of the voltages and currents. However, for proper representation, measurements must be made over a period of time and the statistical characteristics of the harmonic components and the total distortion should be determined.

Combined Disturbance and Harmonic Analysers

With the advances in digital signal processing technology, recent instruments have combined harmonic sampling, energy monitoring and disturbance monitoring functions into a single instrument. The output is graphically based and the data is remotely gathered over phone lines into a central database. Statistical analysis can then be performed on the data. The data is also available for input and manipulation by different programs such as spreadsheets etc.

1.4 Review of Methods to Detect Power Quality Events

The effective prediction and monitoring of voltage and current waveforms are key to improved power quality. Sampled data is typically used. This section reviews some of the commonly used methods to detect power quality events.

1.4.1 The Fourier Algorithm

The Fourier Algorithm (FA), is based on the Fourier series. It is a traditional tool for the study of non-stationary signals by virtue of its relatively low computational complexity. The performance of the FA was investigated by considering it as a band pass filter. This was based on the sine and cosine filters [8], [9]. Due to the implicit rectangular window, the Magnitude Frequency Properties (MFP) of the sine and cosine filters are not identical, but rather asymmetrical with side lobes. As a result, the measurement accuracy of the FA deteriorates severely in the presence of frequency

deviation, decaying DC offsets, and signal components other than the measured one (e.g. harmonics, inter-harmonics and noise can affect the measurement of the fundamental component during frequency deviations from the nominal).

To overcome this drawback, other types of windows were used to replace the rectangular window in the FA [10]. Modified orthogonal filters have been proposed to achieve desirable measurement accuracy in all service conditions. However, the new windows were longer than the rectangular window in FA. Hence the dynamic responses of the modified filters were slower. Moreover, the computational complexities are also increased significantly due to the lack of a recursive algorithm. On the other hand, recursive algorithms based on FA are proposed to further reduce the computational complexity. However these algorithms could not improve the performance significantly [6],[7].

1.4.2 Wavelets

Disturbances that are non-periodic or non-stationary require a more powerful mathematical technique than the Fourier series. Wavelet analysis is a windowing technique, similar to the Short Time Fourier Transform, with variable-sized windows. It allows the use of long time intervals, when lower frequency information is sought, and shorter intervals, when higher frequency information is required. Wavelet analysis is capable of revealing aspects of data that other signal analysis techniques can miss, including aspects such as trends, breakdown points, discontinuities and self-similarity. It is also often used to compress or filter a signal without any appreciable degradation. Wavelets were first proposed for application to power engineering by Ribeiro and Pillay [11]. Since then, several papers were devoted to the application of wavelet transformations in current and voltage signal processing [12], [13], [14], [15], [16], [17], [18]. The most common fields of application of wavelet transformations in electrical power engineering include:

- Power quality analysis

- Condition monitoring
- Relay protection
- Transient measurement

Although wavelets have been widely used, there are some disadvantages. The disadvantages are:

- Wavelets have a relatively high complexity.
- It requires a substantial amount of processing power for implementation on a signal processor.
- Wavelet analysis uses historical data for analysis.

It is evident from the disadvantages that wavelet analysis does not satisfy real-time measurement requirement.

1.4.3 Adaptive Filters

Adaptive filtering algorithms are more suitable for applications with real-time requirements.

Kalman Filters [19]

The Kalman filter is just one of many adaptive filtering or estimation algorithms. Despite its elegant derivation and often excellent performance, the Kalman filter has two drawbacks:

- The derivation and consequent performance of the Kalman filter depends on the accuracy of initial assumptions. The performance deteriorates if the assumptions are erroneous.
- The Kalman filter is computationally demanding. This can limit the utility of Kalman filters in high rate real time applications.

Enhanced Phase Locked Loop

A new algorithm proposed by Ghartemani [20] can be used with great success for online signal analysis to track the magnitude and frequency of signals in general and the power system supply in particular. The drawback of this algorithm is that it is sensitive to frequency variations.

Nonlinear Adaptive Filter

The research proposed by Ziarani and Konrad [21], has led to an algorithm capable of extracting or tracking the sine wave as well as tracking variations of amplitude, phase and frequency of the sinusoidal over time. The signal processing algorithm has a very simple structure that makes it easy to implement on a digital signal processor. The proposed approach is significantly faster and more precise in detecting and discriminating the type of disturbance events than conventional approaches. This algorithm is proposed for this research.

1.4.4 The S Transform (ST)

The S transform is an extension of the idea of the CWT and is specifically based on a moving and scalable Gaussian window [22]. The ST can provide improved time-frequency representation of a signal with time varying characteristics, e.g. a narrow time window for a high frequency signal (like the CWT). At the same time, it can maintain a direct relation with the Fourier spectrum in the frequency domain. The ST can be realised and applied efficiently by taking advantage of the Fast Fourier Transform (FFT).

The ST has been used in electric power systems for the identification of power quality events. However, unlike the CWT, the ST is based on the block processing manner and hence it does not satisfy the real-time requirement. On the other hand, because

the width of a frequency window in the ST is also in proportion to its central frequency, the problem in the CWT also exists in the ST. This results in an incorrect measurement of harmonics.

1.4.5 The Quadratic Transforms (QT)

The quadratic transforms also represent a signal with time varying characteristics in the timefrequency plane and have been used in many engineering fields. As a branch of the QT, the WignerVille distribution (WVD) and its modifications have been used to analyse and classify power quality events [23]. However, the WVD is also based on the block processing method and hence it does not satisfy the real-time requirement. On the other hand, the interference terms that are due to the existence of multiple signal components in the waveform, may also appear in the timefrequency plane. This phenomenon may affect the identification and measurement accuracy of harmonics/inter-harmonics.

1.4.6 Curve Fitting and Optimization Techniques

The power disturbance waveform with time varying characteristics is assumed as the sum of a dc component, the fundamental component, a number of integer harmonic components and the additive random noise.

$$v_s(t) = v_1(t) + \sum_{k=2}^{\infty} v_k(t) + n(t) \tag{1.1}$$

where $v_1(t)$ is the fundamental component of the signal, k the harmonic number and $n(t)$ the signal noise. The coefficients (weights) in the model can be estimated by minimising the total square errors between the actual sample values and the model outputs via curve fitting or unconstrained optimisation techniques, e.g. the Least Squares fitting and Newton type algorithm [24]. Some of these techniques have the attribute of recursive computation and hence can be used in real-time applications. These methods include Recursive Least Square fitting [25], Recursive Newton type

algorithm, Kalman filtering [26] and Artificial Neural Networks [27] and in particular the Adaptive Linear Combiner (ADALINE) [28]. However, in practical power systems, the actual number of signal components in a given waveform is usually unknown, the fundamental frequency may deviate and the inter-harmonic components, which are ignored in this model, may also exist. Therefore, the performance of these methods may not be satisfactory due to model mismatch or frequency deviations (some methods require frequency information a priory or assume it is constant). It is also impossible to obtain any information about inter-harmonic components using this model.

1.4.7 Comparison of Current Techniques

Table 1.1: A comparison of techniques to track power signals.

Method	**Measurement Accuracy**	**Dynamic Response Response**	**Real-Time Capability**
Fourier	very good	poor	poor
Wavelets	good	good	poor
Adaptive Filters	poor	good	good
S-Transform	poor	good	poor
Quadratic Transform	poor	good	poor
Curve Fitting	poor	poor	poor

Table 1.1 shows a comparison of the different techniques based on the measurement criteria outlined in the previous section. Only adaptive techniques are able to satisfy the real-time criteria. Some techniques demonstrate poor accuracy under conditions of frequency deviations, noise and harmonics. Therefore limitations exist with current techniques.

1.5 Research Questions and Objectives

Recent work in the field of signal processing has led to a nonlinear adaptive filter that can extract a single non-stationary sinusoidal signal from a given multi-component

input signal. The filter is adaptive and is capable of estimating the amplitude, phase and frequency of a non-stationary sinusoidal. The main objective of this thesis is the application of the nonlinear filter to various nontrivial power system problems and to compare the performance against existing methods such as the Root Mean square (RMS), Fourier transform etc. The objective is achieved through detailed investigation of the following research questions associated with the thesis:

1. Can the nonlinear filter be used to improve the ability to estimate time-varying amplitude, phase and frequency deviations?
2. Is it possible to dynamically estimate symmetrical components?
3. How can the proposed technique be applied to characterise sags/swells for analysis?
4. How can the nonlinear filter be used to effectively synchronise and protect wind generators under conditions of disturbances?
5. What is the impact of these techniques for custom power applications?
6. How does the performance of the nonlinear adaptive filter compare to other algorithms that has been used?
7. Does the performance of the filter change for a range of different power quality events?
8. How can the filter perform in the presence of noise, unbalance and harmonics?
9. What improvements in power quality mitigation can be obtained by using the nonlinear filter as compared to conventional algorithms?

The first question is answered through a detail consideration of amplitude, phase and frequency estimation. Chapter THREE applies the nonlinear adaptive method to detecting sags/swells. This forms the basis for testing the amplitude tracking ability of the proposed method. The phase and frequency estimation ability is considered

in chapter FOUR. Question two is answered through the application of the tools developed in reply to question one as well as the application of these tools in order to develop a dynamic symmetrical components mathematical model. This is considered in chapter FIVE. The core building blocks of a new method for application to diverse areas of power systems are developed through the detailed consideration of questions one and two. The application examples in chapters SIX and SEVEN utilise the core building blocks developed. This is used to answer questions three to five. Performance aspects of the new method are considered throughout the thesis by answering questions six to nine.

1.6 Research Design and Methodology

This section explains the design and methodology that were used for the research.

1.6.1 Framework

The study is quantitative in nature, relying on data obtained from experiments and field recording. The framework of this project is as follows:

- Empirical - laboratory and field experiments will be conducted.
- Primary - new data will be obtained.
- Numeric - the nature of the data is numeric.
- Control - medium, i.e. highly structured (laboratory work and simulations) as well as natural (field installations at Eskom and customer sites).

1.6.2 Data Collection Techniques

The following data collection techniques were used:

Computer simulation

Computer simulation was used to test the nonlinear filter before laboratory implementation. It will also be used to determine the performance of the filter with different convergence parameters. The application for noise reduction will be simulated.

Laboratory Testing

Laboratory testing was done for convergence and sag detection.

Field Testing

For field testing, monitoring equipment was installed at the Eskom substations. From the substations, this instantaneous fault information was logged for analysis.

Existing Test Data

The IEEE 1159 working group is tasked with the recommended practice on monitoring electric power quality [1]. Test waveforms for sag events are available to download from the website. Waveforms are available for specific sag event types such as transformer energisation, faults, motor starting etc.

1.6.3 Analysis

Existing methods of analysing power quality events were implemented. The nonlinear filter was compared to these methods. Graphs and tables are used to quantitatively indicate the performance improvements achievable with the algorithm. Mathematical and statistical methods are applied to the data.

1.6.4 Strengths

The nonlinear filter has already been implemented for applications such as Electrocardiogram (ECG) analysis [21], power line communication [29] etc. Stability has already been proved [30]. An important attribute of the nonlinear filter for power

system applications is the ability to accurately track key parameters in the presence of frequency deviations.

1.6.5 Weaknesses

Although the nonlinear filter has the ability to accurately track steady state phenomena, it has not been applied successfully to system transients. Transients require response times that are not possible to achieve using the algorithm. For transient studies it has to be applied in conjunction with other methods such as wavelet analysis. In [31] it has been applied successfully with wavelet analysis. The scope of such work is not pursued in this thesis.

1.7 Original Contribution

The original contribution of this thesis is the development of new techniques that can be used for improved power system operation. These include:

- Improvement of existing methods of sag detection under varying conditions of sag magnitude, rate of change, point on wave and frequency deviations.
- Application of the algorithm to the challenge of real-time symmetrical component estimation. This is achieved by using the nonlinear filter to convert the instantaneous voltages into a real-time phasor. The phasors are then used to estimate the time-domain symmetrical components.
- A novel approach to protect and synchronise distributed generation applications.
- A new real-time approach to single and three-phase phase and frequency estimation under non-stationary conditions. This can be used for reactive power compensation etc.
- An online method of sag characterisation based on the method of Bollen and Zhang [32]. The proposed method can be implemented in signal processors for

real-time characterisation of sags as well as to determine sag indices.

1.8 Outline of Thesis

This thesis is broadly organised as follows: Chapters ONE and TWO provide the theoretical framework of the thesis. Amplitude estimation is tested through the application of sag detection in chapter THREE. Phase and frequency estimation are investigated in chapter FOUR. In chapter FIVE, a new method is proposed to determine symmetrical components. Chapters THREE to FIVE provide the core building blocks for further applications in subsequent chapters.

Specifically: Chapter TWO presents a mathematical model of the algorithm. The governing equations and a mathematical description of the system are given. Convergence of the nonlinear adaptive algorithm is demonstrated in the time and frequency domain through experimental results. In chapter THREE, the algorithm is used to detect and track the amplitude of sags and swells. The proposed system is compared to the RMS, peak voltage and Fourier methods. Simulation, experimental data and field data are used to evaluate the performance of the proposed method. The influence of magnitude, point-on-wave and rate-of-change is presented. Phase and frequency estimation for single and three-phase systems are presented in chapter FOUR.

A positive sequence extractor is described in chapter FIVE. The algorithm is used to convert the instantaneous signals into phasors. The real-time phasors are converted into instantaneous symmetrical components using the standard transformation matrix. Simulation and field data are used to evaluate the performance of the system with respect to variations in amplitude, phase and noise. A method of characterising sags in real-time is presented in chapter SIX. The method uses the instantaneously estimated symmetrical components from chapter FIVE and the method of phase and frequency estimation of chapter FOUR. The influence of sag propagation is described. The system is extended to determine sag indices. Simulation and field data are used

to test the proposed method. With the increased demand for power, distributed generation applications have received considerable attention in recent years. Chapter SEVEN proposes the use of the algorithm for synchronisation, protection and control. The system is used to synchronise and protect a doubly-fed induction generator under abnormal system conditions. Simulations and experimental studies of the wind generator under fault conditions are used to demonstrate the proposed approach. Finally, concluding remarks, including an outline of future research directions and the main features of the application are presented in chapter EIGHT.

Chapter 2

Mathematical Model of the Nonlinear Adaptive Filter

This chapter presents the mathematical formulation and operational features of the nonlinear adaptive filter. The key to the filter is the nonlinear tracking model that continuously minimises the error between the input and output signals. The information presented in this chapter forms the technical basis required for the understanding of the subsequent chapters. Much of the theory described in this chapter can be found in [33].

2.1 Fourier Analysis Revisited

Digital Signal Processing (DSP) is one of the most powerful technologies that is shaping science and engineering in the twenty-first century. One of the reasons for the tremendous growth in the use of digital signal processing over the last few decades is the development of the Discrete Fourier Transform (DFT) and its computationally efficient alternative, Fast Fourier Transform (FFT). The principle of the DFT is closely related to the Fourier series representation of periodic signals. In essence, DFT of a set of sampled data provides Fourier series coefficients of a periodic signal, a single period of which is given by the set of sampled data. In this section, the inherent assumptions behind the Fourier series analysis and its limitations are reviewed.

The proposed algorithm emerges as a generalisation of FA. It attempts to eliminate assumptions intrinsic to Fourier analysis which, limits its applicability to a wide range of time-varying applications. Given a periodic signal $u(t)$ with period T_0, the best approximation of the signal, $\hat{u}(t)$, in a space spanned by a number of sinusoids $\sin(i\omega_0 t + \delta_1),\ i = 0 \cdots N-1$, each having a frequency of a multiple integer of fundamental frequency $\omega_0 = \frac{2\pi}{T_0}$ (in rad/sec) and a constant phase δ_i (in rad), written as $\hat{u}(t) = \sum_{i=0}^{N-1} A_i \sin(i\omega_0 t + \delta_i)$ is achieved by the minimisation of the least squares error

$$\|e\|^2 = \frac{1}{T_0} \int_{T_0} [u(t) - \hat{u}(t)]^2 dt \tag{2.1}$$

In general, when the approximation of $u(t)$ is in the form of linear combination of the basis vectors, the approximating coefficients are given by the inner products of $u(t)$ and the basis vectors. Therefore,

$$\begin{aligned} a_0 &= \tfrac{1}{T_0} \int_{T_0} u(t)dt \\ a_i &= \tfrac{1}{T_0} \int_{T_0} u(t)\cos(i\omega_0 t + \delta_i)dt, \quad i = 1 \cdots N-1 \\ b_i &= \tfrac{1}{T_0} \int_{T_0} u(t)\sin(i\omega_0 t + \delta_i)dt, \quad i = 1 \cdots N-1 \end{aligned} \tag{2.2}$$

One can easily verify that the least squares error can be redefined as

$$e(t)^2 = [u(t) - \hat{u}(t)]^2$$

i.e. as the instantaneous value of error, and still obtain the same expressions for the Fourier coefficients $a_0,\ a_i,\ b_i,\ i = 1 \cdots N-1$, although in this case the defined error would not be mathematically well defined.

If the frequency (hence total phase) of the signal $u(t)$ drifts from $f_0 = \frac{1}{T_0}$, the Fourier coefficients that is obtained by the minimisation process still provides the best approximation that can be given in terms of the bases $\sin(i\omega t + \delta_i),\ i = 1 \cdots N-1$; to use a geometrical interpretation, $\hat{u}(t)$ thus obtained is the orthogonal projection of the vector $u(t)$ onto the space spanned by the vectors $\sin(i\omega t + \delta_i),\ i = 1 \cdots N-1$.

However, the space onto which the projection is made, is fixed and is not necessarily the best N-dimensional space for the representation of a signal whose frequency is no longer known. Herein lies a shortcoming of Fourier analysis: there is an inherent fixed frequency assumption involved in Fourier analysis.

Granted, the frequency of the signal is now fixed and known. Fourier analysis provides coefficients a_i and b_i for each basis sinusoid $A_i \sin(i\omega_0 t+\delta_i) = a_i \cos(i\omega_0 t)+b_i \sin(i\omega_0 t)$, which in turn provide estimates for the amplitude A_i and constant phase δ_i of the sinusoidal components. Where needed, the sinusoidal component $A_i \sin(i\omega_0 t+\delta_i)$ itself is yet to be somehow synthesised, a task which is not trivial and often involves the use of a synchronisation scheme such as a phase-locked loop. This presents another inherent shortcoming of the Fourier analysis: it only provides a means of estimation of amplitude and constant phase of individual sinusoids. As regards the shortcoming of the Fourier analysis due to its fixed frequency assumption, the ideal method would be one which finds not only the best approximation in a given space, but also the best space onto which the projection is to be made. This means that the method would have to be inherently adaptive and the estimation process would be a closed loop process.

2.2 Formulation of the Nonlinear Adaptive Filter

Let *u(t)* represent a voltage or current signal. In the case of power systems this function is usually continuous and almost periodic. A sinusoidal component of this function

$$v(t) = V \sin(\omega t + \phi_V) \tag{2.3}$$

is a fundamental component of the input signal where V is the amplitude, ω is the frequency and ϕ_V is the constant phase.

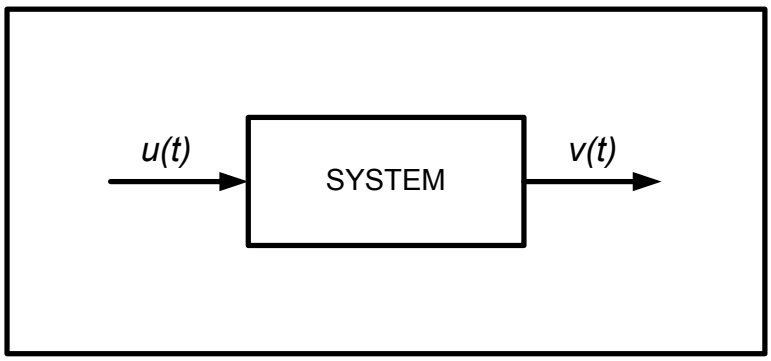

Figure 2-1: Simple black box

The input voltage $u(t)$ can be represented as follows

$$u\left(t\right)=\sum_{i=0}^{\infty}V_{i}\sin\left(\omega_{i}t+\phi_{iv}\right)+n\left(t\right) \tag{2.4}$$

in which $n(t)$ denotes the superimposed disturbance or noise. In practice, the power system parameters in (2.4) will change in time. This is due to the system loading and faults. In the proposed algorithm, the objective is to extract more or less a specified sinusoidal component, $v(t)$. Such a desired component may be defined as $v\left(t\right)=V\sin\phi\left(t\right)$, incorporating all phase variations in the $\phi\left(t\right)$ term. To explicitly incorporate the concept of instantaneous frequency into the total phase, one may define the output as

$$v\left(t\right)=V\left(t\right)\sin\left(\int^{t}\omega\left(t\right)d\tau+\delta\left(t\right)\right) \tag{2.5}$$

Let M be a manifold denoting all pure sinusoidal signals

$$\mathrm{M}=\left\{\begin{array}{l} V(t)\sin(\omega(t)t+\phi_{v}(t)) \\ \left|V(t)\in\left[V_{\max},V_{\min}\right],\omega(t)\in\left[\omega_{\max},\omega_{\min}\right],\phi_{v}(t)\in\left[\phi_{v\,\max},\phi_{\min}\right]\right. \end{array}\right\} \tag{2.6}$$

where

$$\Im(t)=\left[V(t),\omega(t),\phi_{v}(t)\right]^{T} \tag{2.7}$$

is the vector of parameters that belong to the parameter space

$$\vartheta = [V, \omega, \phi_v]^T \Big| V \in [V_{\min}, V_{\max}], \quad \omega \in [\omega_{\min}, \omega_{\max}], \quad \phi \in [\phi_{\min}, \phi_{\max}] \tag{2.8}$$

and superscript T denotes the transposition matrix. The output is defined as the desired sinusoidal component, namely

$$v(t, \Im(t)) = V(t) \sin(\omega(t)t + \phi_v(t)) \tag{2.9}$$

To extract a certain sinusoidal component of *u(t)*, the solution has to be an optimum that minimises the distance function d between $u(t)$ and the desired component $v(t)$.

$$\Im_{opt} = \arg \min_{\Im(t) \in \vartheta} d[v(t, \Im(t)), u(t)] \tag{2.10}$$

The instantaneous distance function d is used

$$d^2(t, \Im(t)) = u(t) - v(t, \Im(t)) \triangleq e^2(t) \tag{2.11}$$

The cost function is defined as

$$J(\Im(t), t) \triangleq d^2(t, \Im(t)) \tag{2.12}$$

The parameter vector $\Im$ is defined and estimated using the gradient decent method

$$\frac{d\Im(t)}{dt} = -\mu \frac{\partial [J(t, \Im(t))]}{\partial \Im(t)} \tag{2.13}$$

where the positive diagonal matrix μ is the algorithm regulating constant matrix. The values of the entries of this matrix control the convergence rate as well as the stability of the algorithm. Gradient descent method is guaranteed to yield the desired solution if the cost function is globally quadratic in parameters. Otherwise, e.g. if the form of the cost function is not quadratic, as is the case here, or not clearly described, a mathematical proof should be given to guarantee the convergence of

solutions of the gradient descent method to the minimum point of the cost function. Therefore, formulation of the nonlinear algorithm calls for direct mathematical proofs of convergence and stability. The estimated parameter vector is denoted by

$$\hat{\Im}(t) = \left[\hat{V}(t), \hat{\omega}(t), \hat{\delta}(t)\right] \tag{2.14}$$

Therefore $\hat{V}(t)$, $\hat{\omega}(t)$ *and* $\hat{\phi}(t)$ represent estimated values of amplitude, frequency and constant phase respectively. The diagonal matrix μ is defined as

$$\mu = \begin{bmatrix} m_1 & 0 & 0 \\ 0 & m_2 & 0 \\ 0 & 0 & m_3 \end{bmatrix} \tag{2.15}$$

Carrying out the mathematical manipulations indicated in (2.13), namely

$$\begin{bmatrix} \frac{d\hat{V}(t)}{dt} \\ \frac{d\hat{\omega}(t)}{dt} \\ \frac{d\hat{\phi}(t)}{dt} \end{bmatrix} = - \begin{bmatrix} m_1 & 0 & 0 \\ 0 & m_2 & 0 \\ 0 & 0 & m_3 \end{bmatrix} \begin{bmatrix} \frac{\partial}{\partial \hat{V}(t)} \left[v(t) - \hat{V}(t) \sin\left(\int^t \hat{\omega}(\tau)\, d\tau(t) + \hat{\phi}(t) \right) \right] \\ \frac{\partial}{\partial \hat{\omega}(t)} \left[v(t) - \hat{V}(t) \sin\left(\int^t \hat{\omega}(\tau)\, d\tau(t) + \hat{\phi}(t) \right) \right] \\ \frac{\partial}{\partial \hat{\phi}(t)} \left[v(t) - \hat{V}(t) \sin\left(\int^t \hat{\omega}(\tau)\, d\tau(t) + \hat{\phi}(t) \right) \right] \end{bmatrix} \tag{2.16}$$

one can write

$$\frac{d\hat{V}(t)}{dt} = 2m_1 e(t) \sin\left(\int^t \hat{\omega}(\tau)\, d\tau(t) + \hat{\phi}(t) \right) \tag{2.17}$$

$$\frac{d\hat{\omega}(t)}{dt} = 2m_2 e(t) \hat{V}(t)\, t \cos\left(\int^t \hat{\omega}(t)\, d\tau(t) + \hat{\phi}(t) \right) \tag{2.18}$$

$$\frac{d\hat{\phi}(t)}{dt} = 2m_3 e(t) \hat{V}(t) \cos\left(\int^t \hat{\omega}(t)\, d\tau(t) + \hat{\phi}(t) \right) \tag{2.19}$$

Let θ be the total phase. Since $\hat{\theta}(t) = \int^t \hat{\omega}(\tau)\, d\tau(t) + \hat{\phi}(t)$, one may write the following augmented equation:

$$\frac{d\hat{\theta}(t)}{dt} = \hat{\omega}(\tau) + \frac{d\hat{\phi}(t)}{dt} \tag{2.20}$$

A factor of time variable t appears on the right-hand side of (2.18) since the partial derivative of $\int^t \omega d\tau$ with respect to ω is equal to t. In other words, a time-varying set of equations in which the time variable t is explicitly presented is obtained. Such a time-varying system has been observed to be unstable and hence of no value. This of comes as no surprise given that the non-convex cost function formulation of the algorithm does not enjoy the performance guarantees furnished by the gradient descent theory. Again, given that the formulation is heuristic and non-conforming to the gradient descent method, direct mathematical proofs (i.e. independent of algorithm formulation) are necessary. The heuristic method employed to render the system time-invariant is to replace the time variable t by a constant m_4. This process converts the time-varying system to a time-invariant system which performs very well in practice, as will be shown in subsequent sections. Although the development of these equations is inspired by the concepts of least-squares minimisation and steepest descent, it does not comply with the conditions under which these concepts may be legitimately employed. This implies that the mathematical properties of the proposed algorithm such as stability, convergence and uniqueness of the solution have to be proved. A complete mathematical proof using the Poincare map theorem is presented in [33].

2.2.1 Governing Equations of the Nonlinear Adaptive Algorithm

The filter can be represented by the following set of nonlinear differential equations

$$\dot{V} = \mu_1 e \sin \phi_v \tag{2.21}$$

$$\dot{\omega} = \mu_2 e V \cos \phi_v \tag{2.22}$$

$$\dot{\phi} = \mu_3 e A \cos \phi_v + \omega \tag{2.23}$$

$$v(t) = V \sin \phi_v \tag{2.24}$$

$$e(t) = u(t) - v(t) \tag{2.25}$$

A block diagram of the nonlinear filter is shown in Figure 2-2. The filter comprises of three subsystems. An exploded view of all subsystems is shown in Figure 2-3. The amplitude is tracked in subsystem A. Equation (2.21) mathematically describes this subsystem. Amplitude variations are typically the result of reactive power changes on the power system [34]. The component $e(t) \times \sin(\phi) \times \mu_1$ of subsystem A influences the response time. For a large variation in the amplitude $V(t)$, the error $e(t)$ is large. This increases the response time. The other parameter that influences the response time of subsystem A is parameter μ_1. Equations (2.22) and (2.23) track the system frequency and phase variations of the input signal. This is graphically illustrated in subsystem B. The parameters μ_2 and μ_3 control the speed of the transient response with respect to variations in the frequency of the input signal. Once an estimate of the amplitude and total phase of the fundamental component is known, a specific sinusoidal component of interest can be extracted using (2.24). This is shown in subsystem C of Figure 2-3.

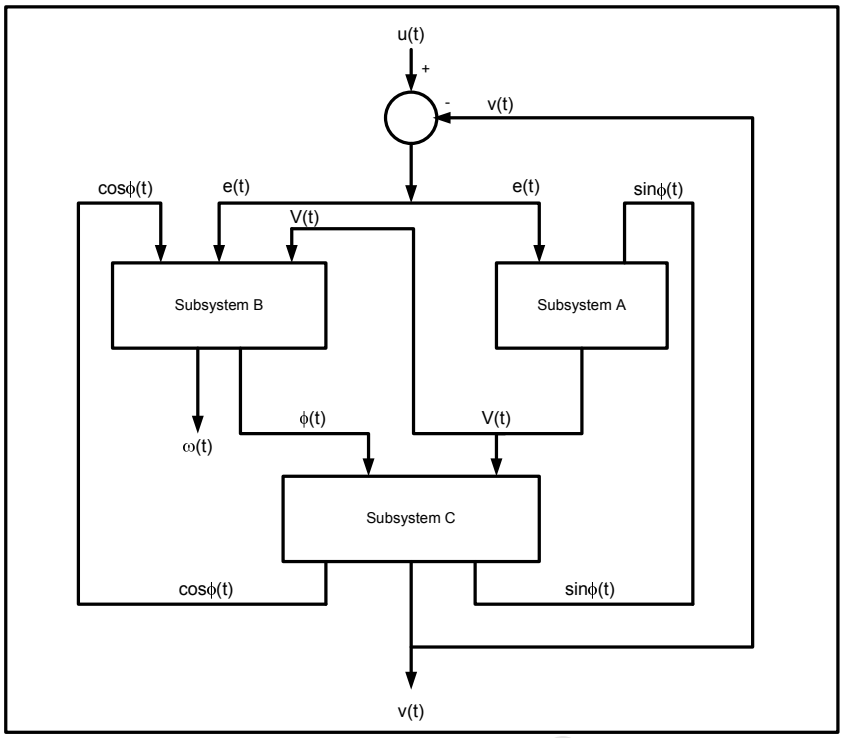

Figure 2-2: Block diagram of the algorithm.

For the nonlinear filter to be of any practical use, it must be able to be implemented on a signal processor. For this, a set of discrete equations is required. The filter can be converted from differential equations into a discrete format as follows

$$V[n+1] = V[n] + 2T_S\mu_1 e[n]\sin(\phi_v[n]) \tag{2.26}$$

$$\omega[n+1] = \omega[n] + 2T_S\mu_2 e[n]V[n]\cos(\phi_v[n]) \tag{2.27}$$

$$\phi_v[n+1] = \phi_v[n] + 2T_S\omega[n] + 2T_S^2\mu_2\mu_3 e[n]V[n]\cos(\phi_v[n]) \tag{2.28}$$

$$v_s[n] = V[n]\sin(\phi_v[n]) \tag{2.29}$$

$$e[n] = v[n] - v_s[n] \tag{2.30}$$

For this to hold, a first order approximation of the derivatives is assumed. The time derivative of any quantity Y is approximated by $(\mathrm{Y}\,[\mathrm{n}+1] - Y\,[\mathrm{n}]) \times \frac{1}{T_s}$. The discrete estimated amplitude is represented as $V\,[n+1]$, the total phase by $\phi_v\,[n+1]$ and the

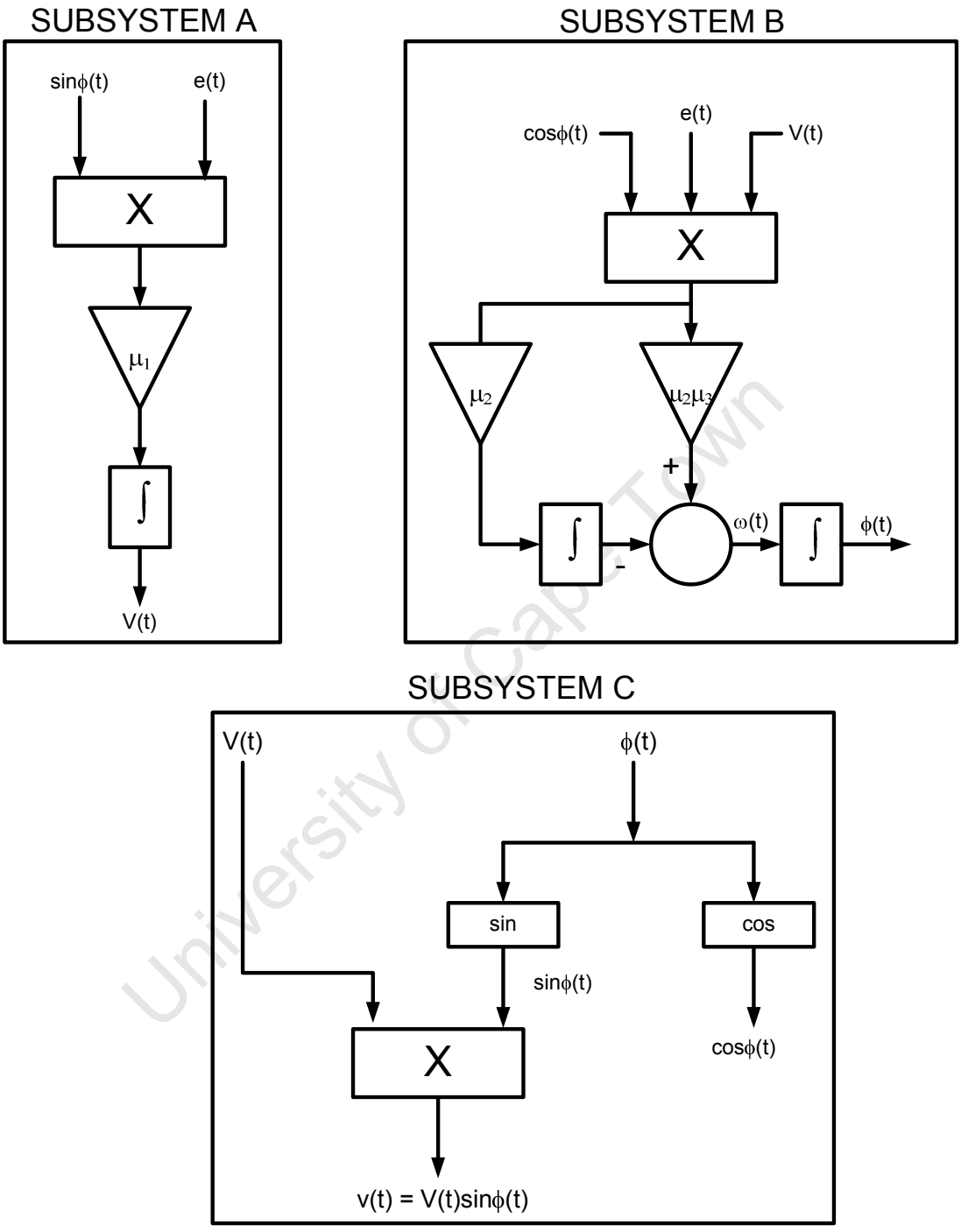

Figure 2-3: Exploded view of subsystems.

angular frequency by $\omega[n+1]$. The sampling time is represented as T_s and the time step index by n. The extracted sinusoidal component of interest is v_s [n] The discrete error $e[n]$ can be tracked at any time step n.

2.3 Performance of the Nonlinear Filter

2.3.1 Convergence

Figure 2-4 shows a snapshot of the frequency convergence performance of the nonlinear filter when a typical power system is energised. The frequency of the input signal jumps from 0 Hz to 50 Hz and the amplitude from 0 to 1 pu respectively. Figure 2-5 shows the convergence of the algorithm in the time domain from experimental results.

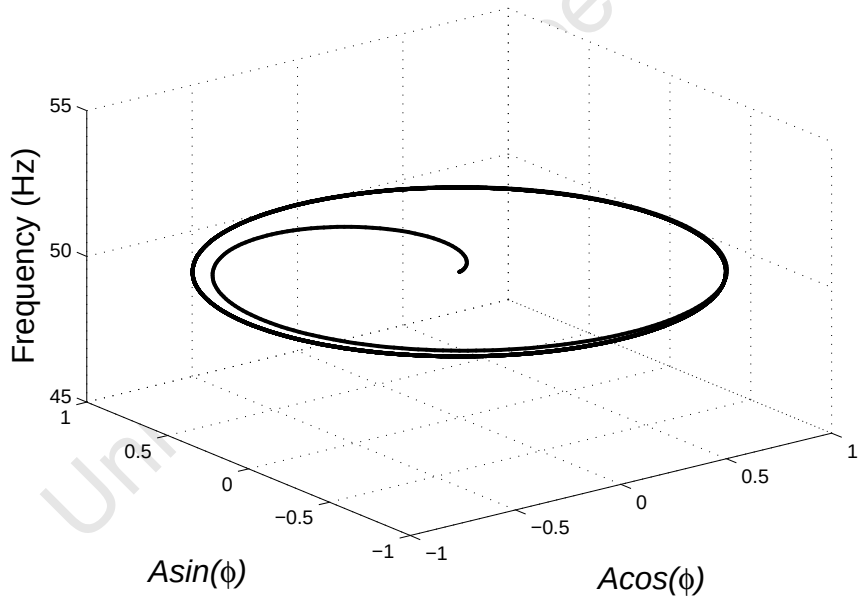

Figure 2-4: Convergence in the frequency domain.

2.3.2 Optimisation of Parameters

One of the issues that need to be considered when using the algorithm is the setting of its parameters. The values of the parameters determine the convergence speed

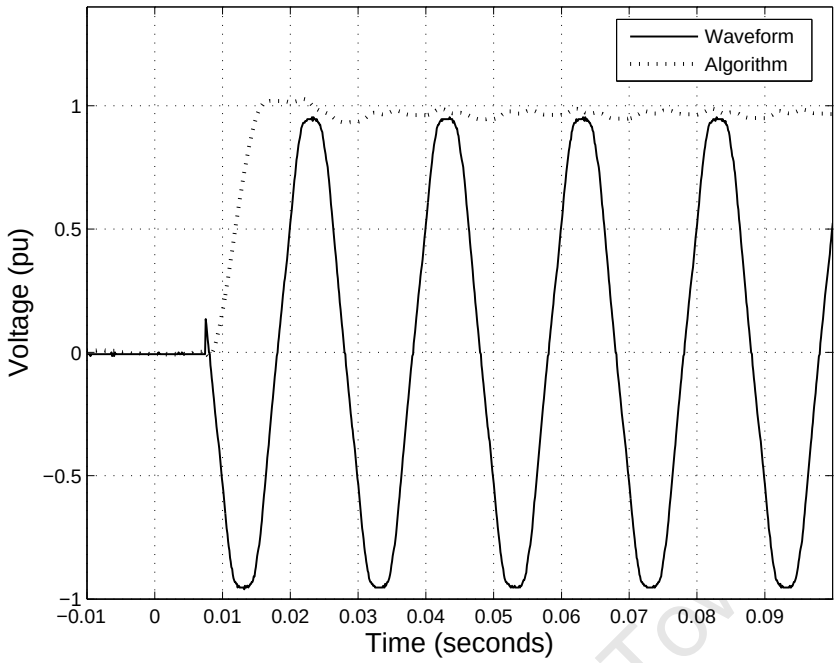

Figure 2-5: Convergence in the time domain.

versus error compromise. Specifically, parameter μ_1 controls the speed of the transient response of the algorithm with respect to variations in the amplitude of the interfering signal. Parameters μ_2 and μ_3 mutually control the speed of the transient response of the algorithm with respect to variations in the frequency of the interfering signal. Speed is traded off by the steady state error. As long as the frequency of the input signal is close to its nominal value (e.g. 50 Hz), this trade-off does not introduce a significant constraint. As the frequency of the input signal deviates from its nominal value, the algorithm introduces more significant trade-off between the speed and steady state error, e.g., within a range of frequency variations of the nominal frequency. The nonlinear algorithm can be adjusted to catch up a step change in the amplitude of the desired sinusoidal within cycles with less than steady state error. Figure 2-6 shows the estimation process under different μ parameters. The higher the μ value is chosen, the shorter the convergence time becomes. The convergence time is about 20 ms for the highest values of μ presented and about 200 ms for the lowest values of μ with the middle set having a convergence time of approximately 80 ms.

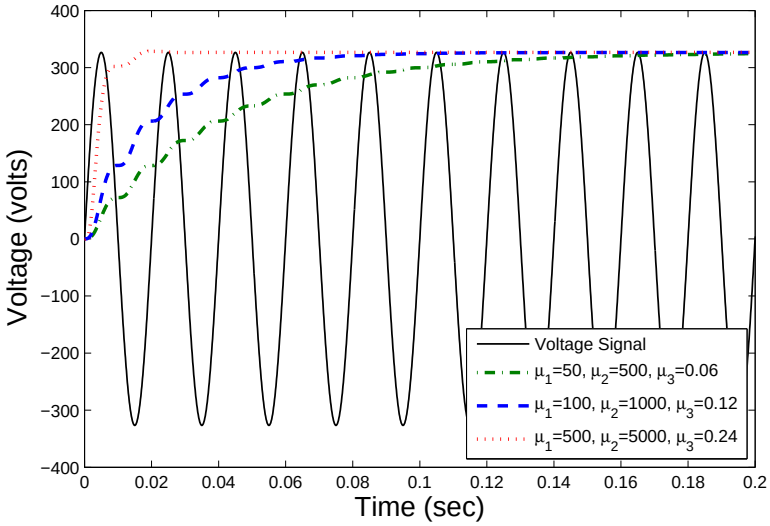

Figure 2-6: Convergence of the core algorithm under different μ parameters.

2.3.3 Influence of Frequency Deviations

The proposed algorithm is capable of tracking time-variations of the characteristics of the power signal over time. An important aspect is that it can accommodate frequency variations within the signal. Figure 2-7 shows the influence of frequency

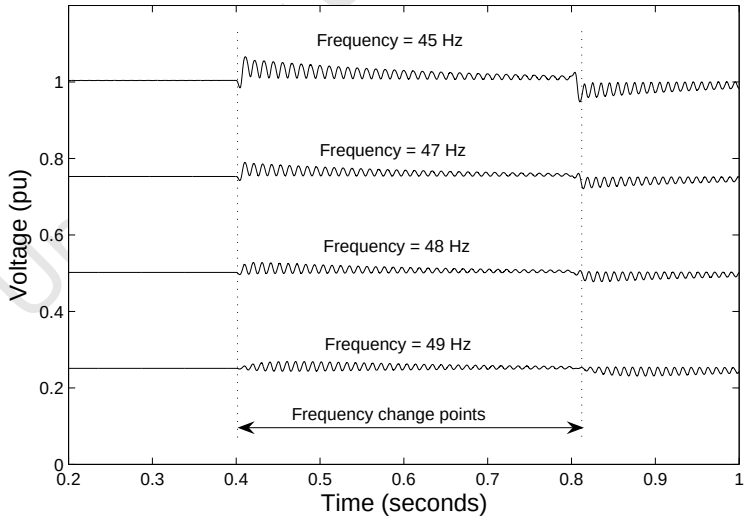

Figure 2-7: Influence of frequency deviations

variation on the proposed algorithm when the frequency of the power signal undergoes a step change in signal. The graph shows simulations with a frequency deviation from

the fundamental frequency of 50 Hz from t = 0.4 s until t = 0.8 s. At a step change in frequency of 5 Hz, the maximum error is 4%. This error reduces with time. At a frequency of 49 Hz, the error is 1.2%. In practice, the power systems control and protection equipment will contain the system frequency to within 2 Hz. Therefore errors associated with a frequency deviation will be small.

2.3.4 Employing a Multiplicity of Core Units

The core algorithm presented so far is intended to extract one single sinusoidal com-

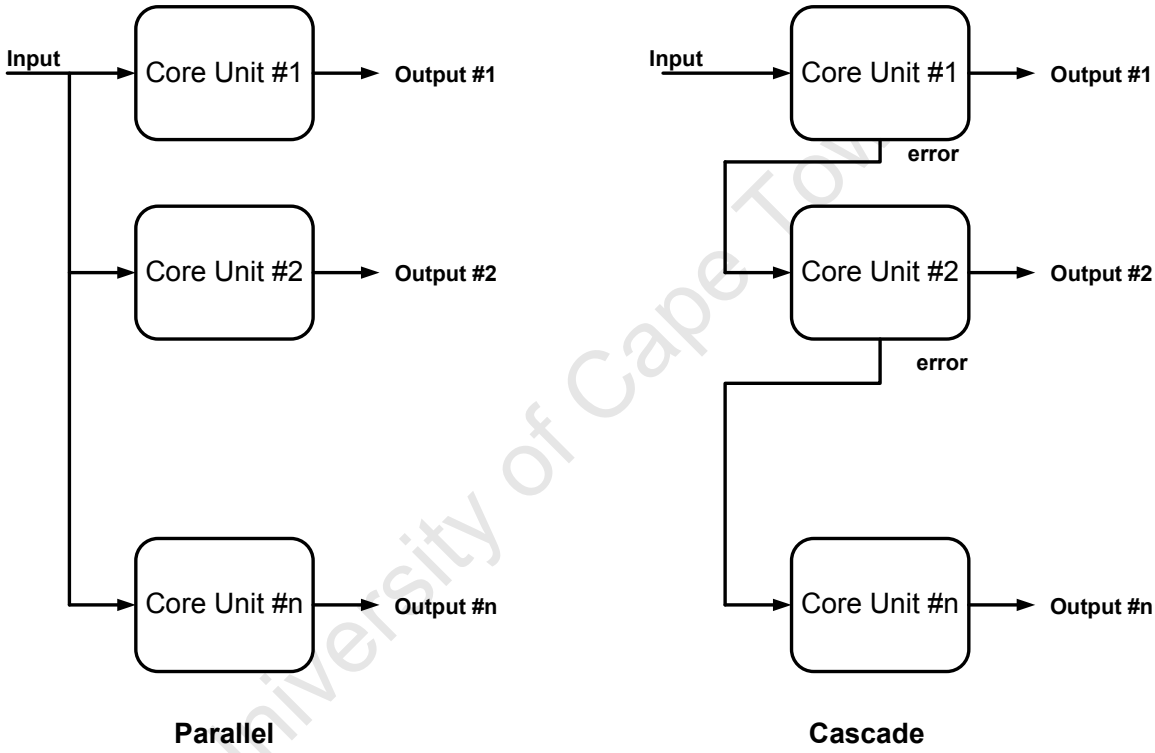

Figure 2-8: Possible ways of employing a multiplicity of core units [33].

ponent of the input signal. A multiplicity of core units may be employed in parallel or alternatively cascaded in order to decompose a multi-component input signal into its constituent sinusoidal components. Figure 2-8 shows two possible combinations, both of which are useful for different applications. For example, in harmonic analysis where a 5th harmonic is to be tracked, the algorithm can be tuned to the resonant frequency for active filtering. Alternatively, the error between the fundamental and

input signal could be used for motor signature analysis as demonstrated in [31].

2.4 Concluding Remarks

This chapter presented a mathematical model of the algorithm. The governing equations are presented and described. Convergence in the time and frequency domain is demonstrated through simulation and experimental results. Finally, the influence of parameter optimisation in order to obtain the desired response was discussed.

Chapter 3

Sag and Swell Detection

Power quality has been the focus of considerable research in recent years. Voltage sags, in particular, can cause expensive downtime. Voltage sags are defined as a decrease in RMS voltage at the power frequency for durations from 0.5 cycles to 1 minute [35]. The duration of a voltage sag is the time measured from the moment the RMS voltage drops to below 0.9 pu of nominal voltage to when it rises above 0.9 pu of nominal voltage. It is therefore possible for sags of short duration to cause problems in some sensitive equipment. Voltage sags may be caused by the switching of operations associated with a temporary disconnection of supply, the flow of inrush currents associated with the starting of motor loads or the flow of fault currents. These events may emanate from the customer's system or from the public supply network. Lightning strikes can cause momentary sags. Voltage swells are brief increases of RMS voltage that sometimes accompany voltage sags. They appear on the unfaulted phase of a three-phase circuit that has developed a single-phase short circuit. Various solutions have been proposed to mitigate sags. An example is a Dynamic Voltage Restorer (DVR) where the basic principle is to inject a voltage in series with the supply when a fault is detected. Figure 3-1 shows a broad overview of the mitigating process. Two approaches to improve ride-through capability include:

- Improve hardware performance
- Improve sag detection time

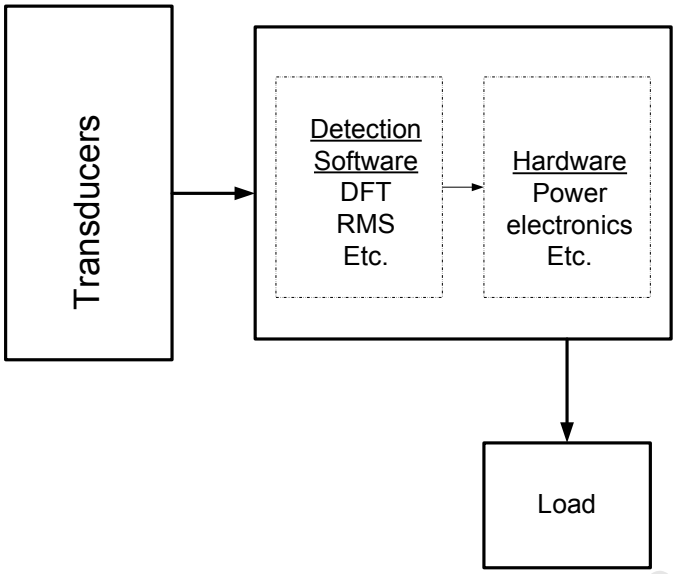

Figure 3-1: Broad overview of sag mitigation.

Much of the research in recent years has focused on the hardware performance of mitigation devices [36], [37], [38]. Generally, the RMS method is used to detect the sag before mitigation is initiated. The disadvantage of this method is that a window of historical data has to be obtained, processed and only then can a mitigation signal be sent to the hardware. Limitations associated with the RMS method are discussed in [39], [40]. The authors use a low pass filter and instantaneous reactive power theory to extract the sag. This is complex for implementation in a digital signal processor or microcontroller. A method for determining the start and end time of a sag using wavelets is presented in [41]. This is done to verify proper breaker operation after the sag has occurred.

3.1 Existing Methods

3.1.1 Root Mean Square (RMS)

Voltage and current measurements are often expressed in RMS values [39]. The sag is detected after data for a window period has been processed. The RMS voltage is

expressed as

$$V_i^{rms} = \sqrt{\frac{1}{N} \sum_{j=i}^{i+N-1} V_j^2} \tag{3.1}$$

where N is the samples per cycle of the fundamental, V_j is the j^{th} sample of the recorded voltage waveform and V_{irms} is the i^{th} sample of the calculated RMS voltage. V_{rms} is delayed relatively to the phase voltage by *N-1* sample points due to the N-sample window used in (3.1). If the sample rate is such that N is not an integer, rounding it off will produce some error, but it is still acceptable. The start and drop time of the sag can be defined in a number of ways depending on the chosen RMS voltage thresholds. The start time is taken as the first point of when V_{rms} drops below 0.9 pu. To find the end time, search for an interval where V_{rms} drops below 0.9 pu for at least half a cycle. The recovery time is then chosen as the first point in this interval. Since the RMS voltage is in effect a moving average calculated using a one-cycle window, there can be a lag of up to one cycle from the time the voltage actually starts or clears and the time that the RMS value falls below the given threshold.

3.1.2 Peak Voltage (PV)

The Peak Voltage (PV) can be used to detect sags and swells. The following equation can be written as

$$PV = \max |V(t - \tau)| \qquad 0 < \tau < t \tag{3.2}$$

where $V(t)$ is the sampled waveform and t is an integer of one half cycle. For each sample, the maximum of the absolute value of the voltage over the preceding half cycle is calculated.

3.2 Experimental Setup and Test Procedure

For experimental testing of the performance of the nonlinear filter, a voltage sag generator was required that is capable of generating sags of varying magnitudes and duration.

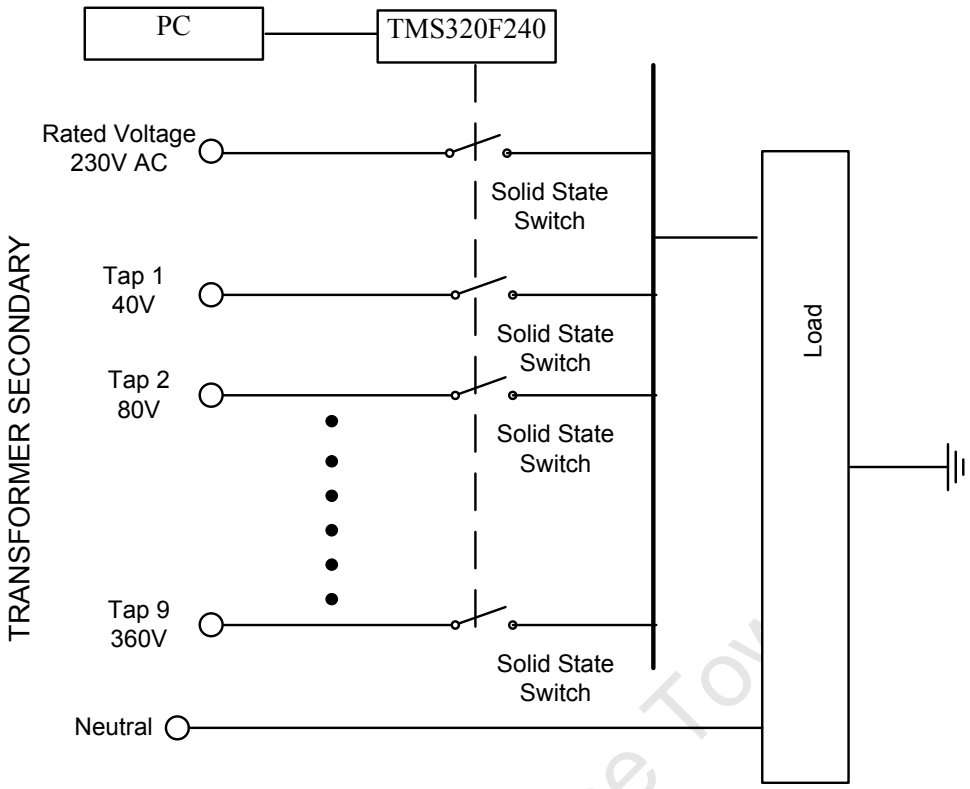

Figure 3-2: Experimental setup of system for laboratory testing.

Figure 3-2 shows the experimental setup that was arranged to conduct the experiments. A 10 kVA transformer with multiple taps on the secondary was used to switch rapidly between two output voltages. The first output was set to 100% of the rated voltage. The second output was set to the required sag magnitude value. The taps can be set from 40 V to 400 V in steps of 40 V. A Texas Instruments, TMS320F240 processor was used to log data and switch solid state relays rapidly between the two outputs to obtain the desired sag magnitude and duration. When testing the performance for rate of change, a cascaded configuration was used. The equipment which underwent testing was the load.

3.3 Sag Detection Results

3.3.1 Comparison of RMS and Nonlinear Filter for Sag Detection

The results in this section are based on experimental results using the experimental test setup. For the experiment, sag down to 0% was generated. The utility supply frequency of 50 Hz is used and a low sampling frequency of 20 samples per cycles was used. Figure 3-3 shows the sag inception point, the RMS and the algorithm. The algorithm detects the sag in 2 ms and the RMS in 9 ms. The difference in detection time between the two methods is 7 ms.

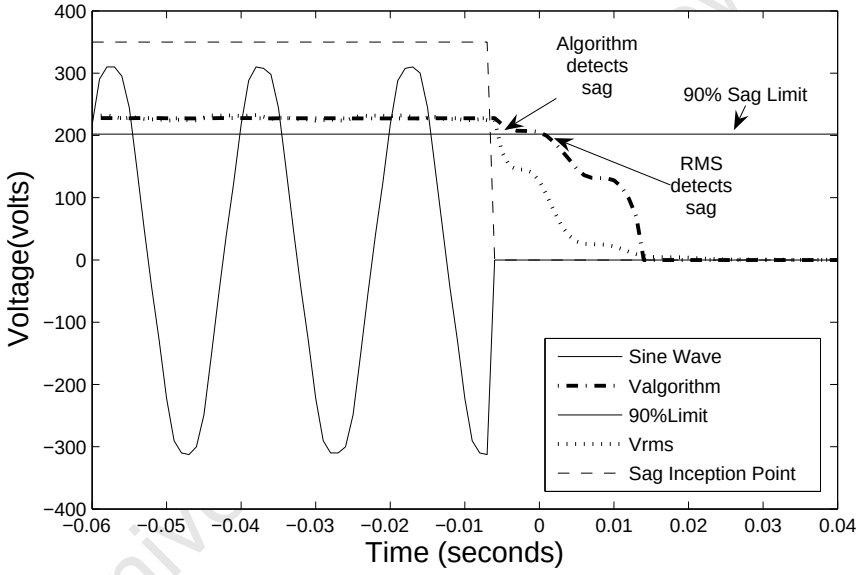

Figure 3-3: Experimental results comparing RMS and the nonlinear algorithm.

3.3.2 Comparison of Peak Voltage Method and Nonlinear Algorithm for Sag Detection

Figure 3-4 shows the performance of the peak voltage method when compared to the nonlinear algorithm. The nonlinear algorithm detects the sag in 2 ms and the peak voltage method in 20 ms. That results in a difference in sag detection time of 18 ms.

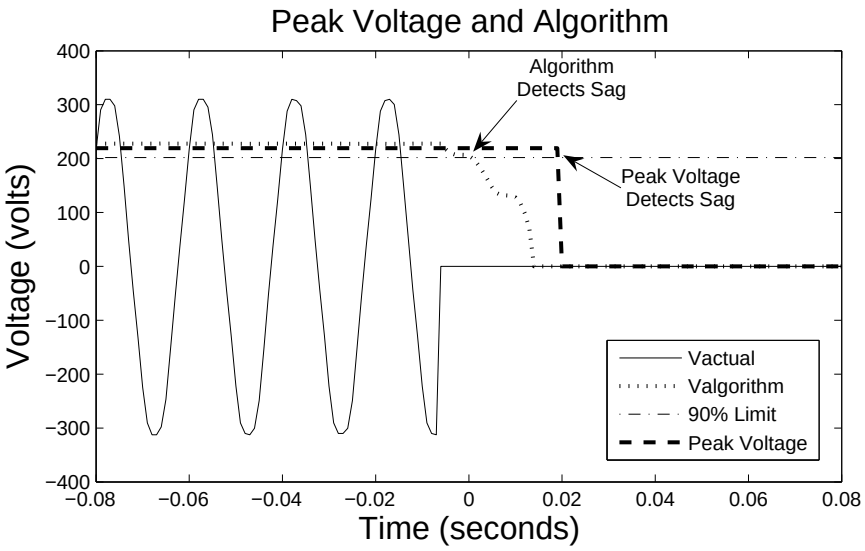

Figure 3-4: Experimental results comparing peak voltage method and nonlinear algorithm.

3.4 Swell Detection Results

A voltage swell is most often caused by a line-to-ground fault on a poly-phase transmission line or feeder. A voltage swell can also be caused by removing a large load or by switching a capacitor bank that is too large for the prevailing conditions. Failure to limit a swell can result in damage to power system and end use equipment. Thus far, only comparisons have been made for voltage sag detection. The algorithm can be used to isolate equipment when the declared voltage increases above pre-defined thresholds.

3.4.1 Comparison of RMS and Nonlinear Adaptive Algorithm for Swell Detection

Figure 3-5 shows a comparison of the nonlinear algorithm with the RMS for detecting a swell in real-time. The difference in detection time from the swell inception point is 17 ms.

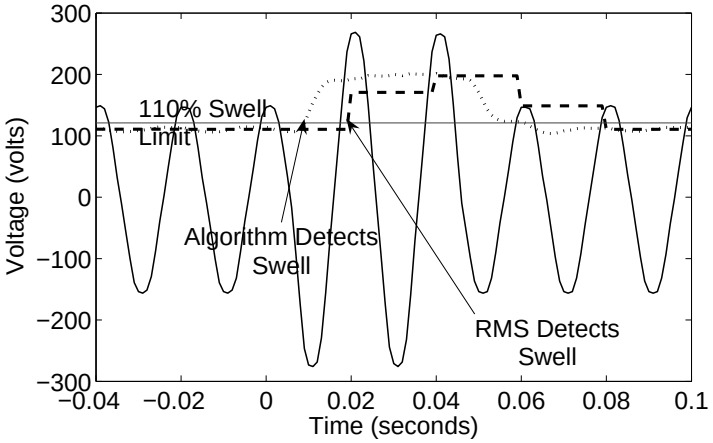

Figure 3-5: Experimental results comparing the RMS and the nonlinear algorithm for swell detection.

3.4.2 Comparison of PV and Algorithm for Swell Detection

Figure 3-6 shows a comparison of the nonlinear algorithm to the PV method for detecting a swell in real-time. The difference in detection time from swell inception is 17 ms.

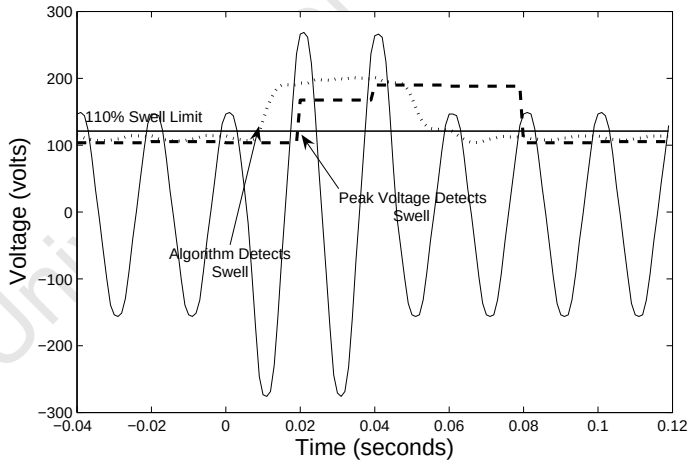

Figure 3-6: Experimental results comparing the Peak Voltage Method and the nonlinear algorithm for swell detection.

3.5 The Effects of Noise on Sag or Swell Detection

For waveforms with a high noise content, simulations demonstrate that the error associated with the peak voltage method is very high. Tables 3.1 and 3.2 show the results from the study. Maximum errors of 40%, 9% and 0.94% were measured from the peak voltage, RMS and nonlinear filter respectively for sag detection. This corresponded to a noise level of $\sigma^2 = 0.1$. For swell detection, the maximum errors were 16.5%, 3.8% and 0.93% respectively for the peak voltage, RMS and nonlinear filter. The input parameters of the nonlinear filter used were $\mu_1 = 100$, $\mu_2 = 10000$ and $\mu_3 = 0.02$.

Table 3.1: Influence of noise on detection of sags.

	% **Error**		
σ^2	**PV**	**RMS**	**Alg**
0.005	1.800	0.767	0.140
0.01	3.317	1.150	0.180
0.03	11.200	2.700	0.347
0.05	19.533	4.383	0.517
0.08	32.033	7.100	0.767
0.1	40.350	9.033	0.937

Table 3.2: Influence of noise on detection of swells.

	% **Error**		
σ^2	**PV**	**RMS**	**Alg**
0.005	0.793	0.564	0.275
0.01	1.293	0.721	0.307
0.03	4.064	1.364	0.425
0.05	7.636	2.021	0.564
0.08	12.993	3.057	0.782
0.1	16.557	3.771	0.929

3.6 Influence of Point on Wave

The point on the wave is the instant on the sinusoidal when a disturbance begins. In practice, one cannot control the point on the wave when a fault occurs. Hence for a sinusoidal waveform, the point on the wave is at its minimum near the zero-crossing area and at its maximum near the peak value of a waveform. For simulations presented in this section, $Matlab/Simulink^{TM}$ is used as the computational tool.

3.6.1 Sag Detection

Figure 3-7 shows the algorithm tracking an 80% voltage sag at the 0°, 90° and 180° points on the wave. The point on the wave was simulated for different sag magnitudes. The best scenario recorded a detection time of 1 ms. This corresponded to a 20% sag at 90° point on wave. Results from simulations show that detection time is affected more by sag magnitude than by the point on the wave. The worst delay time recorded was 4 ms (less than a quarter of a cycle). This corresponded to an 80% sag at the 180° point on wave.

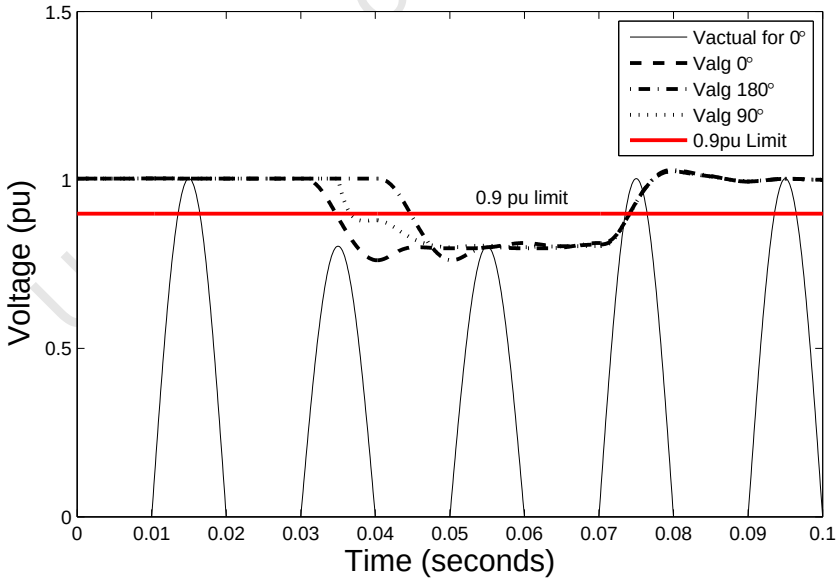

Figure 3-7: Influence of different point on wave on sag detection.

3.6.2 Swell Detection

Figure 3-8 shows tests for point on wave influence on swell detection for a 150% voltage swell. The best detection time of 1 ms corresponded to a 180% voltage swell and a 90° point on wave. The worst detection time recorded was 5 ms. This corresponds to a 120% swell at 180° point on wave.

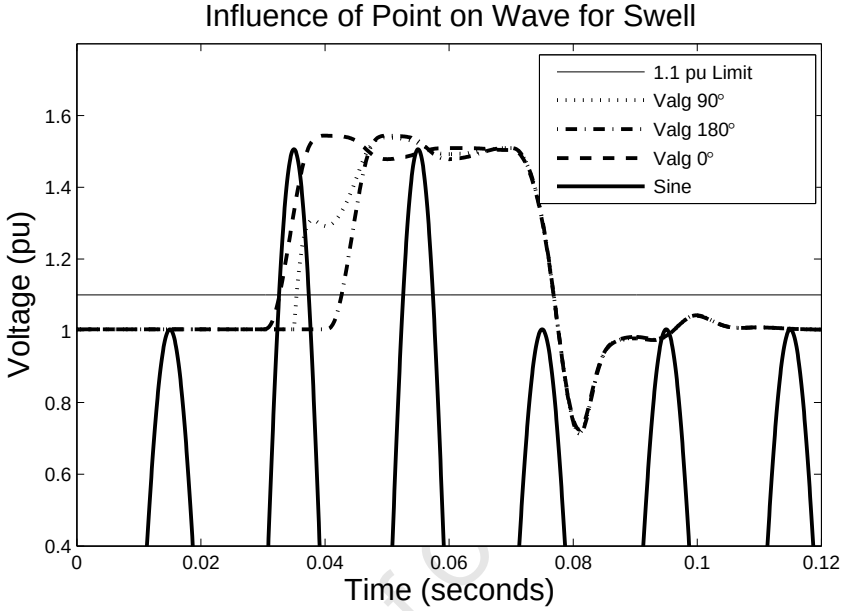

Figure 3-8: Influence of point on wave for swell detection.

3.7 Influence of Rate of Change of Voltage on Detection Results

This section tests the algorithm for detection ability for different rate of changes. Figure 3-9 shows a sag with a small gradient. The gradient was obtained by switching from rated voltage to 203, 180, 158 and 135 V for one-cycle (20 ms) each. A steeper gradient was generated by decreasing the rated voltage to 203, 135, 42.5 and 22 V for one cycle each. This is shown in Figure 3-10. In both cases, the algorithm is able to track the sag within 4 ms. Figures 3-11 and 3-12 are field recorded voltage sags from [11].

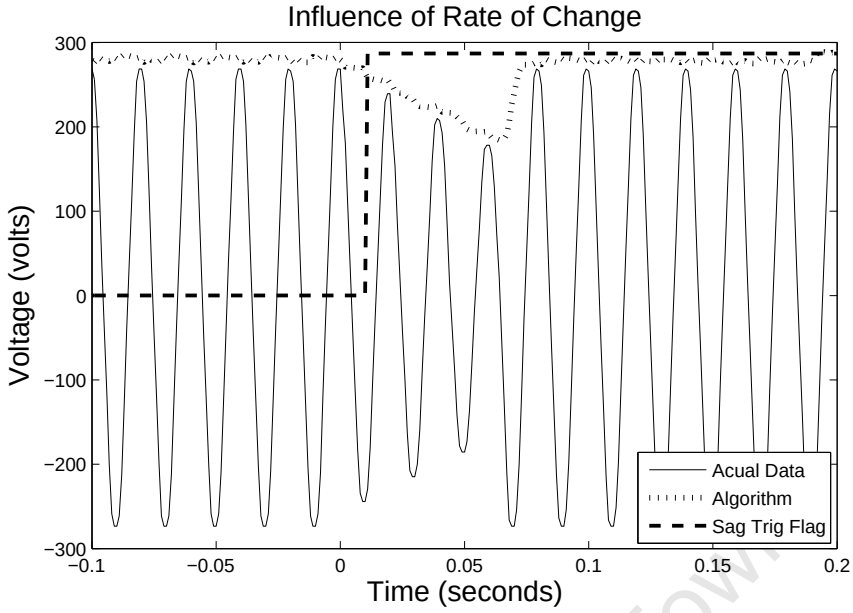

Figure 3-9: Experimental results showing the influence of rate of change for small gradient.

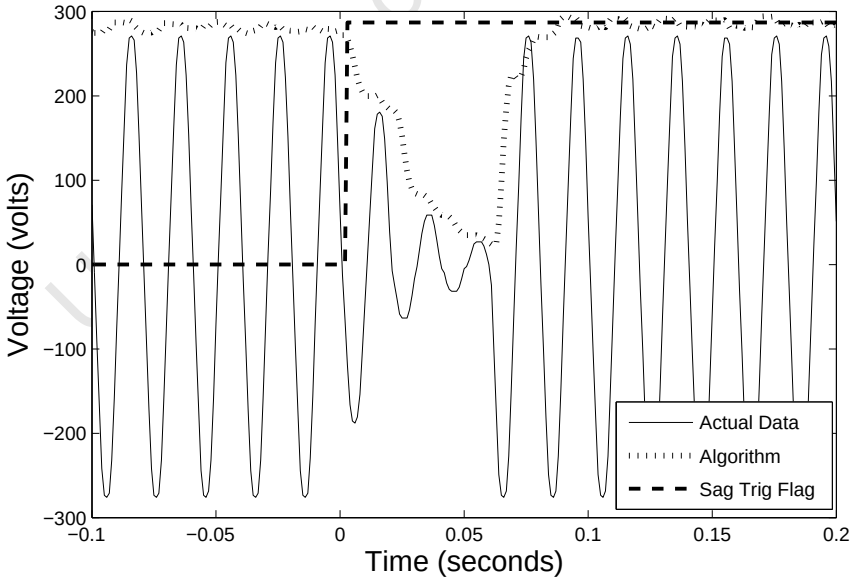

Figure 3-10: Experimental results showing the influence of rate of change for large gradient.

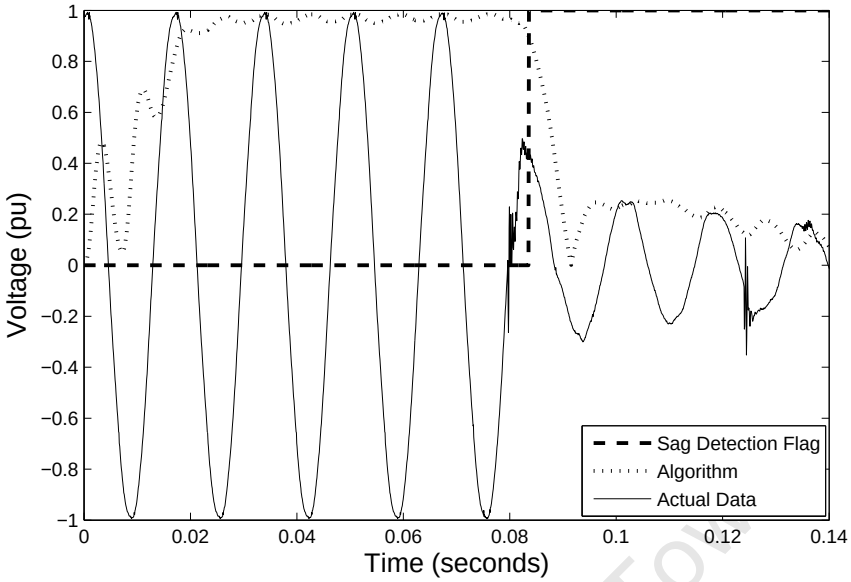

Figure 3-11: Field recorded voltage sag [11].

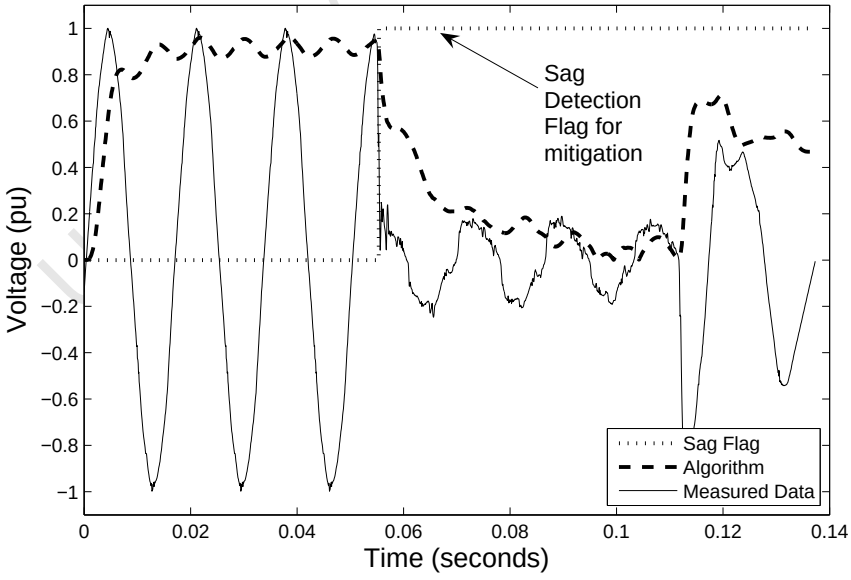

Figure 3-12: Field recorded voltage sag [11].

3.8 Influence of Sag/Swell Magnitudes

From results of the previous section, it is evident that sag magnitude has the biggest influence on detection time. Figure 3-13 shows the influence of sag/swell magnitude on the algorithm.

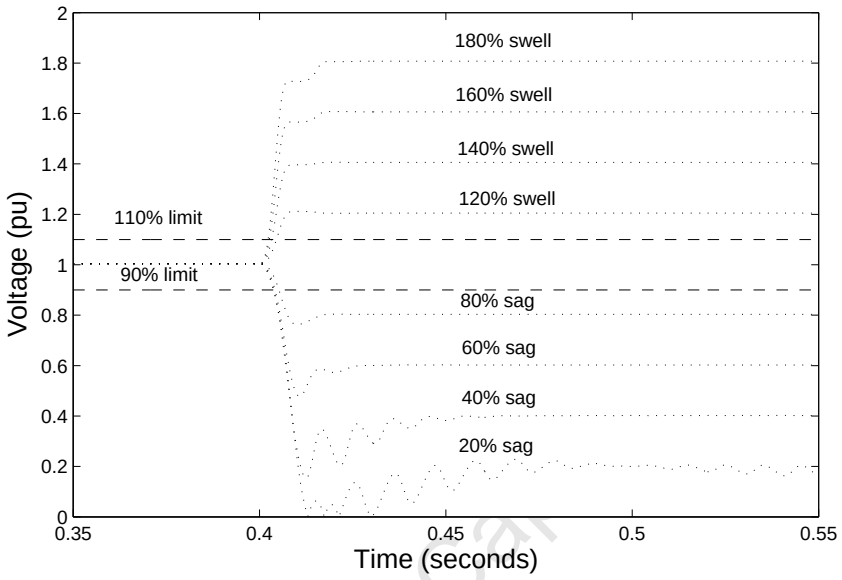

Figure 3-13: Tracking sags and swells.

Results from the study indicate that the algorithm is able to respond within 1 ms for deep sags and swells (i.e. sags $< 30\%$ and swells $> 160\%$). For other sags and swells, it is able to respond within 4 ms. This is in line with mitigation requirements since the sags and swells that require the fastest response time are the ones with the largest magnitude variation.

3.9 Effects of a Change of Input Parameters

The influence of a change in input parameters is shown in this section. The three parameter sets used for the study are:

- Parameter Set 1: $\mu_1 = 400$, $\mu_2 = 3000$ and $\mu_3 = 0.4$
- Parameter Set 2: $\mu_1 = 100$, $\mu_2 = 1000$ and $\mu_3 = 0.12$

- Parameter Set 3: $\mu_1 = 50$, $\mu_2 = 500$ and $\mu_3 = 0.06$

The voltage was varied from 20% to 180% of the nominal voltage for a ten cycle sag. The detection time is determined and it is summarised in Table 3.3. The results indicate that the selection of input parameters does influence the detection time. For optimised detection time, the parameters should be chosen for a desired response.

Table 3.3: Influence of input parameters on detection time.

% Nominal Voltage	Parameter Set 1	Parameter Set 2	Parameter Set 3
20%	10.4	8.1	2.5
40%	10.6	8.3	2.3
60%	11.2	10	4.3
80%	15	13.3	7.4
120%	13	11.2	5.3
140%	11.2	9.1	4.7
160%	10.6	8.4	2.1
180%	10.4	8.2	2.1

3.10 Case Studies

The fundamental issue behind the symptoms related to sag is the amount of energy transferred to the equipment for it to operate satisfactorily. The equipment may malfunction if the DC voltage applied to integrated circuits drop as a result of inadequate energy transferred to the power supply. If this happens, the device will shut down, lock up, or operate incorrectly [42]. If the device shuts down, it can restart as soon as enough energy returns to the power supply. On the other hand, if too much energy is transferred to the equipment, it can cause damage. The effects of a swell can often be more destructive than those of a sag. The temporary over-voltage condition may cause breakdown of components in the power supplies of the equipment, even though the effect may be a gradual, cumulative effect.

3.10.1 Computer Susceptibility

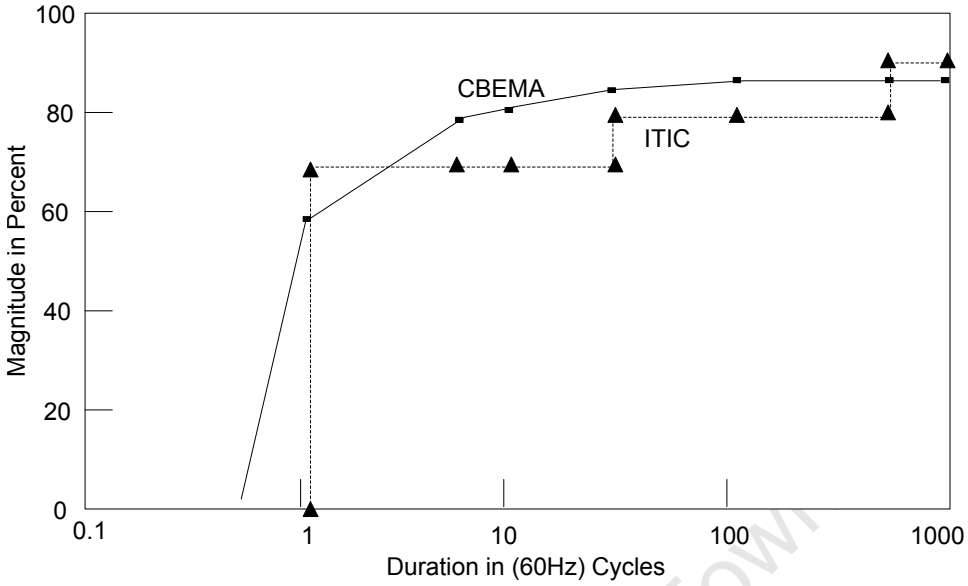

Figure 3-14: Influence of frequency deviations

The Computer and Business Equipment Manufacturers Association (CBEMA) guideline is a realistic, maximum allowable voltage that computer equipment can withstand, without causing damage or mal-operation. The power supply of a personal computer (PC), and most consumer electronic equipment normally consists of a diode rectifier, followed by an electronic voltage regulator. In the case of a PC, a capacitor is connected to the non-regulated dc bus to reduce the voltage ripple at the input of the voltage regulator. The time that it takes for the voltage to reach a level V can be calculate by using the following expression:

$$t = \frac{1 - \left(\frac{V}{V_o}\right)^2}{4 \in} T \tag{3.3}$$

Where $\in$ is the dc ripple voltage, V_o the dc bus voltage at sag initiation and T is one cycle of fundamental frequency [42]. From the CBEMA curve shown in Figure 3-14, one can see that a PC will trip for a 50% one-cycle sag. A simulation showing the algorithm because of a one-cycle 50% sag is shown in Figure 3-15. The algorithm detects the sag in 3.44 ms, whereas the one cycle RMS and peak voltage would detect

it in 20 ms. By detecting the sag faster, additional time is provided for mitigation equipment, such as an off-line Uninterruptible Power Supply (UPS) to react. If the RMS method is used to detect the sag, the PC will shut down before it is detected.

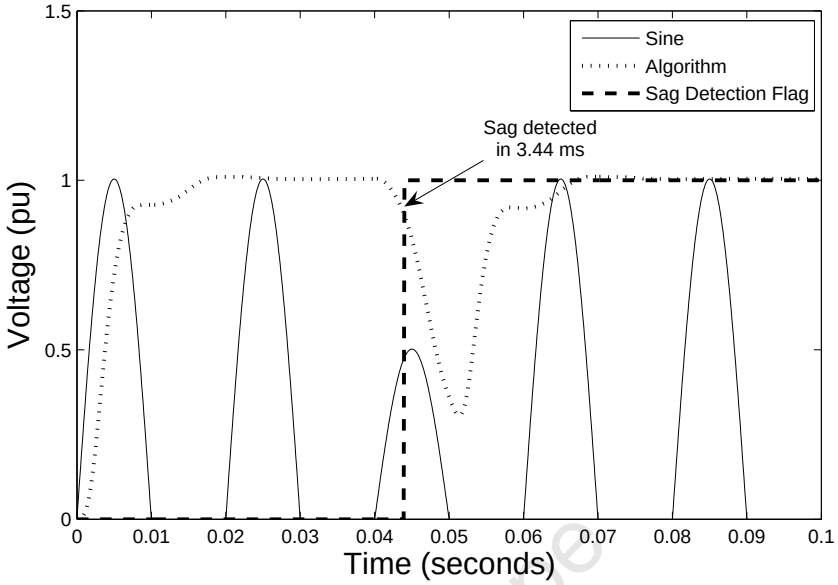

Figure 3-15: Detection for a 50% one-cycle sag

3.10.2 Adjustable Speed Drives

Adjustable speed drives typically trip due to an active intervention by the under-voltage protection when the dc bus voltage reaches a certain value, namely V_{min}. As long as the ac voltage does not reach below this value, the drive will not trip. For sags below this value 3.4 can be used to calculate the time it takes for the dc bus voltage to reach the value V_{min}.

$$t = \frac{C}{2P}\left(V_o^2 - V_{\min}^2\right) \tag{3.4}$$

where C is the dc bus capacitance and P is the loading of the dc bus [42]. A drive with a nominal dc bus voltage, $V_0 = 620\,\text{V}$ and dc bus capacitance $C = 8800\,\mu\text{F}$ powering an ac motor with a load of taking an active power $P = 86\,\text{kW}$ will trip. The drive trips when the dc bus voltage drops to 50% of its nominal i.e. $V_{min} = 330$

V. The time to trip is obtained from (3.4) is 16.7 ms. This is approximately one-cycle for a 60 Hz system.

3.11 Summary of Results

The presentation and performance of the proposed method of sag/swell detection demonstrates its superiority over existing methods. With reference to the discussions presented throughout this chapter, the main features of the proposed method can be summarised as follows:

- **Amplitude Variations** - The nonlinear adaptive filter is able to effectively track variations in amplitude. The magnitude of the sag/swell does influence detection time. A detection time of 1 ms can be achieved for sags $\leq 30\%$ and swells $\geq 160\%$.

- **Robustness and Noise Immunity** - Simulations show that the filter is able to track sags/swells more effectively than existing methods in the presence of noise. For a $\sigma^2 = 0.1$, the PV and RMS methods can produce errors of up to 16.5% and 3.8% respectively. The proposed method is able to contain the error to within 0.95%.

- **Sag Gradients** - The nonlinear filter is able to effectively track different sag gradients to within 0.1%.

- **Input Parameters** - The selection of input parameters does influence the sag detection time. Optimisation is necessary for the desired response. This was demonstrated through the application of different parameter sets as shown in Table 3.3.

- **Point on Wave** - The filter is able to effectively track sags/swells occurring at different point on waves. Sags/swells occurring at close to 90° can respond by up to 3 ms slower than sags occurring at the zero crossing.

3.12 Concluding Remarks

The algorithm has been presented and applied to the detection of sags and swells in power systems. It has been compared to existing methods. The nonlinear algorithm has a distinct advantage when mitigation is concerned. Time saved can be translated into reducing the component of lost energy during the sag. The influence of amplitude variations, noise, point on wave and rate of change has been investigated. It was found that sag/swell magnitude and the selection of input parameters have the greatest influence on the detection time. For optimal parameter selection, it was shown that the proposed algorithm can at worst detect voltage sags within 4 ms. The main contribution of the chapter is the presentation of a new method that offers improved detection time over conventional methods.

Chapter 4

Phase and Frequency Estimation

Phase and frequency estimation is critical for the operation of many power system functions that involve synchronisation, protective relaying and control circuits. Power conditioning equipment such as the Pulse Width Modulation (PWM) rectifiers, UPS's and active harmonic filters, rely on the phase angle of the line voltage as a reference.

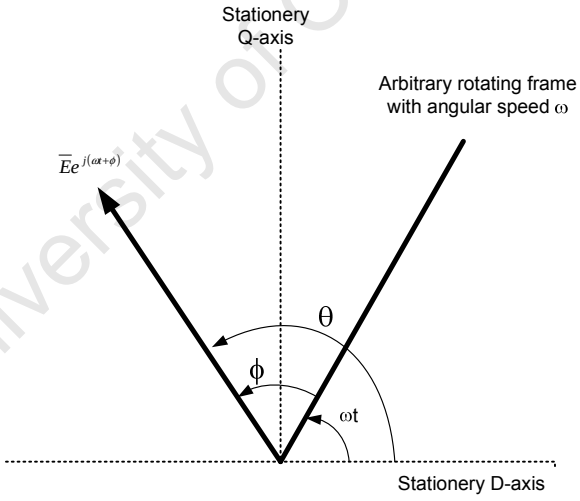

Figure 4-1: Phasor representation of the system voltage [43].

When the amplitude, phase or frequency changes in a step manner, the conventional phase angle detector, such as the Phase Locked Loop (PLL) or low pass or notch filter typically generates a phase delay. This results in a delayed response and can negatively impact time-critical operations. One can enhance the tracking speed of

a PLL or filter by reducing the time-constant. This makes the PLL very sensitive to harmonic disturbances and measurement noise. The challenge is to achieve both fast tracking and robustness against harmonics and noise. Figure 4-1 shows a phasor representation of the system voltage. In recent decades, many algorithms have been published on phase and frequency estimation for both single and three-phase applications. Some of these algorithms are based on known signal processing techniques, such as Least Squares Error, Kalman filtering, DFT, etc. In [8], an iterative technique for estimating phase and frequency is proposed. This method requires considerable computational effort. It is not suitable to the control of PWM converters as required for real-time application. A very fast phase angle estimation algorithm for single phase systems is presented in [43]. This system has been successfully applied to traction systems. The method is based on the Weighted Least Squares Estimation (WLSE) method with the covariance resetting technique. The influence of noise results in frequent covariance resetting. In [44], a recursive method based on the DFT is used to track system frequency and estimate the phase angle. This method has a long delay and is not suitable to real-time applications. The three-phase PLL is widely used to estimate system phase and frequency. A drawback is that system unbalance, harmonics and noise adversely affect its performance. Various techniques have been proposed to enhance its performance [45].

This section focuses on the application of the nonlinear adaptive algorithm for the estimation of phase and frequency. The proposed method is applied to single and three phase applications. A comparison is done against the DFT, single and three-phase PLL.

4.1 Structure of the Proposed Method

The core system of the nonlinear algorithm of Figure 2-2 comprises two parts. The amplitude or peak is estimated by the top branch. The lower branch estimates the phase angle and frequency and generates the sine and cosine functions. It effectively

tracks variations in frequency of the fundamental component of the input signal, while rejecting noise and harmonics. The time varying amplitude is taken into account when estimating the frequency.

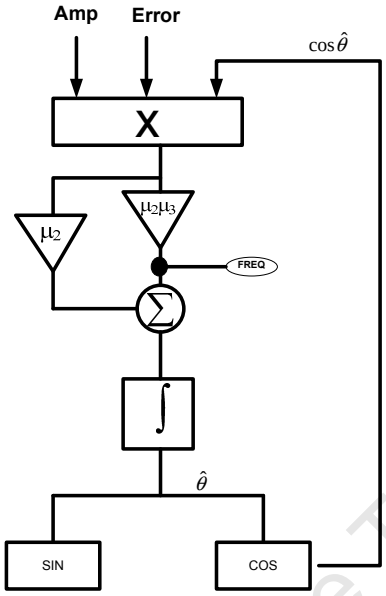

Figure 4-2: Structure of proposed frequency estimation method.

Figure 4-2 shows the structure of the frequency extraction part. One of the issues to be considered in the design of the proposed frequency tracking method is the setting of parameters μ_1, μ_2 and μ_3. The values of μ_1, μ_2 and μ_3 determine the convergence speed versus error compromise. Specifically, parameter μ_1 controls the speed of the transient response of the system with respect to variations in amplitude of the interfering signal. Speed is traded off for steady state error. As long as the frequency is close to its nominal value (e.g. 50 Hz), this trade-off does not introduce a significant constraint. If the frequency of the input signal deviates from the nominal value, the system introduces a more significant trade-off between speed and steady state error. Power system applications under normal operating conditions have frequency deviations of not more than 2%. The load frequency control and protection equipment return the frequency to nominal value under steady state and transient deviations. Parameters μ_2 and μ_3 mutually control the speed of the transient response of the system with respect to variations in the frequency of the interfering signal. The larger the value of μ_2, the faster the convergence is achieved in tracking phase (or frequency)

variations over time. The drawback is a higher steady state error. In the next sections, a number of simulations are presented to demonstrate the performance of the proposed system under non-stationary conditions.

4.2 Frequency Estimation

Frequency is an important operating parameter of the power system. The general problem of fundamental frequency estimation is to take a portion of the signal and to find the dominant frequency of repetition. Difficulties arise if (i) not all signals are periodic, (ii) those that are periodic may be changing in fundamental frequency over the time of interest, (iii) signals may be contaminated with noise, even with periodic signals of other fundamental frequencies, (iv) signals that are periodic with intervals T are also periodic with interval 2T, 3T etc. so one needs to find the smallest periodic interval or the highest fundamental frequency, and (v) even signals of constant fundamental frequency may be changing in other ways over the interval of interest. In this section, the proposed phase angle estimation method is extended to estimate the fundamental component of frequency $\hat{f}$. The general equation for frequency estimation is

$$\hat{f} = \frac{1}{2 \times \pi} \times \frac{(\theta_t - \theta_{t-1})}{dt} \tag{4.1}$$

where θ_t represents the total phase at time t. When the frequency estimate $\hat{f}$ is equal to the actual frequency f, $\hat{\phi}$ (phase angle) is constant in steady state. However, if $\hat{f} \neq f$, then $\hat{\phi}$ is not constant, but varies such that

$$\hat{\phi}_t = \Delta\omega\tau + \hat{\phi}_{t-1} \tag{4.2}$$

From (4.2), the necessary condition for $\hat{\phi} \equiv \phi_t - \phi_{t-1} = 0$ is that $\Delta f = 0$, i.e. $\hat{f} = f$ [43].

4.2.1 Estimating Step Changes in Frequency

For this test, the voltage signal is affected by step changes in frequency. The system was set up to track frequency changes up to ± 20 Hz. Figures 4-3(a) and 4-3(b) demonstrates the estimation of frequency using the nonlinear filter and PLL respectively. Optimised PLL parameters for 60 Hz were available. A nominal frequency of 60 Hz was used. The results indicate that the PLL is only effective in tracking step changes in frequency of up to 5 Hz. To achieve this, there is a delay of up to six cycles for measurement of up to ± 5 Hz. The nonlinear filter is able to effectively track step changes in frequency to within 0.02% and within one cycle. Table 4.1 shows a summary of the results comparing the PLL with the nonlinear filter for step changes in frequency. The results demonstrate the superior performance of the nonlinear filter over the PLL.

Table 4.1: Summary of results for step changes in frequency.

	% Error	
Frequency Deviation (Hz)	**PLL**	**Alg**
-20	-37,95	-0,02
-10	-7,70	0,00
-5	0,02	0,00
-3	0,01	0,00
-1	0,05	0,00
1	-0,05	0,00
3	-0,01	0,00
5	-0,01	0,00
10	5,53	-0,01
20	19,11	-0,02

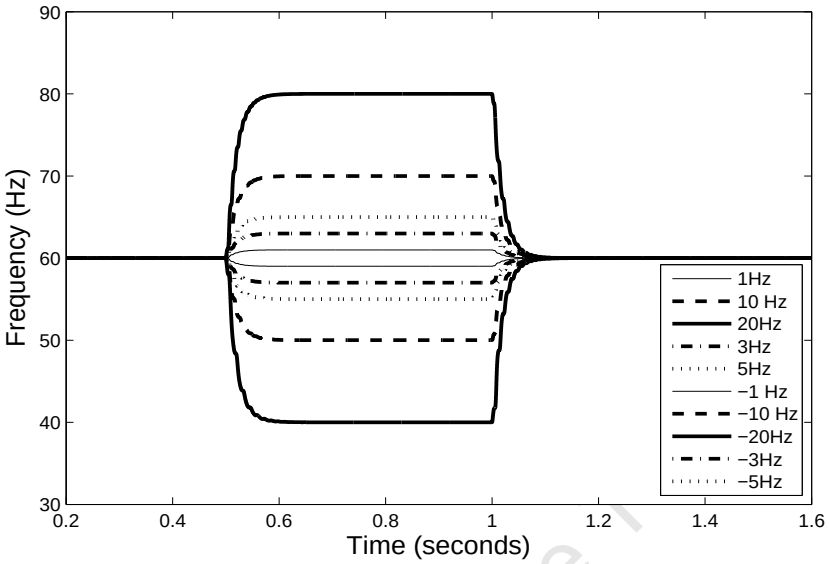

(a) Estimating step changes in frequency using the nonlinear filter.

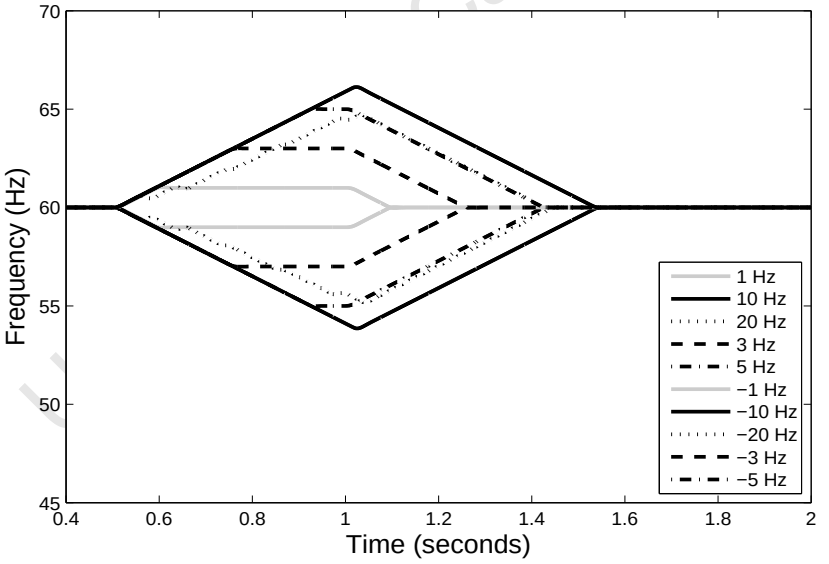

(b) Estimating step changes in frequency using the PLL.

Figure 4-3: Estimating step changes in frequency.

4.2.2 Estimation in Noise, Amplitude and Phase Changes

For this test, an input signal of 1pu amplitude is contaminated with Gaussian noise with zero mean and variance σ^2 for which

$$SNR = 20 \log \left(\frac{A}{\sqrt{2} \times \sigma} \right) \tag{4.3}$$

where A is the amplitude of the utility voltage. In this example, $\sigma^2 = 0.1$ and SNR = 7 db. The input signal is sampled at a rate of 10 kHz. The input signal undergoes a step change in amplitude of -0.5 pu and a phase shift of 30° from t = 0.4 to 0.6 seconds. Figures 4-4(a) and 4-4(b) show the input signal and the tracked amplitudes respectively. Amplitude errors of 2.5% and 0.75% were observed by the DFT method and by the nonlinear algorithm respectively. The tracked frequency is shown in Figure 4-4(c). The maximum frequency error of the algorithm is 1%.

4.2.3 Estimating Frequency During Simultaneous Amplitude and Frequency Changes

For this test, the input signal comprises a noise level of 7 db. The input signal undergoes a step change in amplitude and frequency of -0.5 pu and 3 Hz respectively. Figures 4-5(a)-4-5(c) show the performance of the nonlinear algorithm in tracking a step change in frequency of the input signal from time t = 1 to 3 seconds. The error from the Fourier method increased from 2.35% to 6.4% following the step change in frequency. The maximum amplitude and frequency error of the algorithm are 0.5% and 0.6% respectively.

4.2.4 Estimating a Ramp in Frequency

Figures 4-6(a)-4-6(c) show the influence of a ramp in frequency on a noisy signal. A dynamic change in frequency at a ramp rate of 1 Hz/s of the input signal is simulated from time t = 1 second to t = 5 seconds. Figure 4-6(b) shows that the amplitude error of the Fourier algorithm increases with increasing frequency. 4-6(c).

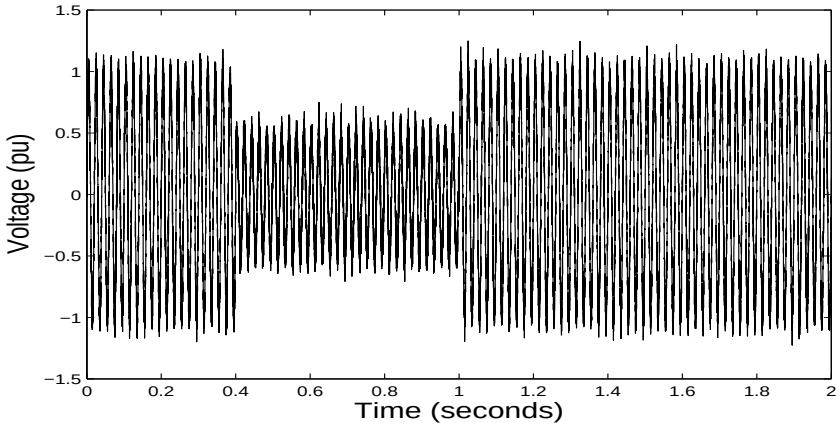

(a) Input signal.

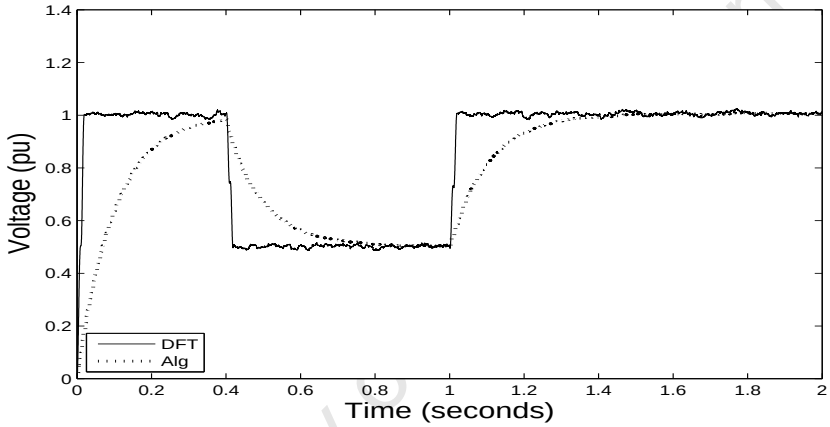

(b) Tracked amplitude.

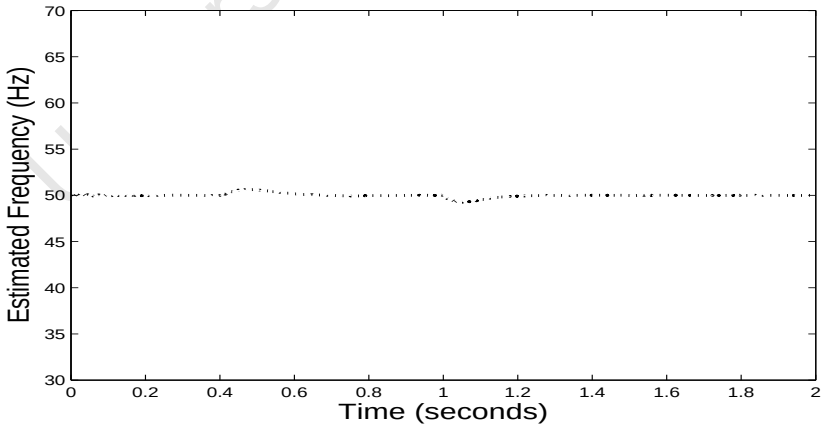

(c) Tracked frequency.

Figure 4-4: Frequency estimation of a noisy signal under a step in amplitude and phase.

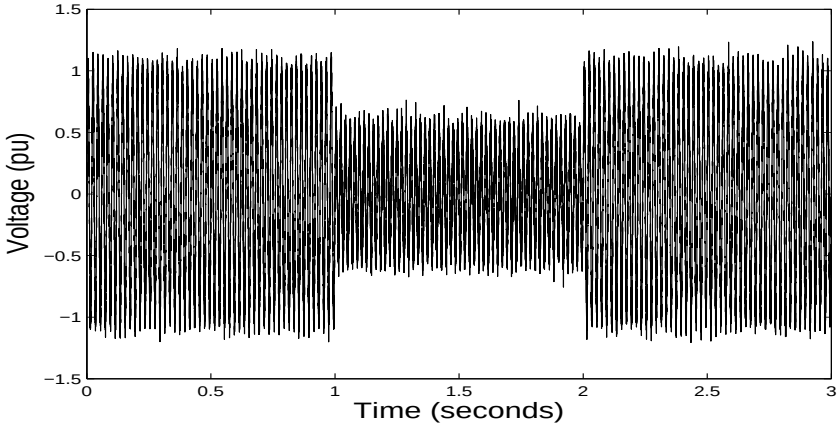

(a) Input signal.

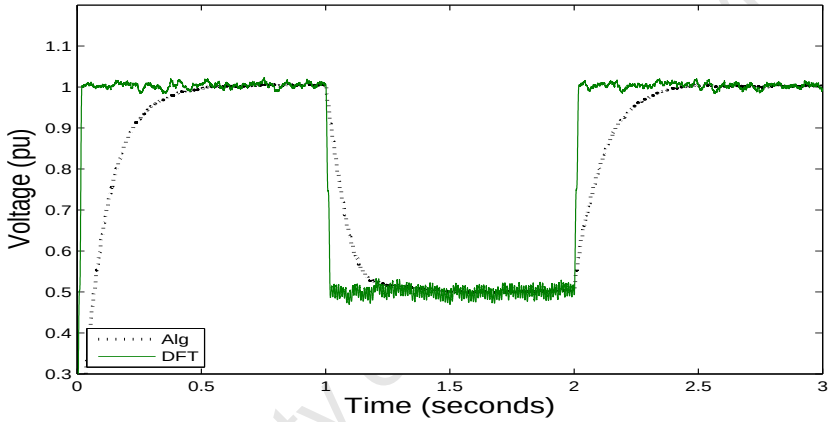

(b) Tracked amplitude comparing the nonlinear algorithm and the DFT.

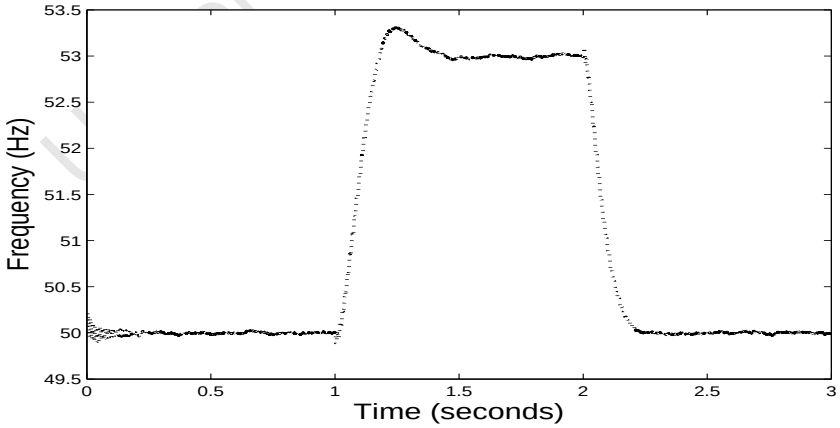

(c) Tracked frequency with the nonlinear algorithm.

Figure 4-5: Influence of a step change in amplitude and frequency.

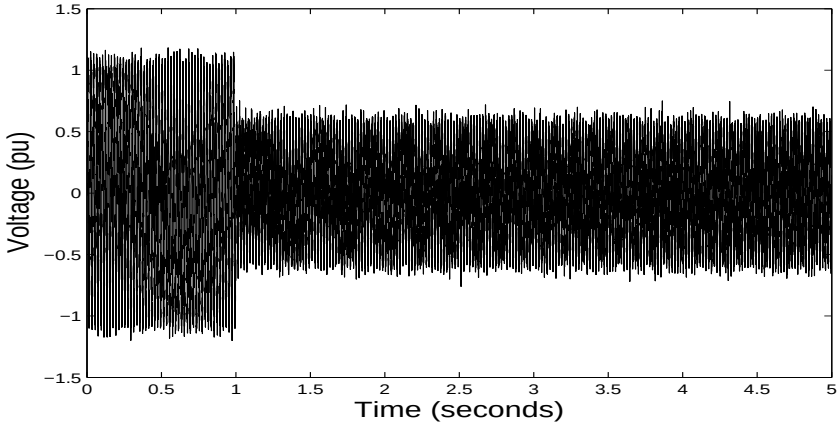

(a) Input signal.

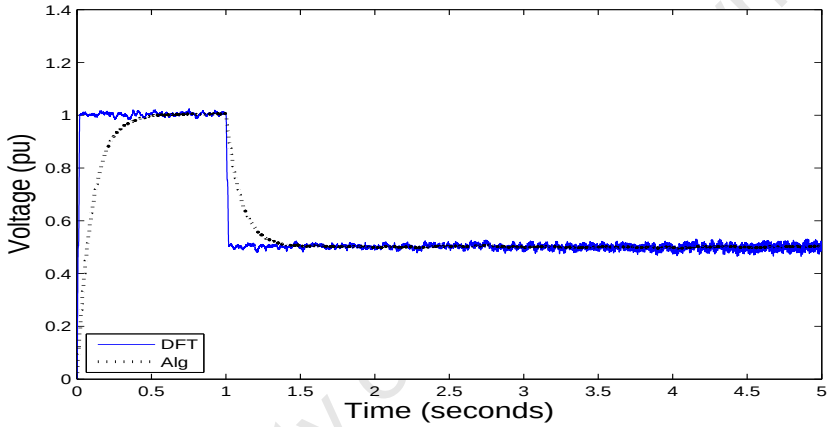

(b) Tracked amplitude comparing the nonlinear algorithm and the DFT.

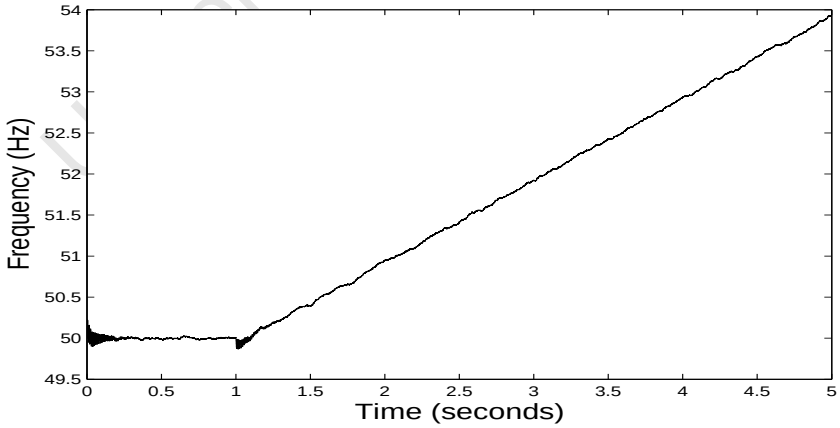

(c) Tracked frequency with the nonlinear algorithm.

Figure 4-6: Influence of a ramp in frequency of 1Hz/s.

4.2.5 Frequency Estimation in a Harmonic Polluted Environment

Harmonics are generally caused by non-linear loads on the power system. Non-linear loads draw non-linear currents. This results in a volt drop across the system impedance at the harmonic frequencies, thereby distorting the voltage at the point of common coupling. A good frequency estimation algorithm should be able to accurately extract the fundamental component of frequency in the presence of harmonics. For the test system, a 20% third harmonic and 10% fifth harmonic is added to a 1 pu, 50 Hz input signal. The total harmonic distortion is given by

$$\%THD = \frac{\sqrt{\sum_{h=2}^{\infty} V_h^2}}{V_1} * 100\% \tag{4.4}$$

where V_1 is the fundamental line-to-neutral voltage (RMS), in volts and V_h is the h^{th} harmonic component of the voltage of the order indicated by the subscript in V. THD is a measure of the effective value of the harmonic components of a distorted waveform, that is, the potential heating value of the harmonics relative to the fundamental. The input signal for this test comprises a THD of 22%. The maximum allowable voltage total harmonic distortion as prescribed by the IEC 61000-3-6 [46] is 8%. Two scenarios are simulated, namely (i) without noise and (ii) with noise. Figures 4-7(a) to 4-7(c) show the input signal, amplitude error and estimated frequency of the fundamental component respectively in a signal without noise. The amplitude estimation using the DFT results in no error. This is because the harmonics are exact integer multiples of the fundamental frequency. In cases where inter harmonics are present, the errors can be high. The steady state error using the algorithm is less than 0.2%. Figures 4-8(a) to 4-8(c) show the input signal and estimated frequency of the fundamental component in a signal with noise of SNR = 7 db. The steady state error using the DFT increases to 2%. The algorithm is able to contain the amplitude error to within 0.3% and the frequency error to within 0.1%.

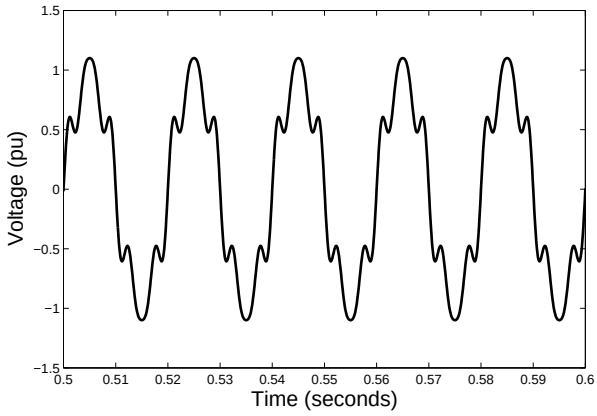

(a) Input signal.

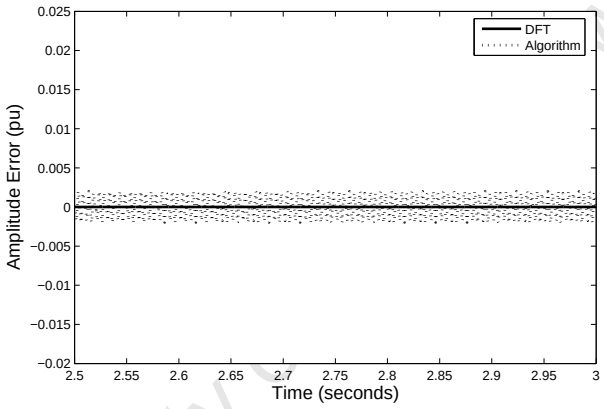

(b) Amplitude error.

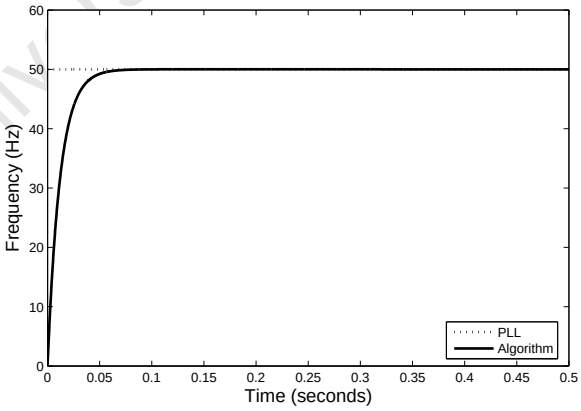

(c) Tracked frequency.

Figure 4-7: Performance in a harmonic polluted environment without noise.

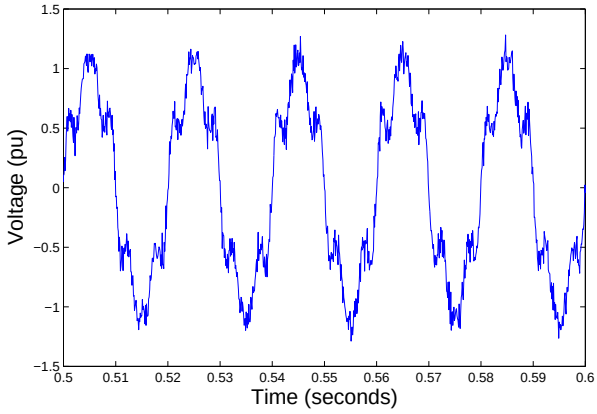

(a) Input signal.

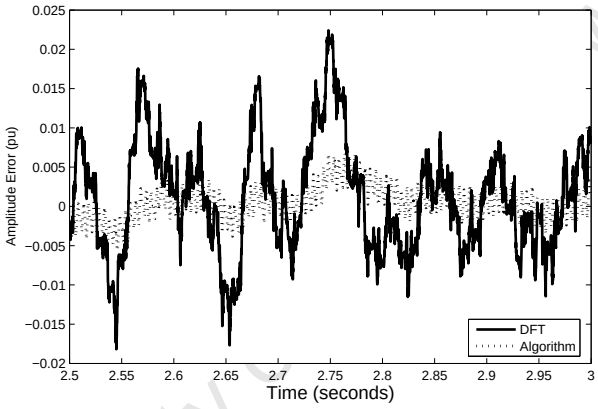

(b) Amplitude error.

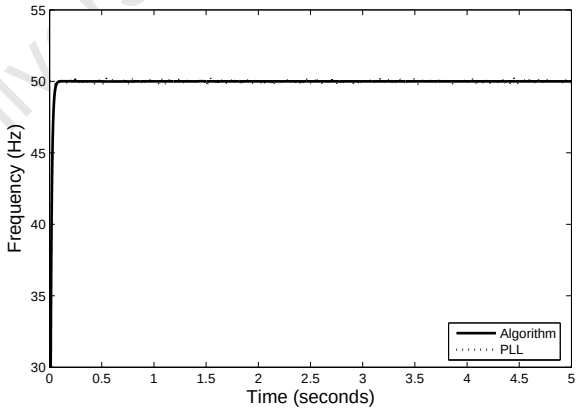

(c) Tracked frequency.

Figure 4-8: Performance in a harmonic polluted environment with noise.

4.2.6 Performance During Frequency Decay/Rise

The proposed technique does not rely on the assumption that the frequency remains constant within a certain period as per [8]. The effectiveness of the proposed technique during frequency decay/rise is tested by synthesising a signal whose frequency oscillates by $\pm$ 3 Hz at a frequency of 3 Hz starting from 50 Hz. The synthesised signal was sampled at a rate of 10 kHz. Figure 4-9 shows the actual frequency of the signal and the frequency estimate using the PLL and nonlinear algorithm. The figure demonstrates that the proposed technique tracks the signal frequency very closely with a delay of 10 ms. The tests were repeated with different rise rates. The results are shown in Table 4.2.

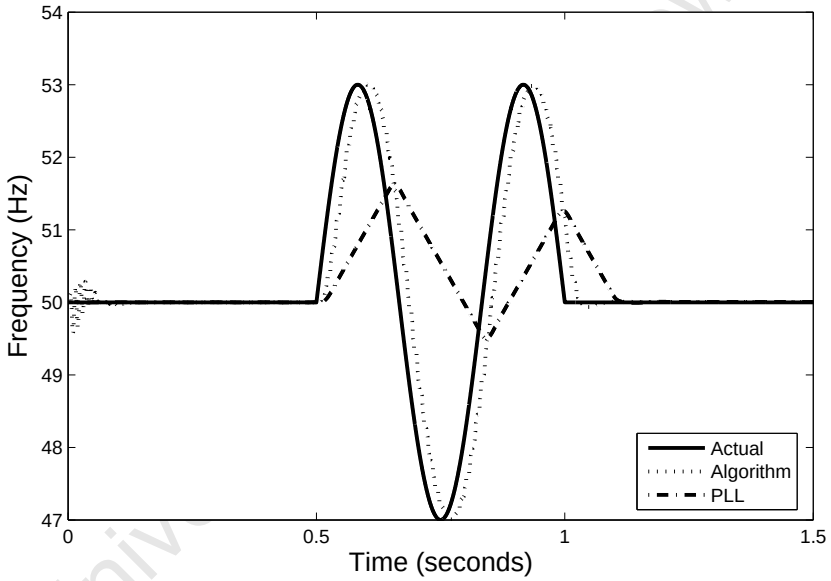

Figure 4-9: Structure of proposed frequency estimation method.

Table 4.2: Summary of results for tracking a modulated frequency.

Modulation	Maximum Error (%)	Delay (ms)
1 Hz	0.01	10.5
2 Hz	0.01	10.5
3 Hz	0.01	11

4.3 Phase Angle Estimation of Single-Phase Systems

The structure of the phase estimation component is shown in Figure 4-10. The algorithm estimates the total phase $\left(\hat{\omega}t + \hat{\phi}\right)$. The frequency output of the proposed method is sent to a discrete PLL. The PLL adjusts the frequency of the saw-tooth generator to the nonlinear algorithm-estimated frequency. This ensures that the instantaneous total phase is stationary with respect to the PLL so that the estimated phase angle remains stable following frequency deviations.

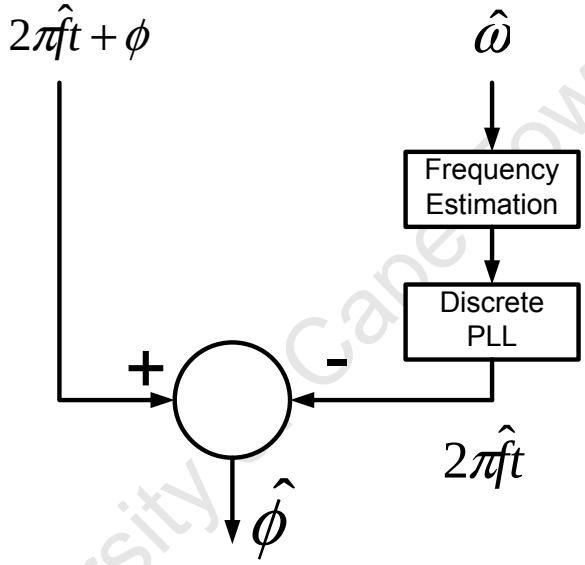

Figure 4-10: Structure of phase estimation component.

The output from the PLL and the nonlinear algorithm are subtracted to provide the instantaneous estimate of the phase angle $\hat{\phi}$. This could be mapped onto the direct and quadrature axis of Figure 4-1 to provide the d and q axis components.

4.3.1 Estimating Step Changes in Phase

Figures 4-11(a)-4-11(c) show the performance of the algorithm and the DFT in estimating step changes in phase. Figure 4-11(a) shows that the algorithm is able to lock onto the stepped phase of the input signal within two cycles of the fundamental frequency. The input signal has an initial phase angle of 30°.

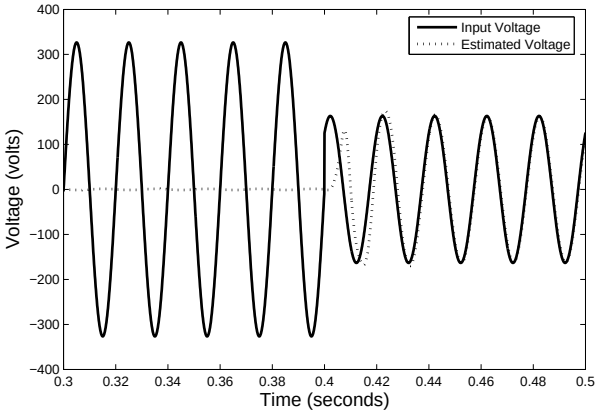

(a) Input and estimated signal.

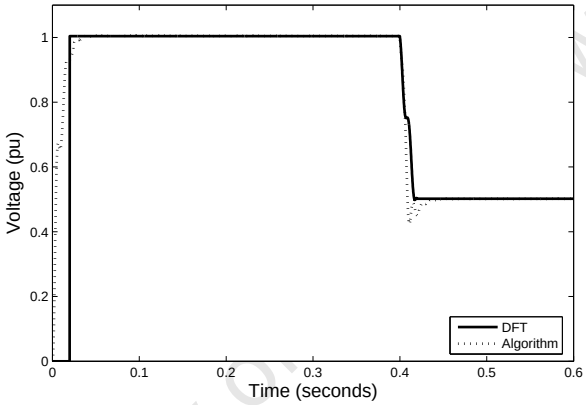

(b) Amplitude estimation comparing the DFT and the proposed method.

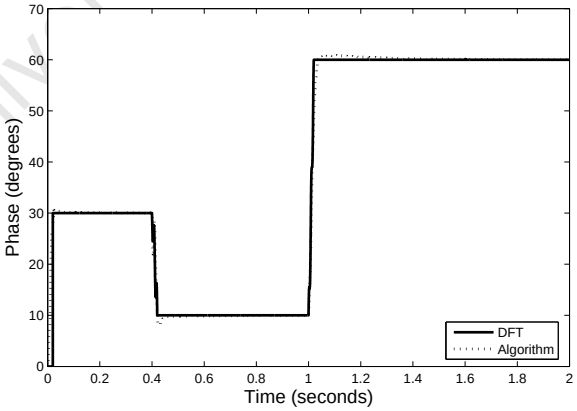

(c) Tracked phase comparing the DFT and the proposed method.

Figure 4-11: Performance for a step change in phase and amplitude.

This is stepped to 10° and from 0.4 to 1 second. During this period, the amplitude is stepped by -0.4 pu. From 1 to 2 seconds, the phase is stepped to 60° and the amplitude is returned to the nominal voltage. The maximum phase steady state error is 0.2% from both the algorithm and DFT.

4.3.2 Estimating Simultaneous Step and Ramp Changes In Phase

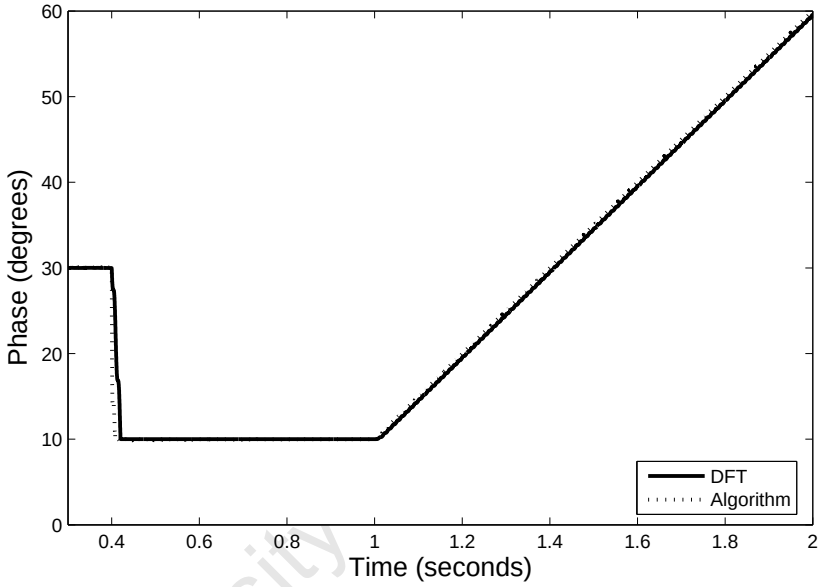

Figure 4-12: Estimating a simultaneous step and ramp in phase with the DFT and the proposed method.

In this test, the algorithm is compared to the DFT for a ramp in phase. The input signal is stepped from 30° to 10° from 0.4 to 1 second. The phase is then ramped at a rate of 50° per second from 1 to 2 seconds. The steady state error from both the algorithm and the DFT is within 0.3%. The algorithm is able to respond by 15ms faster to the new phase value as compared to the DFT. This is shown in Figure 4-12. A close up view is shown in Figure 4-13.

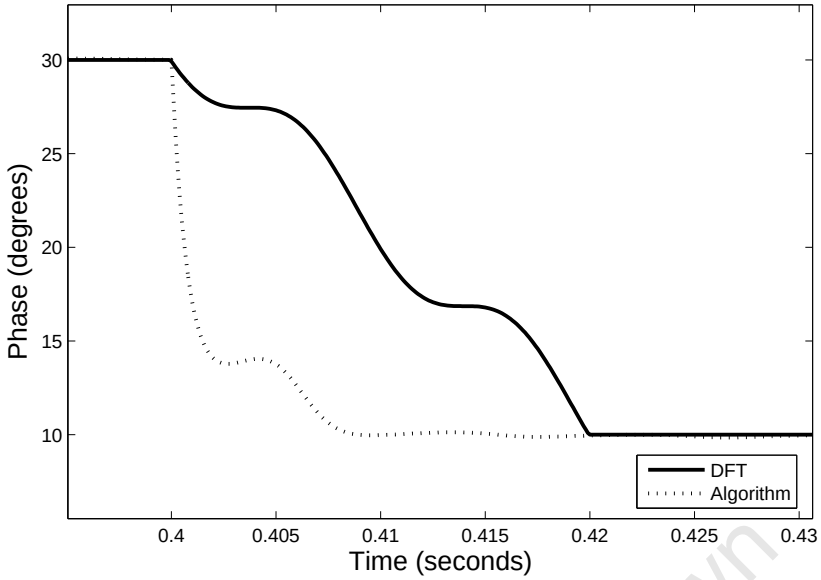

Figure 4-13: Close up showing the responses of the DFT and the nonlinear algorithm to a 50° per second ramp in phase.

4.3.3 Application to Reactive Compensation

Reactive power compensation is a frequent requirement in power systems. The instantaneous reactive power theory based on the transformation technique is a widely accepted approach for high performance compensators. This section shows that the proposed algorithm can be used to extract the reactive current component to be used as a reference signal for a compensator. Figure 4-14 shows a simple system in which a voltage source of 400 V L-L supplies a load of (5000+j2000) VA. From $t = 0.5$ to 1 second, the power requirements are stepped to (2500+j1600) VA. The amplitude is modulated from $t = 1.5$ to 2 seconds with a modulating frequency of 3 Hz and amplitude of 0.2 pu. Based on this loading, the power factor angle θ is 21.8°. The calculated theoretical active and reactive current components are 7.21 and 0.56 amps respectively. The challenge is to determine the apparent, active and reactive components of power in real-time for compensation. The amplitudes of the voltage and current, ϕ_v, ϕ_i and θ, are attainable from the algorithm in real-time. Figures 4-15(a) and 4-15(b) show the response of the filter for the step change in load and modulated amplitude.

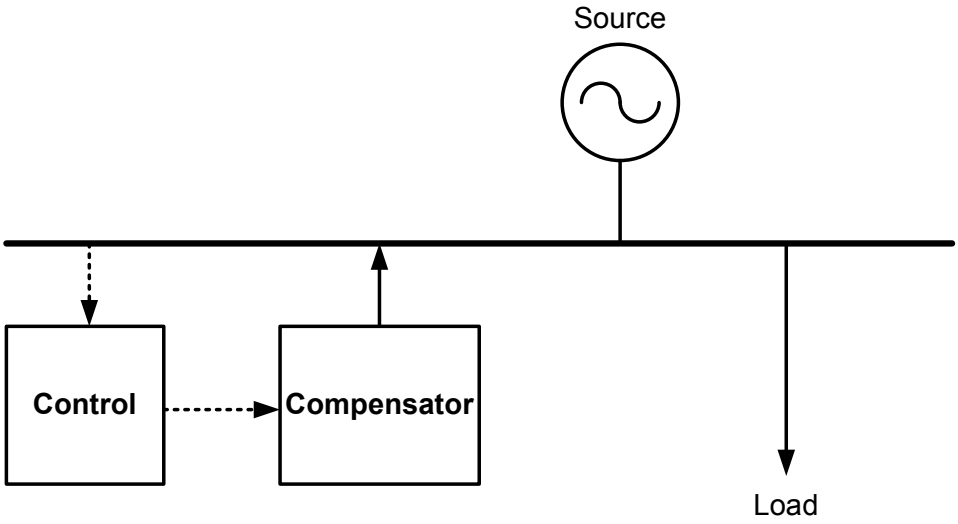

Figure 4-14: System configuration of compensator

The simulations show that the algorithm can be used as a signal to accurately determine the compensation parameters in real time. The advantage of using the algorithm is shown in Figure 4-16. There is a 15ms response time difference between the DFT and the algorithm.

4.4 Phase Angle Estimation of Three-Phase Systems

A trend in recent years has been the increased use of distributed generation. The method used for estimating the phase angle of three-phase systems must be accurate, fast and robust to system changes. This section deals with the application of the nonlinear algorithm for phase angle estimation of three-phase systems. A comparison is done against the DFT, $dq0$ and the three-phase PLL. The $dq0$ and PLL are commonly used methods and were therefore selected for the study.

4.4.1 $dq0$ Method

The direct axis, quadratic axis and zero sequence quantities components are obtained from the abc to $dq0$ transformation. This transform computes the $dq0$ components in

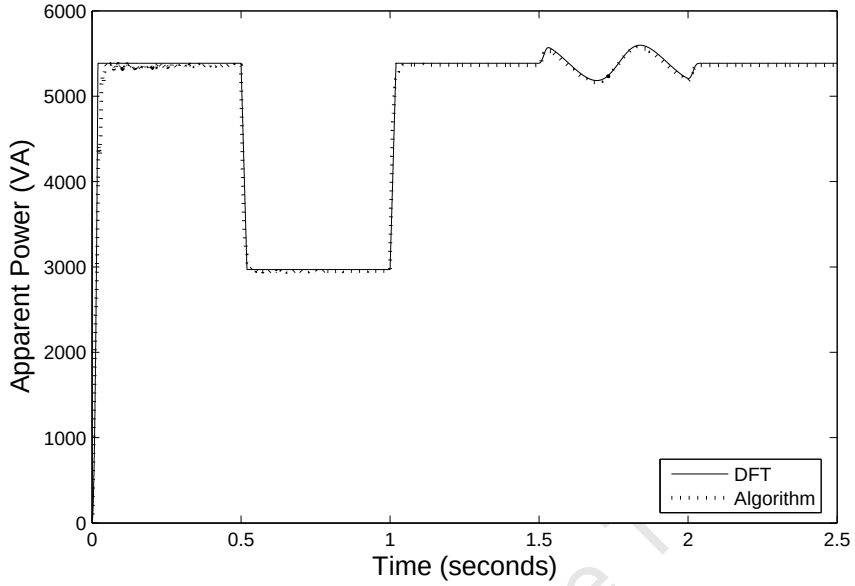

(a) Apparent power estimation.

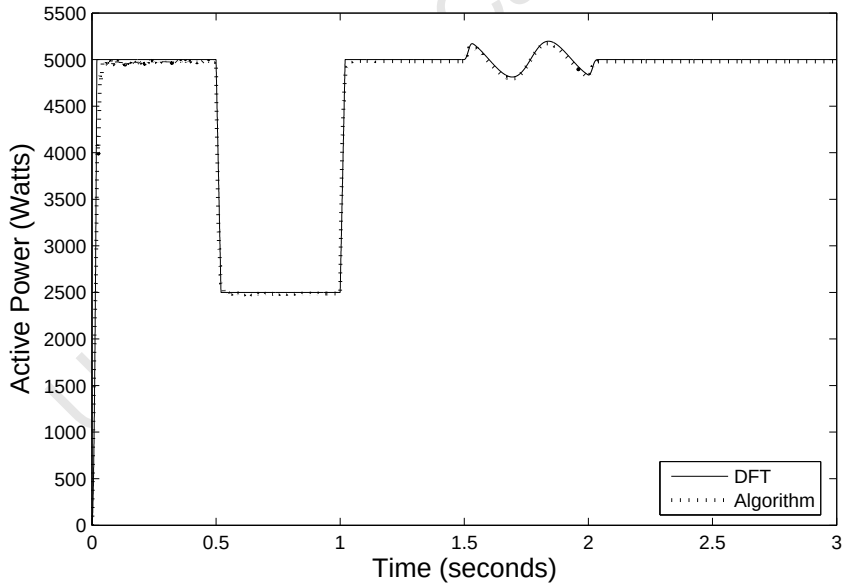

(b) Active power estimation.

Figure 4-15: Performance for a step change in load and a modulated amplitude.

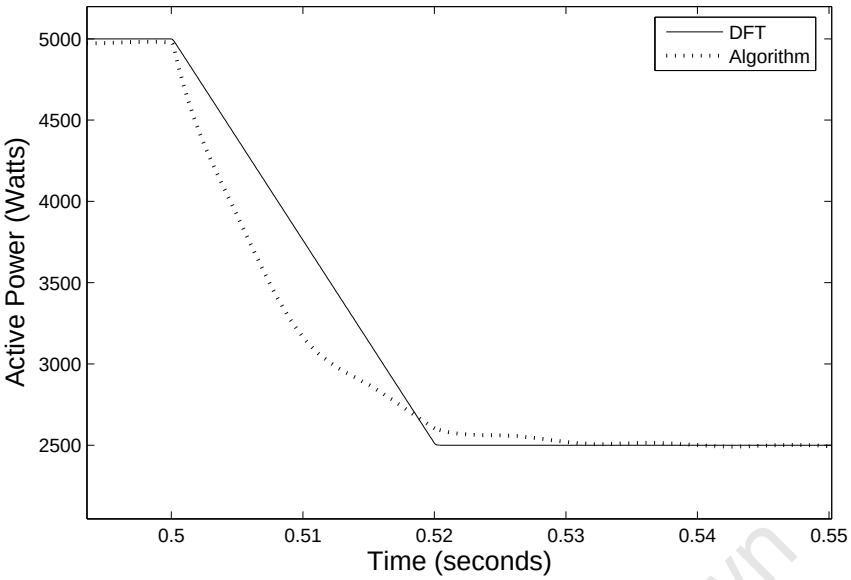

Figure 4-16: Response time comparison for the compensator.

a two-axis rotating reference frame for a three-phase sinusoidal signal, as

$$\begin{bmatrix} V_d \\ V_q \\ V_0 \end{bmatrix} = \begin{bmatrix} \frac{2}{3} \\ \frac{2}{3} \\ \frac{1}{3} \end{bmatrix} \begin{bmatrix} \sin(\omega t) & \sin\left(\omega t - {}^{2\pi}/_{3}\right) & \sin\left(\omega t + {}^{2\pi}/_{3}\right) \\ \cos(\omega t) & \cos\left(\omega t - {}^{2\pi}/_{3}\right) & \cos\left(\omega t + {}^{2\pi}/_{3}\right) \\ 1 & 1 & 1 \end{bmatrix} \begin{bmatrix} v_a \\ v_b \\ v_c \end{bmatrix} \tag{4.5}$$

where ω is the speed of rotation in rad/s of the rotating frame. This transformation is commonly used in three-phase electric machine models, where it is known as a Park transformation. It allows you to eliminate time-varying inductances by referring the stator and rotor quantities to a fixed or rotating reference frame. In the case of a synchronous machine, the stator quantities are referred to the rotor. I_d and I_q represent the two DC currents flowing in the two equivalent rotor windings (d directly on the same axis as the field winding, and q winding on the quadratic axis), producing the same flux as the stator I_a, I_b, and I_c currents. This can be used as part of a control system to measure the positive-sequence component V_1 of a set of three-phase voltages or currents. The V_d and V_q (or I_d and I_q) then represent the rectangular coordinates of the positive-sequence component. From the d and q components, the angle of V_1

can be obtained by

$$\hat{\theta} = \arctan\left(\frac{v_q}{v_d}\right) \tag{4.6}$$

This method of phase angle estimation has a very fast response with little delay. However it is sensitive to harmonics and unbalance.

4.4.2 Three-Phase PLL

The three-phase PLL is widely used for phase angle estimation. Operation of the three-phase PLL is based on the fact that the d-axis component of a balanced set of components is equal to zero. The d-axis component is determined by the phase angle. A control loop is designed to regulate the d-axis component to zero and provide an accurate estimate of the phase angle [45]. If properly designed, the PLL has good noise tracking ability. However, the PLL has problems working under conditions of rapid frequency change and voltage unbalance. A three-phase PLL is shown in Figure 4-17.

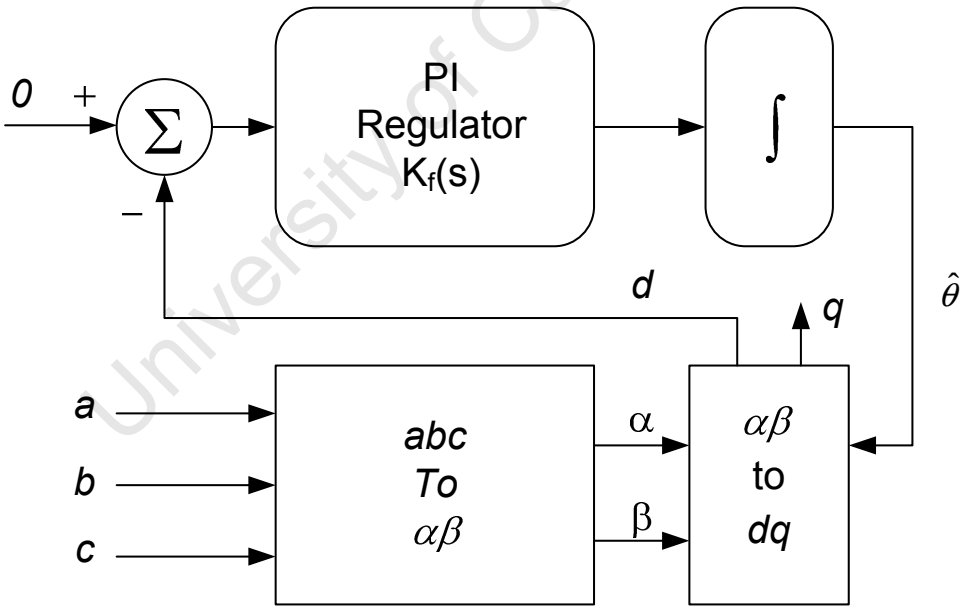

Figure 4-17: Block diagram of three-phase PLL [45].

4.4.3 Effect of Unbalance

True voltage unbalance is given by

$$\%V_{UB} = 100 \times \frac{V_{-ve}}{V_{+ve}} \tag{4.7}$$

where V_{+ve} and V_{-ve} represent the positive and negative sequence of the supply voltage respectively. The maximum unbalance permissible on distribution and transmission networks for voltage unbalance is 2%. However, current unbalance can be many times that of voltage unbalance.

Test System

A test system is used to evaluate the performance of the DFT, $dq0$, three-phase PLL and the nonlinear algorithm for a step in amplitude and unbalanced conditions. A three-phase voltage source is used to generate a 1 pu, 15° positive sequence voltage. At $t = 0.1$ s an unbalance is introduced by adding a 0.25 pu negative sequence component with a phase of $-25°$. The magnitude and phase of the positive-sequence component is evaluated in three different ways namely i) Sequence calculation of phasors using the DFT analysis; ii) *abc* to $dq0$ transformation and iii) three-phase PLL. The magnitude and phase of the positive sequence from the d and q components is then determined using (4.6). The results show the effect of unbalance on the extraction of the positive sequence voltage and phase angle using the different methods. This is then compared against the proposed method.

Test Results

Figure 4-18(a) shows the input signal. The phase angle is tracked using the $dq0$ method. This is shown in Figure 4-18(b). A comparison of the three-phase PLL, Fourier and proposed method is shown in Figure 4-19. A summary of the results is given in Table 4.3. The results indicate that the proposed method is able to offer improved accuracy of amplitude and phase angle under conditions of unbalance. The phase error obtained using the $dq0$ is unacceptable.

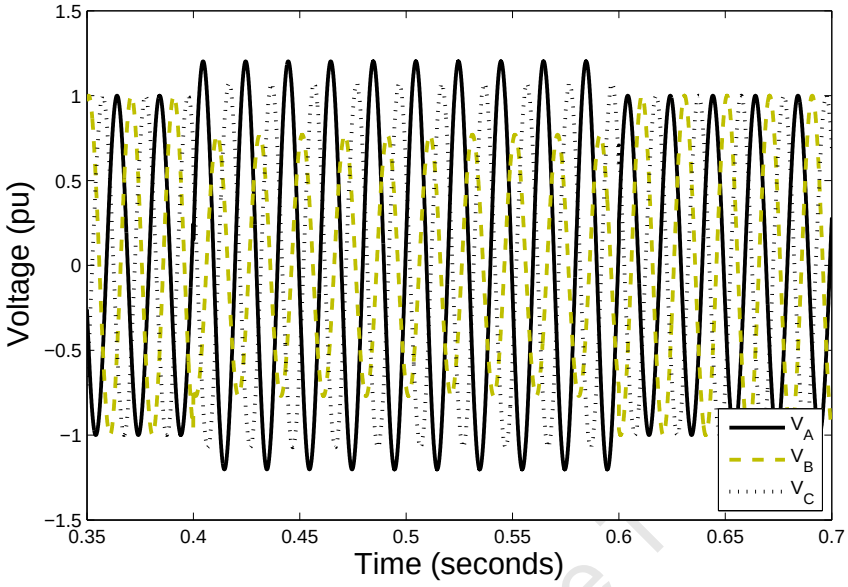

(a) Input signal.

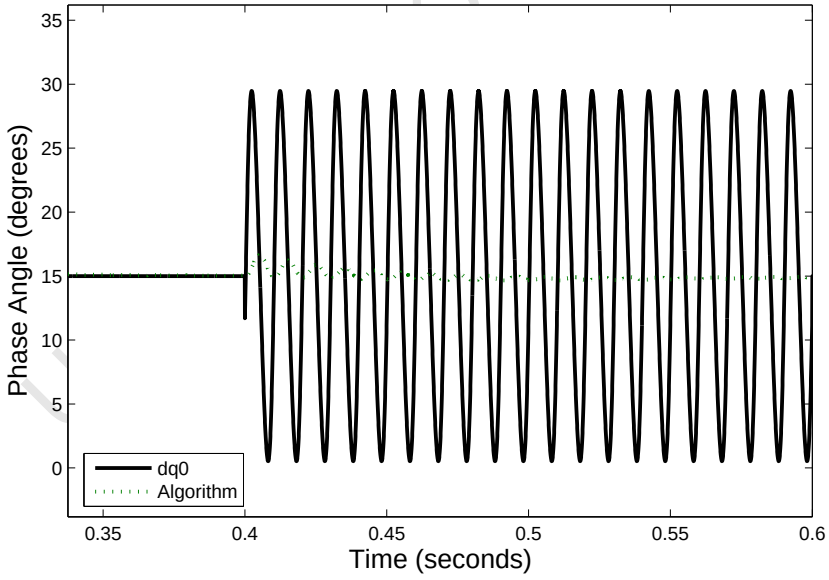

(b) Phase angle estimation the $dq0$ method.

Figure 4-18: Effect of unbalance on determining the positive sequence phase angle.

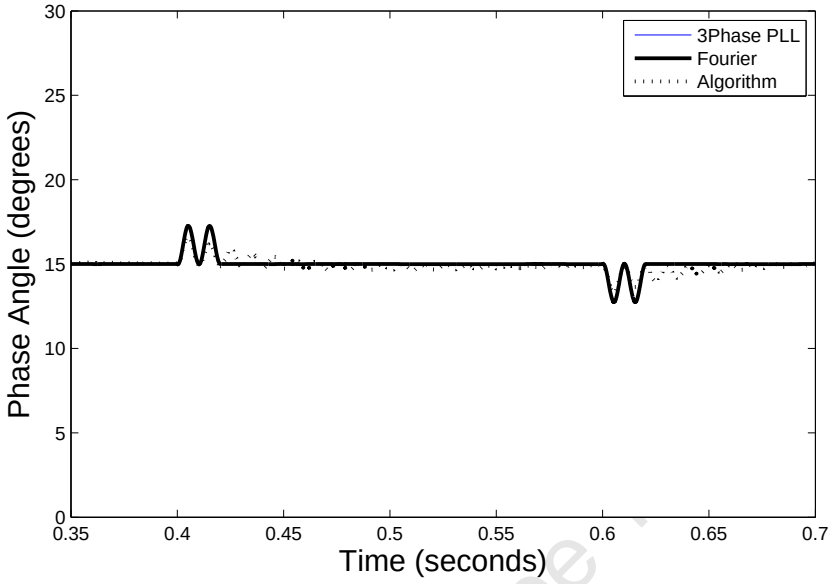

Figure 4-19: Effect of unbalance on determining the positive sequence phase angle.

Table 4.3: Summary of results.

	Magnitude Error (%)	Angle Error (%)
$dq0$	25	96.5
Fourier	2.5	15
Three-Phase PLL	2.5	15
Nonlinear Algorithm	2.3	11

4.5 Summary of Results

With reference to the discussions presented throughout this chapter, the main features of the proposed method can be summarised as follows:

- The nonlinear filter is able to estimate step changes of up to 20 Hz in frequency to within 0.02% accuracy and within a single cycle. A comparison was done against the PLL. The PLL can only accommodate step changes of up to 5 Hz. With this method, there is an error of 0.02% and a delay of up to six cycles.

- In the presence of harmonics and noise (measured up to 22% THD and 7 db noise), the nonlinear filter is able to estimate the amplitude to within 0.3% and the frequency to within 0.1%.

- The nonlinear filter is able to accurately track a modulated frequency of up to 3 Hz to within 0.01% steady state error and 10 ms delay. This is an improvement of 100 ms over the PLL.

- The DFT and the nonlinear filter are both able to estimate step changes in phase to within 2%. However, there is a 15 ms improvement by the nonlinear filter in response time over the DFT.

- For three-phase systems, commonly used methods such as the DFT and $dq0$ suffer in the presence of unbalance. Errors of up to 100% were recorded with the $dq0$ method. The three-phase PLL compares favourably to the nonlinear filter in terms of performance. Errors of 15% and 11% were recorded by the PLL and nonlinear filter respectively.

4.6 Concluding Remarks

This chapter has proposed an online phase and frequency estimation method for single and three-phase power system applications. Design, analysis and computational aspects of the proposed technique have been described. The proposed technique is

found to be more accurate when compared to the DFT in amplitude estimation under frequency deviations. The PLL is unable to effectively track frequency variations of 3 Hz modulation. The proposed method is able to respond to changes in phase to within 15 ms as compared to the DFT, which is unable to do so. This provides an improved reference signal for reactive power compensation. Computer simulations were carried out to thoroughly test the performance of the proposed system. The effects of noise, harmonics, amplitude step/ramp and frequency deviations were studied. Results confirm that the proposed system offers improved performance when compared to conventional methods.

Chapter 5

Real-Time Symmetrical Component Estimation

Power systems worldwide are generally three-phase. The topic of symmetrical components is standard in most text books on electric power systems. A system that is considered balanced has three voltage and current signals that have equal magnitudes and 120° phase-displacements. When these conditions are not met, the system is unbalanced. The theory of symmetrical components indicates that an unbalanced set of signals can be decomposed into three sets of signals as shown in Figure 5-1 [47]. The three sets are 1) a balanced set with 120° phase-shifts called the positive-sequence, 2) a balanced set with −120° phase-shifts called the negative-sequence, and 3) a third set with 0° phase-shifts called the zero-sequence. Assuming that the power system operates at a fixed and known frequency, each sequence component is uniquely determined by its magnitude and its phase-angle. Thus, a total of six parameters for the three sequence components are used to characterise them [48]. Symmetrical components find applications in a variety of power system problems such as protection, fault analysis and classification, reactive power compensation, unbalance mitigation, system modelling and identification. Many papers describe the application of symmetrical components [49], [50], [51], [52], [53]. Fortescue introduced the theory of symmetrical components for complex phasors [47]. It is formulated in terms of a linear matrix transformation involving the unity complex phasor $a = e^{j\frac{2\pi}{3}}$. The con-

cept of symmetrical components was then extended to time-domain signals for use in machine analysis [54].

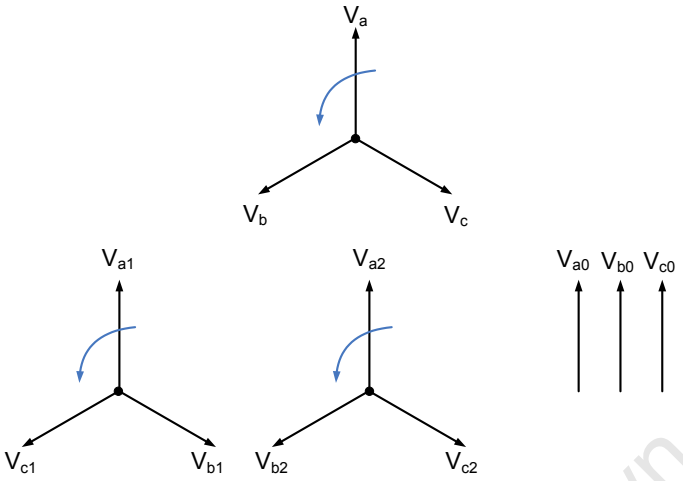

Figure 5-1: Decomposition of waveform into symmetrical components.

Several methods of estimating symmetrical components have been proposed [55], [56], [57], [58], [59]. The different approaches include stochastic estimation theory, Kalman filters, weighted least-squares estimation, and recently the time-domain approach of [48]. In [48], there has been much theory presented with little focus on the influence of frequency deviations and harmonics. Further, the results presented are from simulations and not practical application. This chapter presents a method of decomposing a three-phase set of signals into its instantaneous positive-sequence, negative-sequence and zero-sequence components. The proposed method is based on converting the input signals into phasors. This is done by an estimation of the magnitude, phase-angle and frequency of an input signal. From this, the sequence components are computed in the time-domain. An overview of the proposed approach is shown in Figure 5-2. As the magnitudes and phase-angles are estimated and made available online, the steady-state and dynamic phasors associated with the symmetrical components are also made available by the proposed method. It can be employed as an integral part of the control system of distributed generation systems and renewable energy resources. This is due to the presence of frequency deviations and high distortions commonly encountered in systems in which conventional strategies fail to cope.

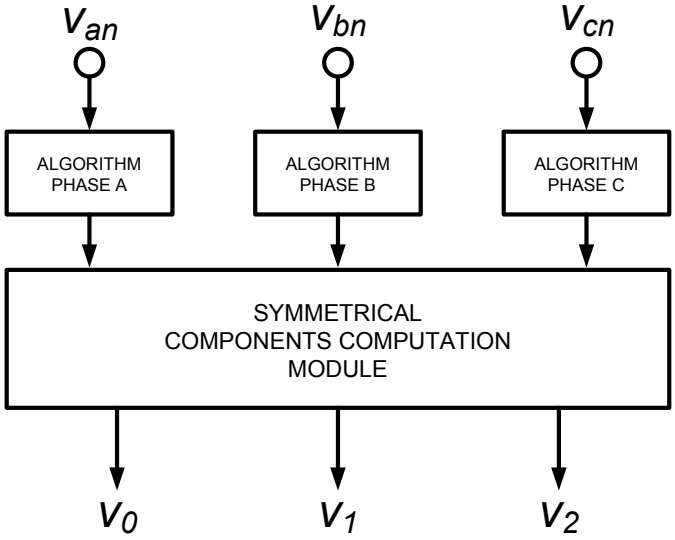

Figure 5-2: Overview of the proposed approach.

5.1 Mathematical Model of Proposed System

Consider the three-phase set of asymmetrical signals

$$U = \begin{bmatrix} u_a \\ u_b \\ u_c \end{bmatrix} = \begin{bmatrix} U_a(t)\sqrt{2}\cos(\omega t + \alpha_a(t)) \\ U_b(t)\sqrt{2}\cos(\omega t + \alpha_b(t)) \\ U_c(t)\sqrt{2}\cos(\omega t + \alpha_c(t)) \end{bmatrix} \tag{5.1}$$

where u denotes the instantaneous magnitude, $U(t)$ the time varying peak amplitude of the waveform, and $\alpha(t)$ the time varying phase of the waveform. (5.1) can be written as the sum of two complex conjugated terms:

$$U = \frac{1}{\sqrt{2}} \times \begin{bmatrix} \underline{U}_a e^{j\omega t} + \underline{U}_a^* e^{-j\omega t} \\ \underline{U}_b e^{j\omega t} + \underline{U}_b^* e^{-j\omega t} \\ \underline{U}_c e^{j\omega t} + \underline{U}_c^* e^{-j\omega t} \end{bmatrix} \tag{5.2}$$

with

$$\begin{bmatrix} \underline{U}_a \\ \underline{U}_b \\ \underline{U}_c \end{bmatrix} = \begin{bmatrix} U_a(t)e^{j\alpha_a(t)} \\ U_b(t)e^{j\alpha_b(t)} \\ U_c(t)e^{j\alpha_c(t)} \end{bmatrix} \tag{5.3}$$

$\underline{U}$ denotes the phasor of u and is determined by estimating the amplitude $U(t)$ and phase $\alpha(t)$ in (5.3). The proposed system for estimating these parameters is shown in Figures 5-3 and 5-4.

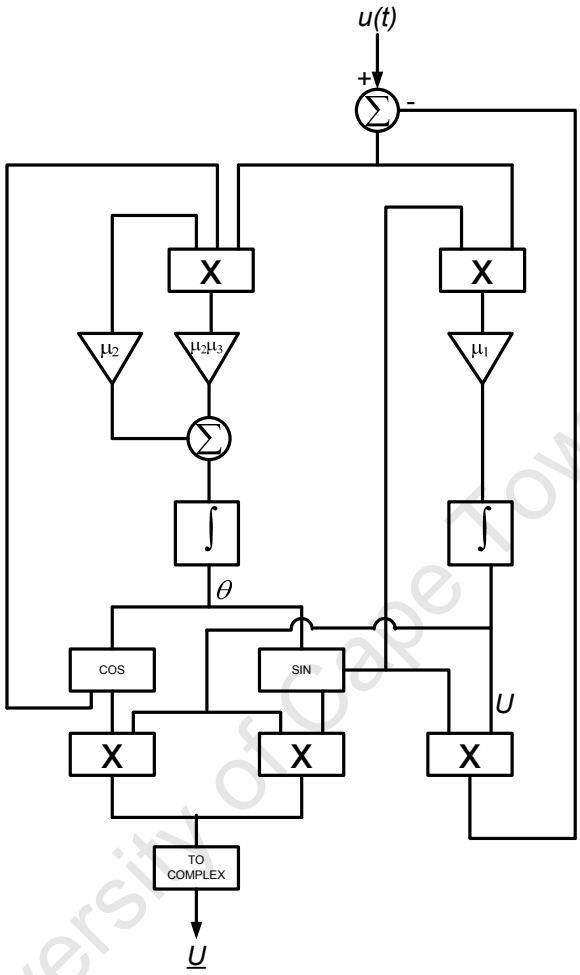

Figure 5-3: Conversion of time domain input signal into a phasor.

The objective of the system shown in Figure 5-3 is to convert the time domain input signal into a phasor. The phasors are then converted into time domain symmetrical components as shown in Figure 5-4. The symmetrical component transformation matrix is

$$S = \begin{bmatrix} 1 & 1 & 1 \\ 1 & a^1 & a^2 \\ 1 & a^2 & a^1 \end{bmatrix} \quad where\, a = \exp\left[j\frac{2\pi}{3}\right] \tag{5.4}$$

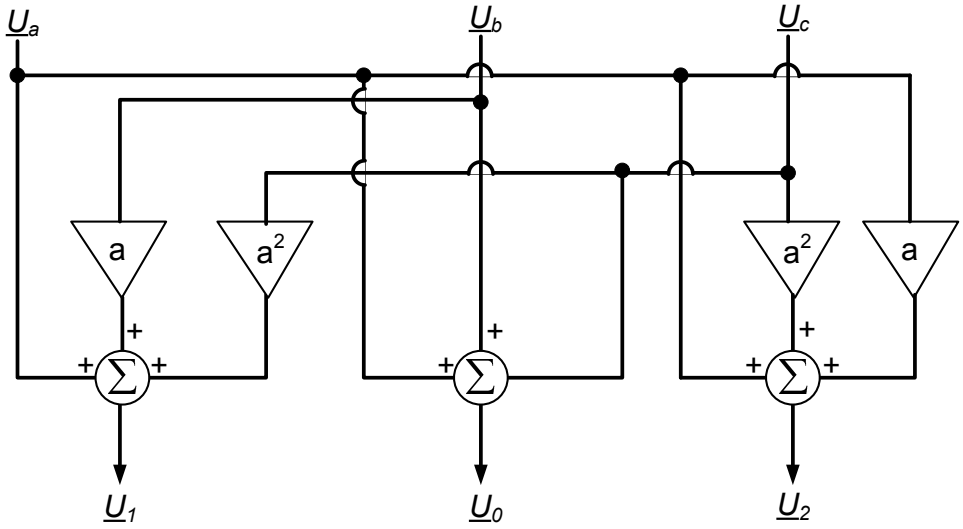

Figure 5-4: Conversion of phasor components to symmetrical components.

Transformation into the symmetrical components time domain $\mathbf{U'}=S^{-1}\mathbf{U}$ yields [55]

$$U' = \begin{bmatrix} u^0 \\ u^1 \\ u^2 \end{bmatrix} = \frac{1}{\sqrt{2}} \times \begin{bmatrix} \underline{U}_0 e^{j\omega t} + \underline{U}_0^* e^{-j\omega t} \\ \underline{U}_1 e^{j\omega t} + \underline{U}_1^* e^{-j\omega t} \\ \underline{U}_2 e^{j\omega t} + \underline{U}_2^* e^{-j\omega t} \end{bmatrix} \tag{5.5}$$

5.2 Performance

This section investigates the performance of the proposed system by means of computer simulations. The following cases are studied:

- Case 1: Symmetrical component estimation for step changes in amplitude.
- Case 2: Symmetrical component estimation for step changes in phase.
- Case 3: Symmetrical component estimation in signals with noise and harmonics.

For each case, the sequence components are theoretically calculated. This is used as a benchmark to compare the performance of the DFT and the algorithm. Performance comparisons are made in terms of speed of response and steady state accuracy.

5.2.1 Case 1: Effects of a Change in Amplitude

Step in Amplitude

Figure 5-5 shows the three phase input voltages. The nominal system voltage is 230 V (325 V peak). The voltage in phase b is reduced by 0.4 pu from time $t = 0.4$ to 0.8 seconds. This is typical of a sag in industry. The input voltages are: $V_a = 1\angle 0°$, $V_b = 0.6\angle 0°$ and $V_c = 1\angle 120°$. This can be converted to its respective symmetrical components using:

$$V_{012} = S^{-1}V_{abc} \tag{5.6}$$

The theoretically calculated sequence components (in terms of the L-N peak) from (5.6) are: $V_0 = 43.3$ V, $V_1 = 282$ V and $V_2 = 43.3$ V.

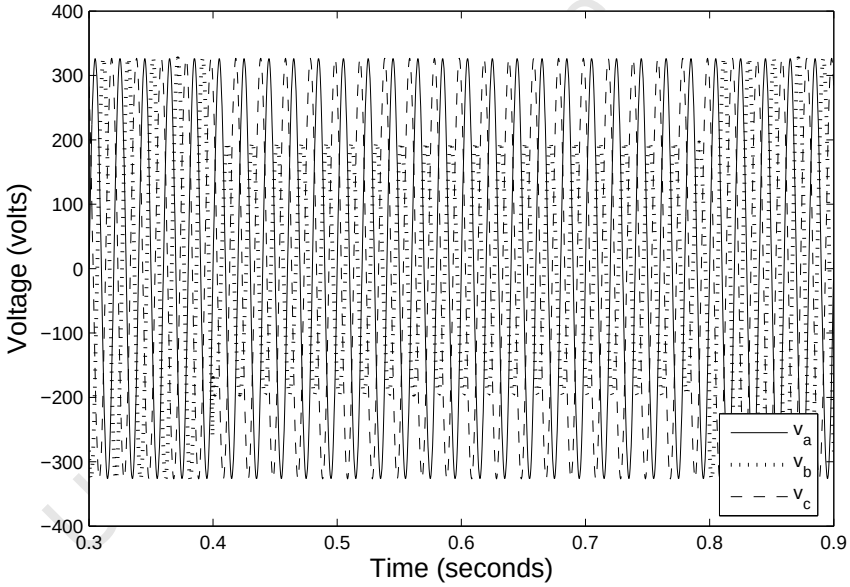

Figure 5-5: Input waveform.

Figures 5-6, 5-7 and 5-8 show a comparison of the response of the algorithm and the Fourier sequence analyser's to the step change in amplitude. From the figures, it is evident that the nonlinear algorithm responds much faster to a change in amplitude when compared to the Fourier method. The maximum response time difference based on a sampling time of 2.5 kHz and is 5 ms.

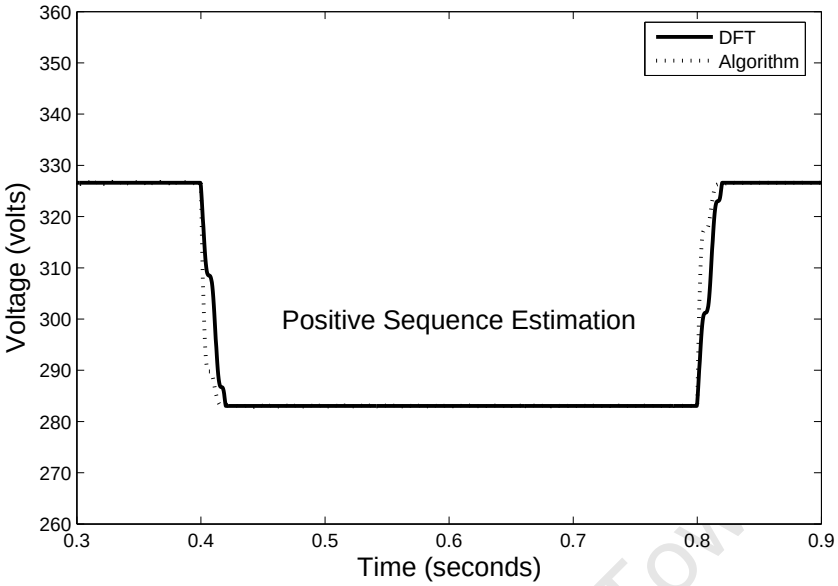

Figure 5-6: Positive sequence extraction for a step change in amplitude.

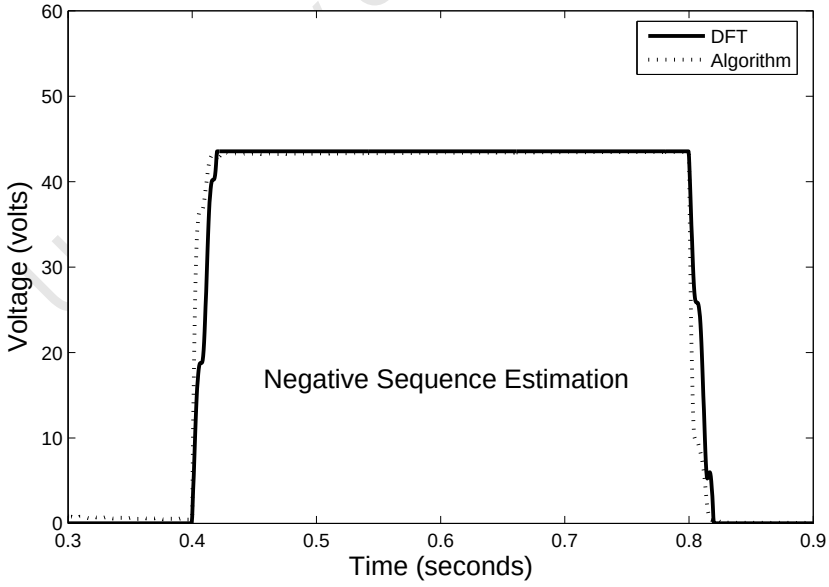

Figure 5-7: Negative sequence extraction for a step change in amplitude.

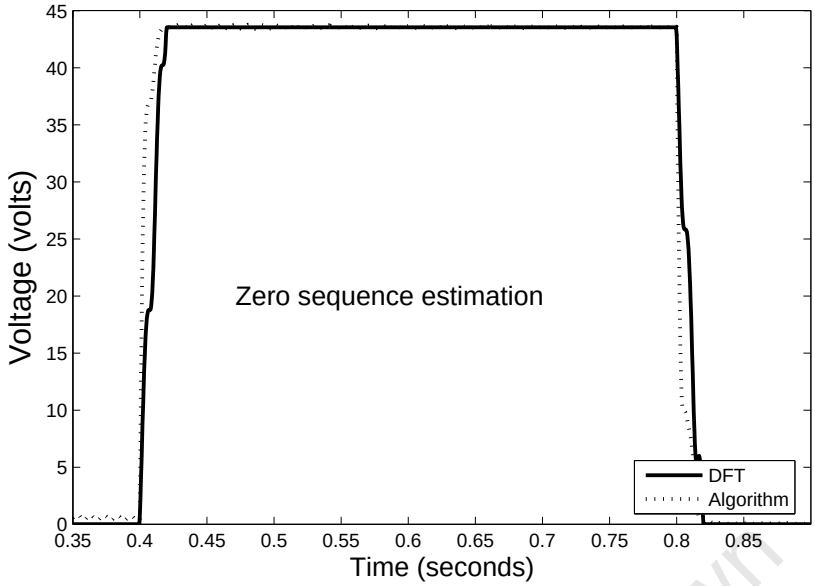

Figure 5-8: Zero sequence extraction for a step change in amplitude.

A faster response time can be achieved with a higher sampling frequency and further optimising the nonlinear algorithm's parameters. In practice, the proposed method should be able to respond to amplitudes of varying magnitude. The maximum steady-state error of the DFT and the proposed method are both 0.35%.

Table 5.1: Summary of results showing the effects of a step change in phase.

Effects of a Change in Amplitude			
Phase B Step in Amplitude	% Error		Response Time Difference (ms)
	DFT	Nonlinear Filter	
0.2	0.35	0.35	5
0.4	0.36	0.36	5
0.6	0.36	0.36	5
0.8	0.38	0.38	5

Table 5.1 shows a summary of the results for various step changes in amplitude. The accuracy compares closely to that of the DFT. A response time difference of approximately 5 ms was measured. Figure 5-9 shows the ability of the algorithm to track changes in varying amplitudes of $\pm$ 0.2, $\pm$ 0.4 and $\pm$ 0.6 pu.

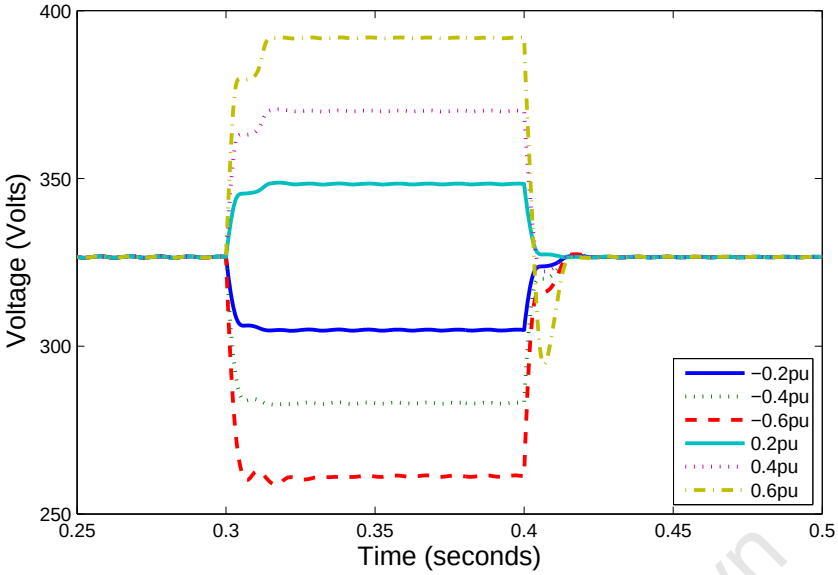

Figure 5-9: Effect of a step change in amplitude with the proposed method.

Ramp in Amplitude

The effect of a ramp in amplitude is shown in Figure 5-10. A ramp rate of 1 pu/sec is used. The figure shows a comparison between the response of the algorithm and DFT to a ramp in amplitude.

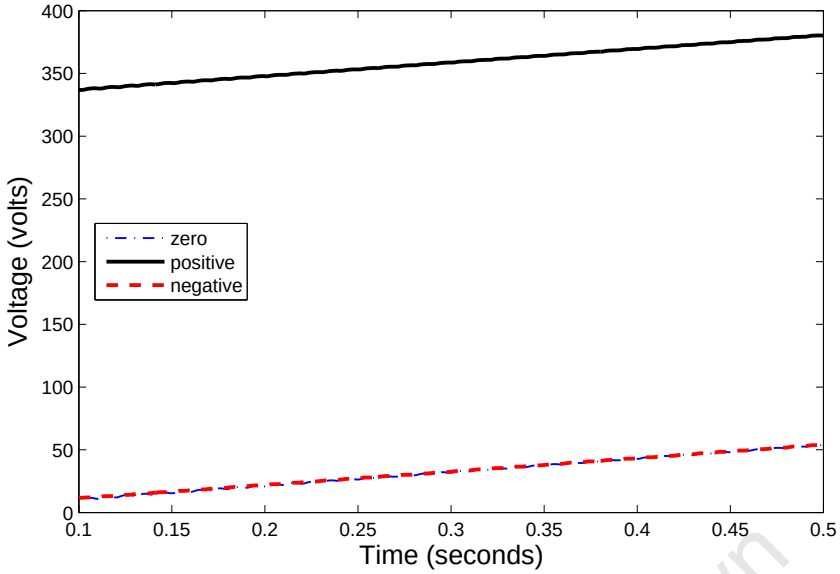

Figure 5-10: Estimating sequence component of a ramp in amplitude using the proposed method.

5.2.2 Case 2: Effects of a Change in Phase

This section studies the response of the nonlinear algorithm and DFT to phase changes.

Step in Phase

In this test, the phase angle of phase B is stepped by 30° from 0.4 to 0.8 seconds. The input voltages are $V_a = 325\angle 0°$ V, $V_a = 325\angle -90°$ V, $V_c = 325\angle 120°$ V. The theoretically calculated symmetrical components following the step change in phase are: $V_0 = 56.1\angle -15°$ V, $V_1 = 315\angle 9.9°$ V, and $V_2 = 56.1\angle -135°$ V. This is used to benchmark the steady state accuracy of the DFT and the proposed technique. Figures 5-11 to 5-13 show the response of both methods to a step change in phase. The results indicate that the steady state error from both methods is within 0.5%. The nonlinear filter is able to respond 10ms quicker to the change in phase as compared to the DFT.

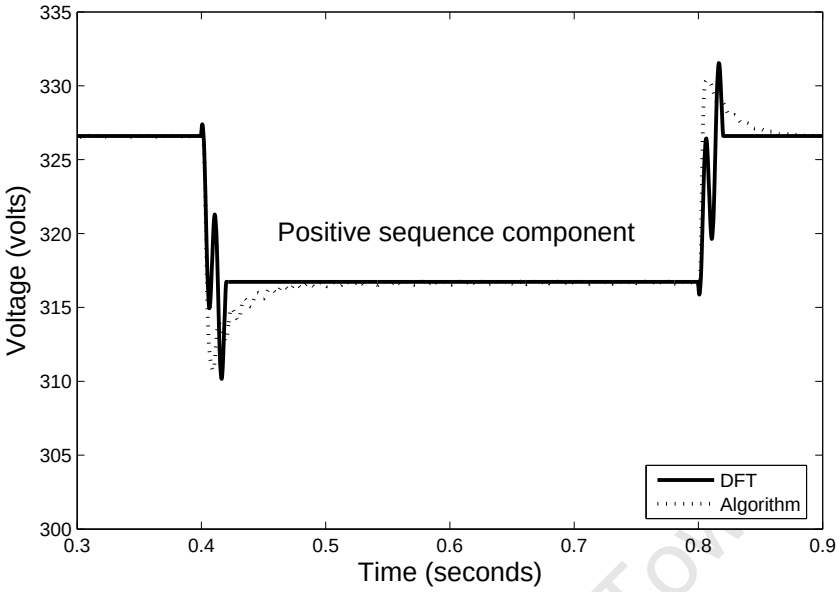

Figure 5-11: Positive sequence extraction for a step change in phase.

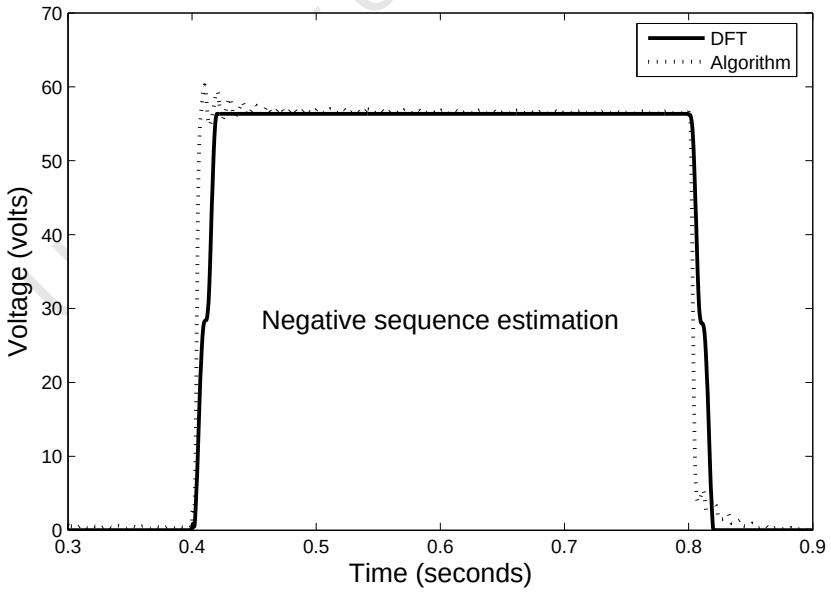

Figure 5-12: Negative sequence extraction for a step change in phase.

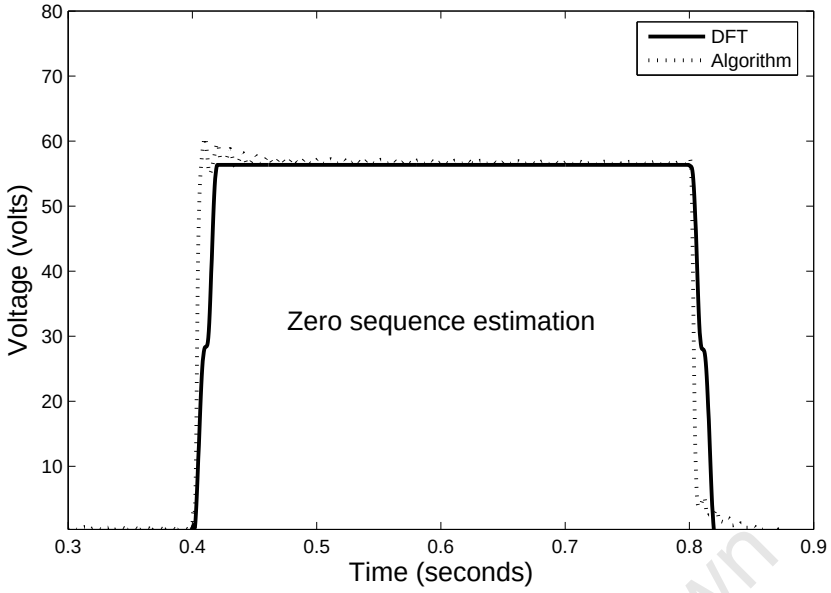

Figure 5-13: Zero sequence extraction for a step change in phase.

Ramp in Phase

The phase angle of v_a is ramped at 80°/s during time intervals of 0.4 to 0.8 seconds. Figure 5-14 to 5-16 show the response of the nonlinear algorithm to the ramp in phase. A 15 ms delay in response of the DFT to the ramp in phase can be observed.

Table 5.2: Summary of results showing the effects of a change in phase.

Effects of a Change in Phase			
Phase B Step in Phase	% Error		Response Time Difference (ms)
	DFT	Nonlinear Algorithm	
10	0.33	0.32	6
20	0.34	0.33	8
50	0.41	0.4	8
100	0.49	0.48	10

A summary of the results for step changes in phase is shown in Table 5.2. The results indicate similar accuracy between the two methods. The nonlinear filter demonstrates the advantages of improved response time.

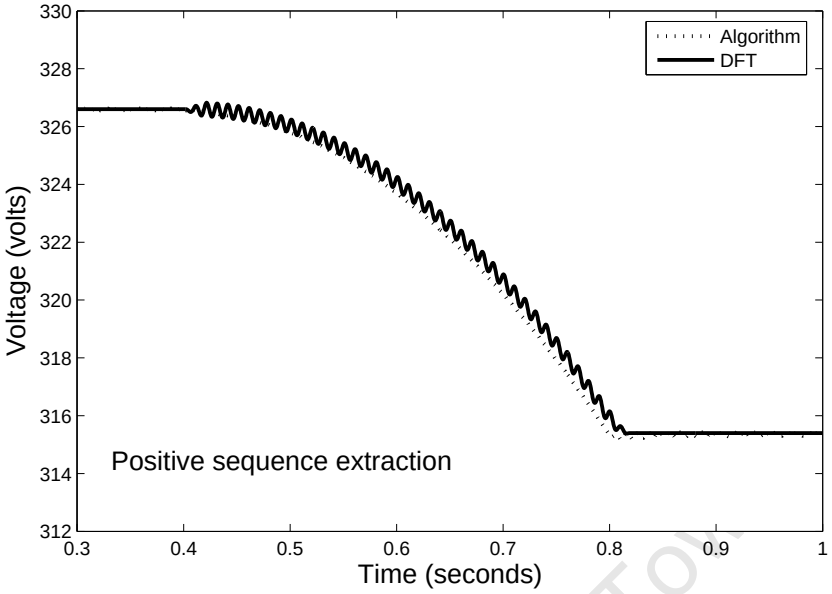

Figure 5-14: Positive sequence extraction for a 80°/s ramp in phase.

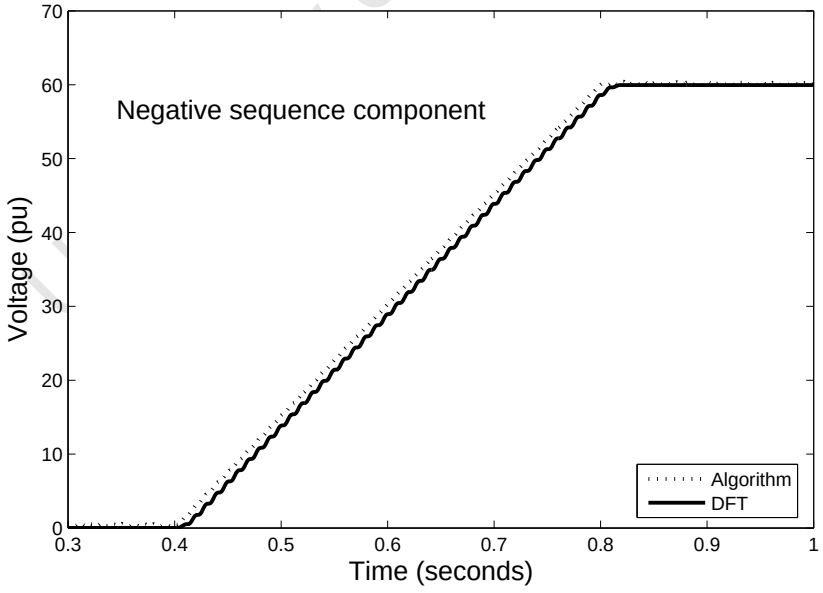

Figure 5-15: Negative sequence extraction for a 80°/s ramp in phase.

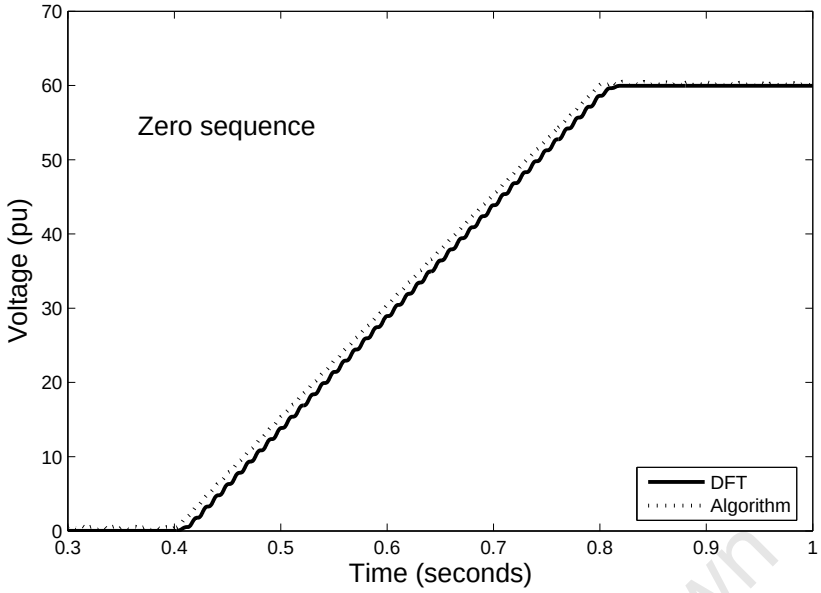

Figure 5-16: Zero sequence extraction for a 80°/s ramp in phase.

5.2.3 Case 3: Influence of Harmonics and Noise

Performance of both methods with regard to noise is demonstrated in this section. The peak amplitudes of the input signal that is shown in Figure 5-17 are 1.0 pu, 0.6 pu and 1.0 pu for phases a, b and c respectively. The input signal is corrupted with a Gaussian noise with zero mean and a variance of σ^2 for which $\sigma^2 = 0.01$ and SNR = 17 db. The DFT is capable of accurately extracting the fundamental component under harmonic conditions. When the frequency of the harmonic is not an exact integer multiple of the fundamental frequency (interharmonic), it poses a problem for the DFT. A 4.5 th interharmonic of 10% magnitude is added to the waveform. Figures 5-19 to 5-21 show a comparison between the response of the DFT and the proposed method in extracting the sequence components of the signal. Errors of 1.4%, 12.5% and 3% were obtained by using the DFT to extract the positive, negative and zero sequence voltages. The errors from the proposed method were 0.35%, 4% and 3.5%. Table 5.3 shows the influence of noise on the nonlinear filter and the DFT. The results show that noise does influence the accuracy. At higher noise levels, the nonlinear filter offers improved accuracy.

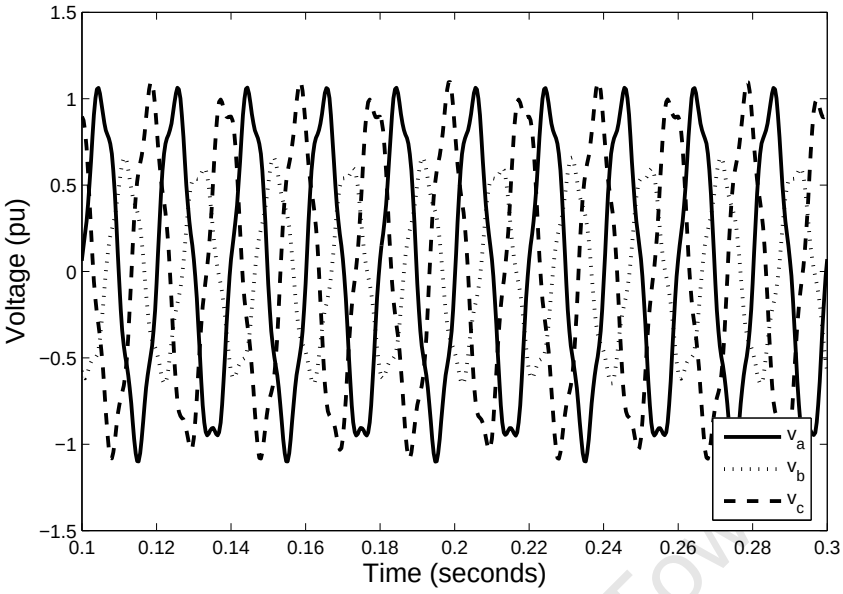

Figure 5-17: Input signal in the presence of noise and harmonics.

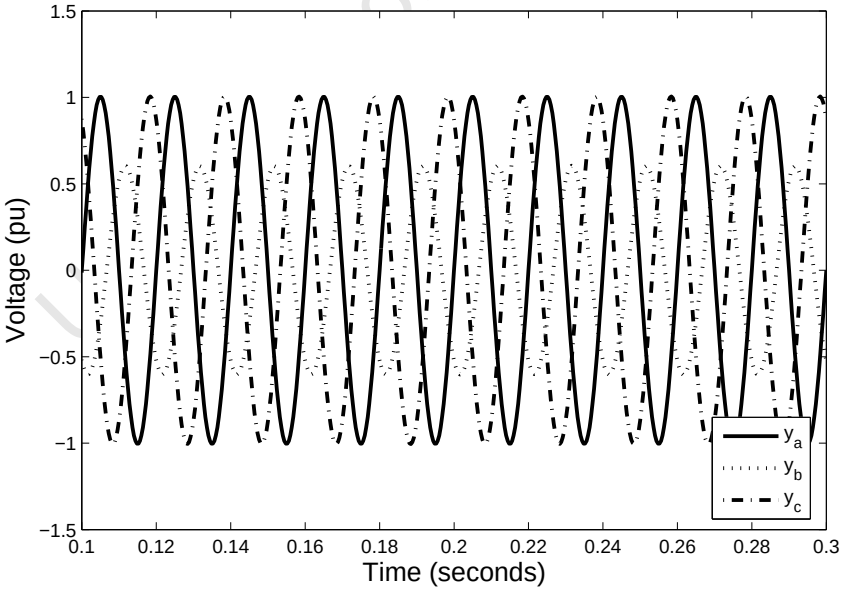

Figure 5-18: Extracted fundamental components in the presence of noise and harmonics.

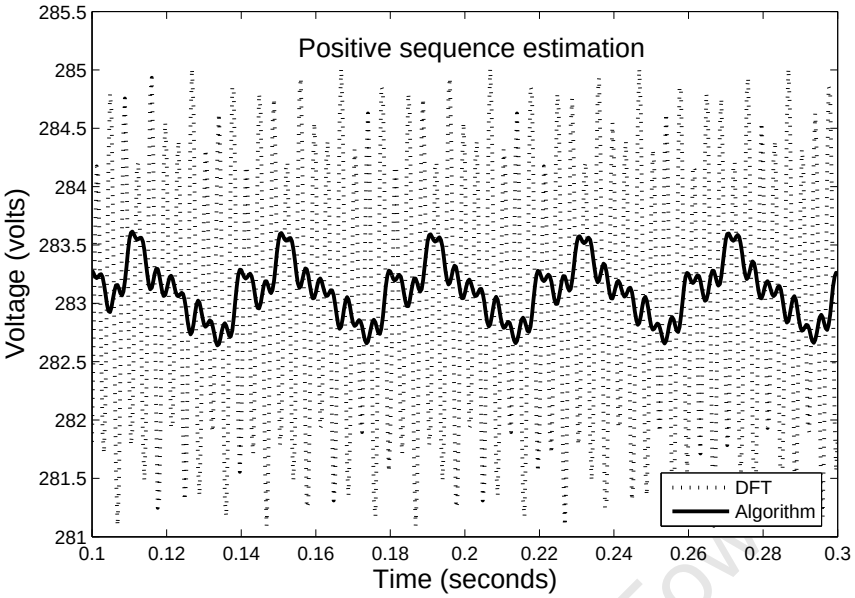

Figure 5-19: Extracted positive sequence component in the presence of noise and harmonics.

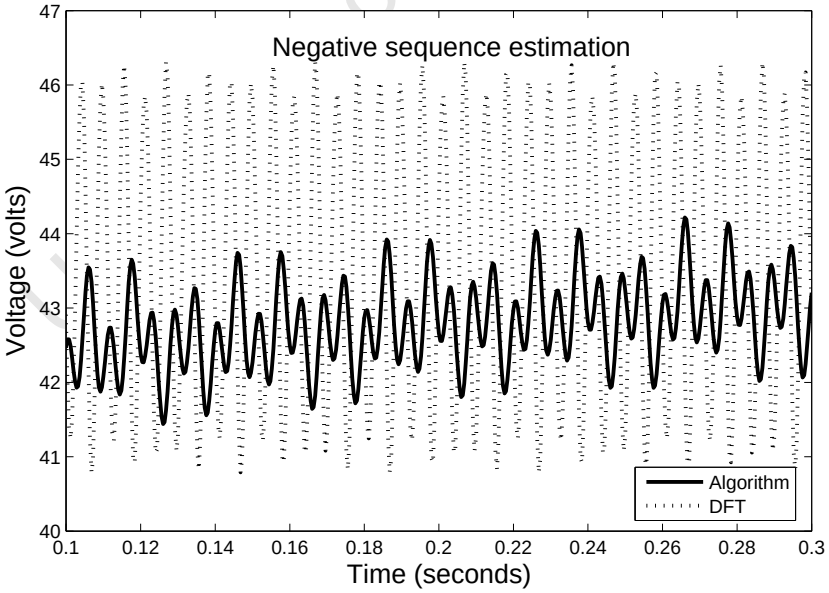

Figure 5-20: Extracted negative sequence component in the presence of noise and harmonics.

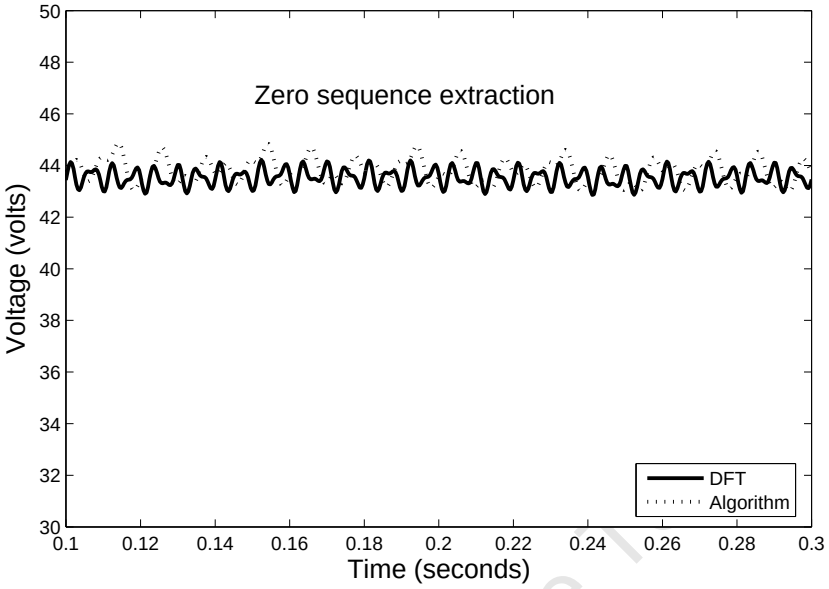

Figure 5-21: Extracted zero sequence component in the presence of noise and harmonics.

Table 5.3: Summary of results showing the influence of noise.

	% Accuracy	
σ^2	DFT	Nonlinear Filter
0.001	0.75	0.6
0.003	3.5	1.5
0.006	6.9	1.9
0.008	10.5	3.8
0.01	12.5	4

5.3 Application to Field Data

In this section, the performance of the proposed method is tested against field data. Two different cases of transmission system fault types are studied. The DFT is used to benchmark the algorithm for the application to field data.

5.3.1 Case 1

Figure 5-22 shows a one line diagram of the system. A fault locator indicated that

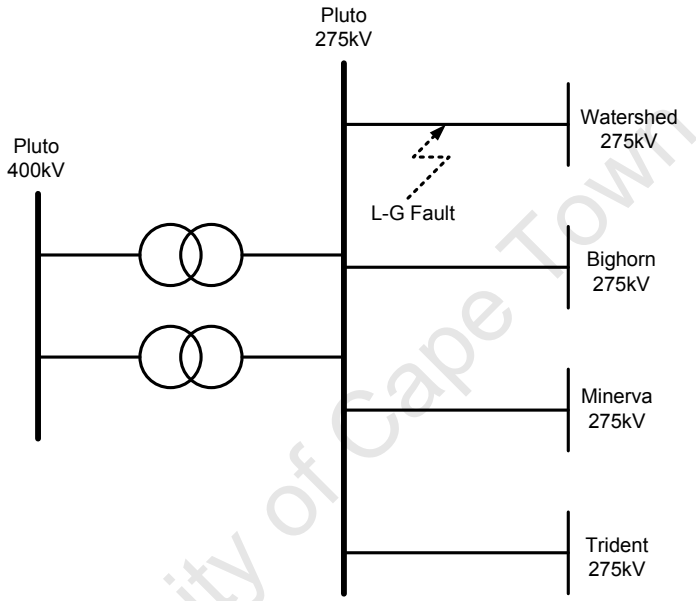

Figure 5-22: One-line diagram of the system under study.

a single line-ground fault occurred 12 kM within the Pluto-Watershed 275 kV feeder. Line inspection revealed that the source of the fault was a bird. Field services staff confirmed that no bird guards were installed on this particular feeder. The sampling frequency was 2.5 kHz i.e. 50 samples/cycle. The pre/post fault voltages on the three phases are shown in Figure 5-23. The fault occurred on phase B at approximately 0.4 seconds. The convergence parameters μ_1, μ_2 and μ_3 which were used for the test was 300, 3000 and 0.24 respectively. The results indicate that the algorithm is able to track the symmetrical components of the voltages to within 0.5% to that of the DFT. Response times from both methods were within 3 ms of each other. Once the fault was detected, the protection relays operated to clear the fault.

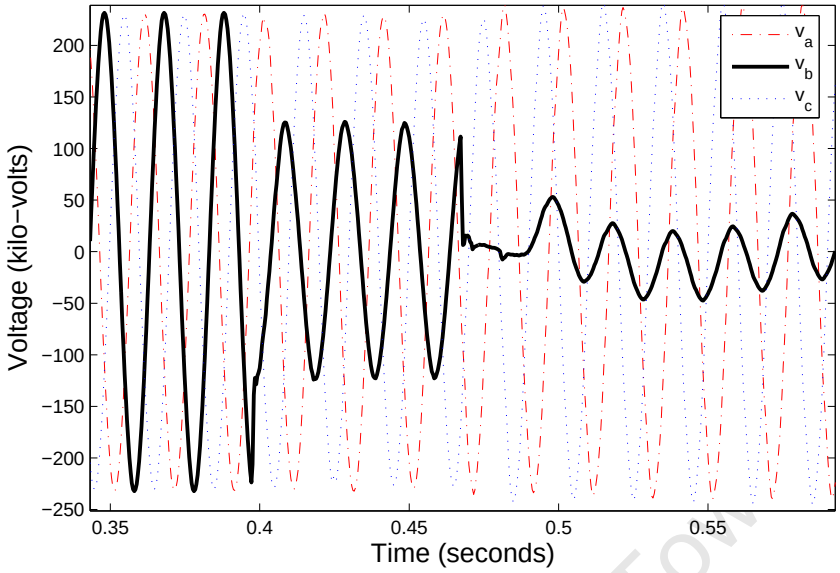

Figure 5-23: Three phase voltage at fault instant for Case 1.

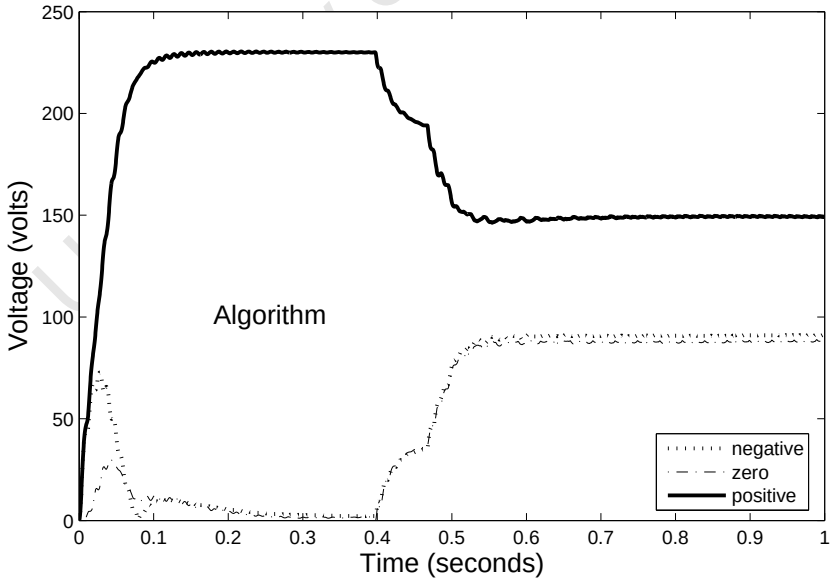

Figure 5-24: Tracking symmetrical components using the proposed technique.

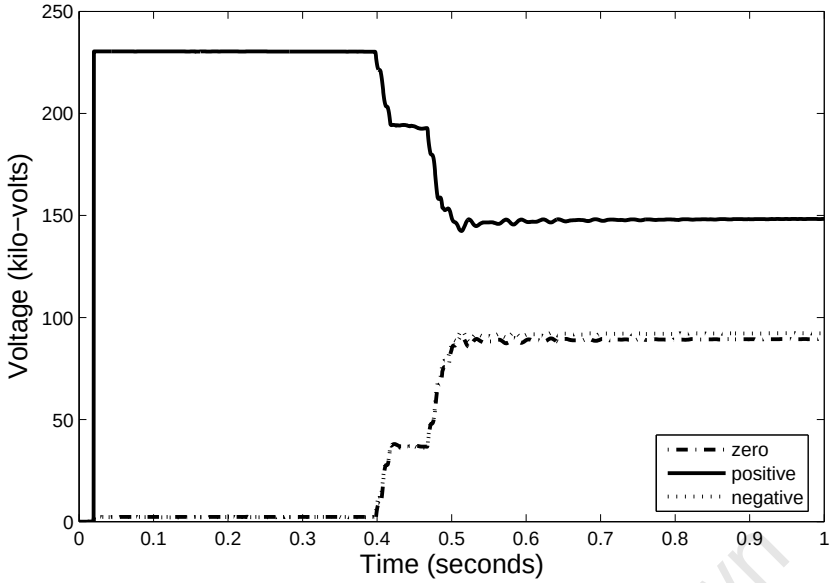

Figure 5-25: Tracking symmetrical components using the Fourier Analyser.

5.3.2 Case 2

A single line-ground fault occurred on the Eskom network. Line inspection revealed that the source of the fault was veld fires. The sampling frequency was 2.5 kHz i.e. 50 samples/cycle. Figure 5-26 shows the fault data. The convergence parameters of case 1 were used for the algorithm. The extracted positive, negative and zero sequence components using the proposed method and DFT is shown in Figures 5-27 and 5-28 respectively. The maximum difference in steady state error is 0.4%. The response times were in close agreement. The response time of the nonlinear algorithm was 3 ms faster than the DFT.

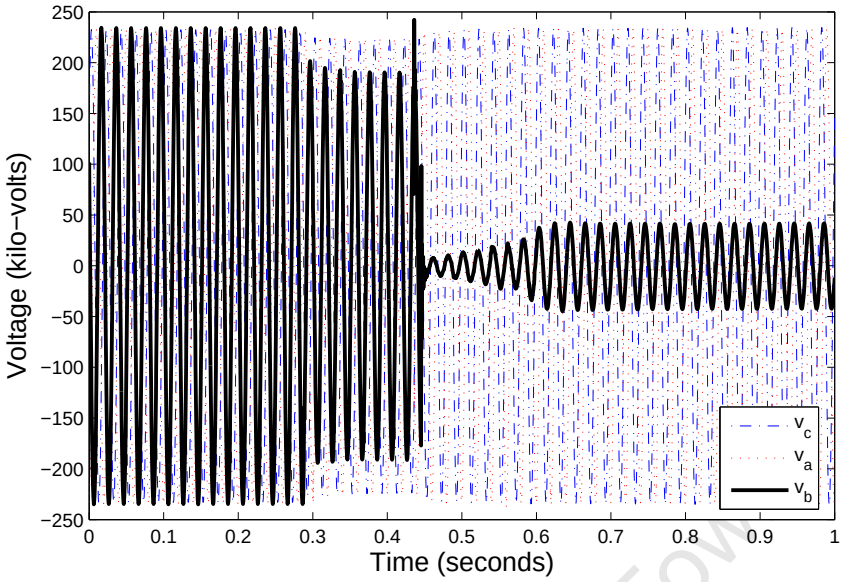

Figure 5-26: Three-phase voltage at fault instant for Case 2.

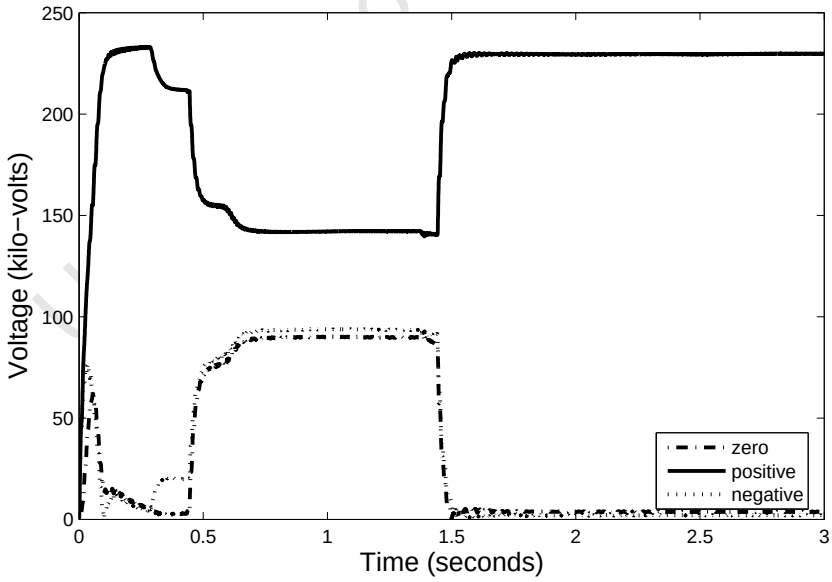

Figure 5-27: Tracking symmetrical components of Case 2 using the proposed technique.

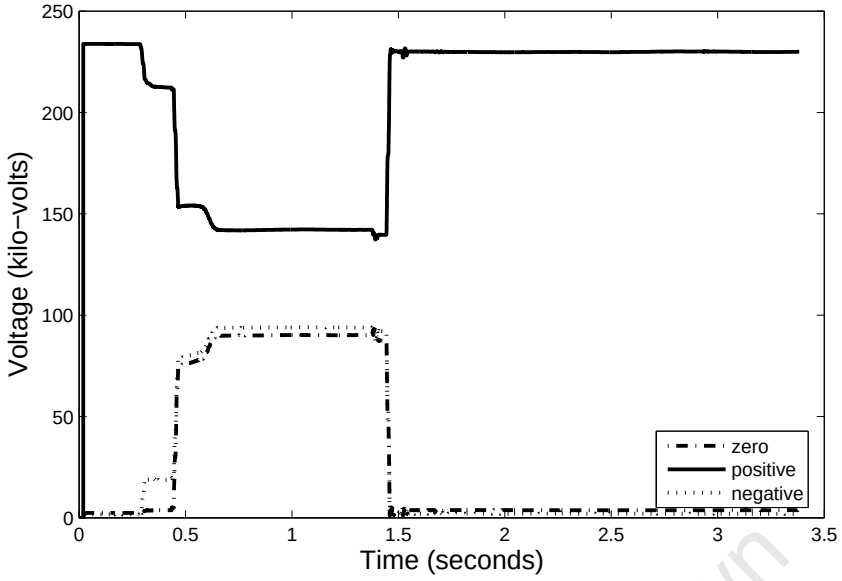

Figure 5-28: Tracking symmetrical components of Case 2 using the Fourier Analyser.

5.4 Summary of Results

The presentation and performance of the proposed method of symmetrical component estimation demonstrates improvement over existing methods. With reference to the discussions presented throughout this chapter, the main features of the proposed method can be summarised as follows:

- For step changes in amplitude, the DFT and nonlinear filter yields approximately the same accuracy. The nonlinear filter offers an improvement in response time of 5 ms.

- For step changes in phase, the steady state error from both the DFT and nonlinear filter is approximately 0.5%. A response time difference of up to 10 ms can be achieved by employing the nonlinear filter.

- For noise levels of $\sigma^2 > 0.03$, the influence of noise impacts the DFT significantly. The nonlinear filter is able to offer improved accuracy.

5.5 Concluding Remarks

In this chapter, a new method was presented to determine symmetrical components in real-time. The method converted a three-phase input signal into a time-domain phasor. The standard symmetrical component matrix was used to convert the three phasors into a positive, negative and zero sequence components in real-time. The system was first tested using simulation data. Theoretical calculations were used for a bench marking to compare the response of the algorithm and DFT. The effects of varying amplitude, phase and noise were investigated. The simulation studies confirm the superior performance of the algorithm as compared to the DFT, especially under conditions of noise and harmonics. Field data was used to test the algorithm against the DFT. The proposed technique yielded a steady state error of within 0.5% to that of the DFT. This makes it an effective and efficient solution for power system applications such as power factor controllers, FACTS devices etc. The proceeding chapters apply the core building blocks developed in chapters THREE to FIVE.

Chapter 6

Online Sag Analysis

To ensure optimal performance of power systems, the monitoring of sags is critical. Monitoring can be used as a vital diagnostic tool to identify problem conditions on a power system before they can cause disturbances or interruptions. A successful power quality monitoring programme requires flexibility, powerful data processing, value adding reports, and easy access to information. Voltage disturbances lasting more than one cycle are normally characterised in terms of voltage magnitude and event duration. These parameters provide an easily understood means of characterising these types of voltage disturbances. However, magnitude and duration are not the only characteristics that affect loads. Many types of loads such as contactors, control systems, and ac/dc drives are also affected by other factors such as the wave shape, the point in the waveform at which the disturbance begins and the phase angle jump during a disturbance [60].

Bollen and Zhang presented a method of characterising voltage dips as experienced by a three-phase load [32]. The method is based on the well-proven theory of symmetrical components and has contributed significantly to the field. The method has this far only been used for off-line sag analysis. This chapter provides an online method of characterising voltage sag by applying the method of Bollen and Zhang. The proposed method can be used in power quality recorders to reduce processing requirements. Additional indices such as sag magnitude, duration, lost voltage-seconds, phase angle

jump and sag energy can determined. The proposed system reduces the processing requirement of power quality recorders to characterise sags. The method relies on the core building blocks as developed in chapters THREE to FIVE, i.e. amplitude, phase, frequency and real-time symmetrical component estimation.

6.1 Sag Characterisation

Voltage sag in transmission and distribution networks generally affect one or more phases. Each phase can have a different magnitude and duration characteristics. Two different philosophies which characterise voltage sag can be found in literature. The first considers the sag in terms of three single phase events, estimating the magnitude and duration for each event. A more common approach is to consider the three phase sag as a single event.

6.1.1 Method of Bollen and Zhang

Bollen and Zhang developed two different methods of sag charaterisation, namely the ABC classification and the symmetrical component classification.

ABC Classification

In the ABC classification, seven types of voltage sags are proposed. This is shown in Figure 6-1. The ABC classification was developed, among other reasons, to analyse the propagation of voltage sag from transmission to distribution levels. The ABC classification is based on a simplified network model and the authors do not recommend its use for characterising field data [61].

Symmetrical Component Classification

A classification of three-phase unbalanced dips was proposed in [32]. The classification considers three-phase, phase-ground, phase-to-phase and phase-to-phase-ground type faults.

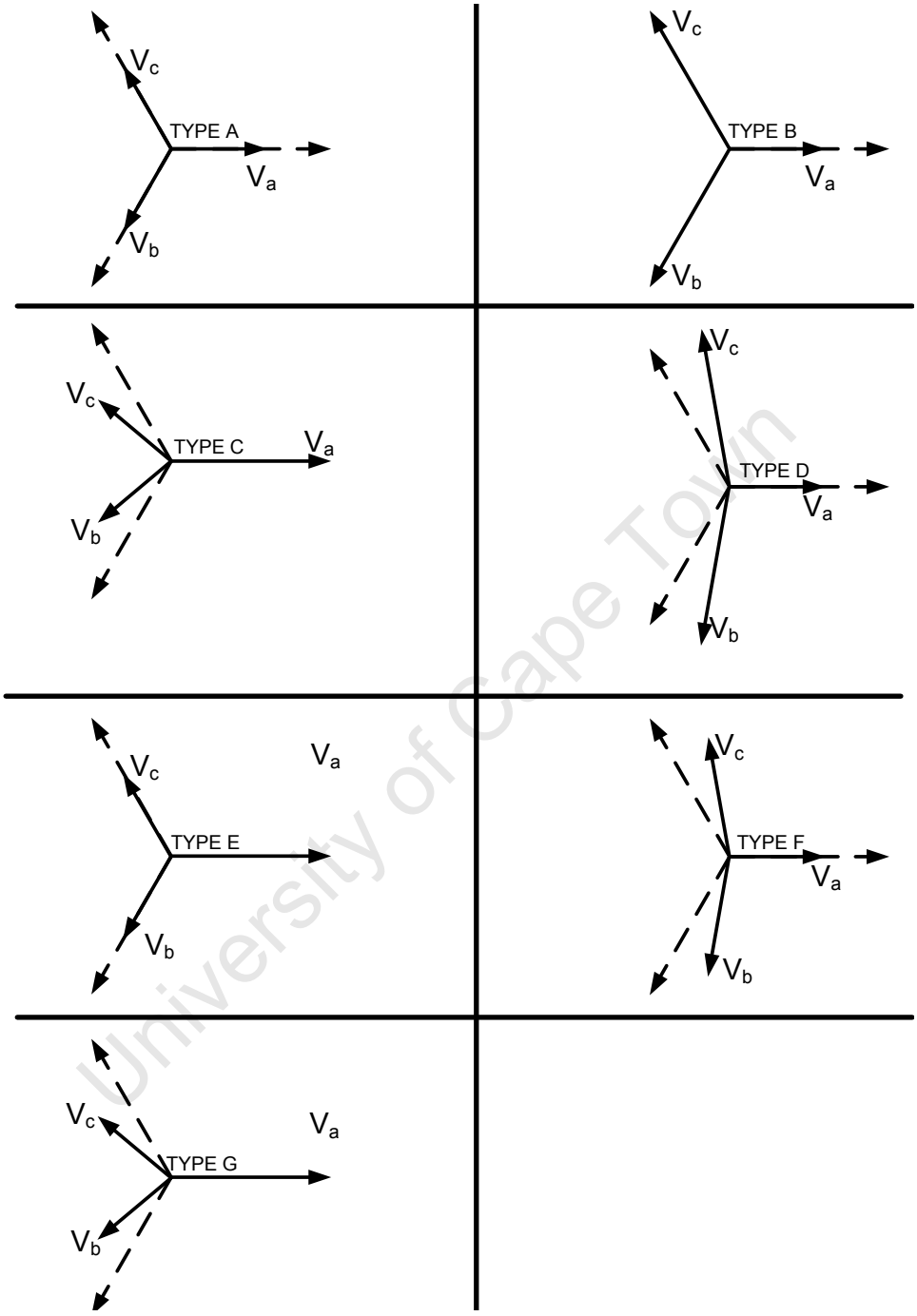

Figure 6-1: ABC classification of sags.

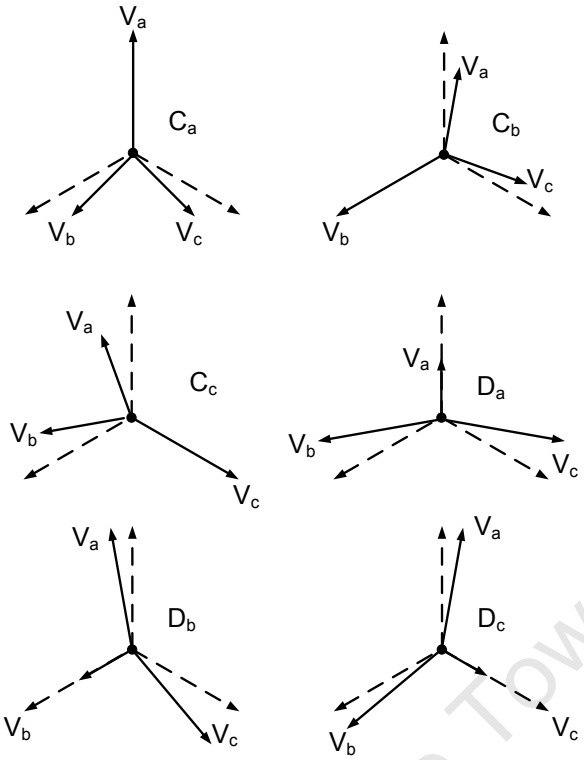

Figure 6-2: Voltage sag classification according to the symmetrical components method.

The method assumes that the positive and negative sequence source impedances are equal. This has been proven to be statistically valid in [32] from actual field data. Four types of three-phase unbalanced sags are proposed. This is shown in Figure 6-2. Type A is due to three-phase faults and types B, C and D are due to single-phase and phase-to-phase faults. Type B contains a zero-sequence component which is rarely transferred down to the equipment terminals. Three-phase equipment is normally connected in delta or in star without neutral connection. Single-phase low-voltage equipment are generally connected between phase and neutral. The percentage of sags originating in the low-voltage system is small. The vast majority of three-phase unbalanced sags at the equipment terminals are of type C or type D. A distinction between type C and D together with a single characteristic magnitude and phase-angle jump is sufficient. The definition of characteristic magnitude and phase-angle jump is such that these quantities do not change when the sag transfers from one voltage level to the other. The characteristic magnitude V_{ch} and phase-angle jump are defined as

the absolute value and the argument of the complex phasor representing the voltage in the lowest phase for a type D dip, and the voltage between the two lowest phases for a type C dip. A sound mathematical basis for the above classification is given in [32] and [61]. It includes a generalisation that holds when positive and negative-sequence source impedances are different. This extension of the classification is based on the theory of symmetrical components. The three (complex) phase voltages in an unbalanced three-phase system can be completely described through symmetrical components. The complex voltages (in pu) for a three-phase unbalanced dip of type C with Characteristic Voltage, V_{ch} are as follows:

$$\begin{aligned} \underline{V}_a &= 1 \\ \underline{V}_b &= -\tfrac{1}{2} - \tfrac{1}{2} j \underline{V}_{ch} \sqrt{3} \\ \underline{V}_c &= -\tfrac{1}{2} + \tfrac{1}{2} j \underline{V}_{ch} \sqrt{3} \end{aligned} \tag{6.1}$$

For a dip of type D the complex voltages (in pu) are:

$$\begin{aligned} \underline{V}_a &= 1 \\ \underline{V}_b &= -\tfrac{1}{2} \underline{V}_{ch} - \tfrac{1}{2} j \sqrt{3} \\ \underline{V}_c &= -\tfrac{1}{2} \underline{V}_{ch} + \tfrac{1}{2} j \sqrt{3} \end{aligned} \tag{6.2}$$

where V_{ch} represents the characteristic voltage. If the complex sequence voltages are known, the voltages in the three-phases can be calculated from:

$$\begin{bmatrix} \underline{V}_a \\ \underline{V}_b \\ \underline{V}_c \end{bmatrix} = \begin{bmatrix} 1 & 1 & 0 \\ 1 & -\frac{1}{2} & -\frac{1}{2} j \sqrt{3} \\ 1 & -\frac{1}{2} & \frac{1}{2} j \sqrt{3} \end{bmatrix} \begin{bmatrix} \underline{V}_0 \\ \underline{V}_1 + \underline{V}_2 \\ \underline{V}_1 - \underline{V}_2 \end{bmatrix} \tag{6.3}$$

Comparing (6.3) with (6.1) and (6.2), the following relations hold for a sag of type C:

$$\begin{aligned} \underline{V}_0 &= 0 \\ \underline{V}_1 + \underline{V}_2 &= 1 \\ \underline{V}_1 - \underline{V}_2 &= \underline{V}_{ch} \end{aligned} \tag{6.4}$$

The equivalent expressions for a sag of type D are:

$$\begin{aligned} \underline{V}_0 &= 0 \\ \underline{V}_1 + \underline{V}_2 &= \underline{V}_{ch} \\ \underline{V}_1 - \underline{V}_2 &= 1 \end{aligned} \tag{6.5}$$

In the proposed characterisation method these relations are used to obtain the characteristic complex voltage. The underlying assumption of (6.4) and (6.5) is that positive and negative-sequence source impedances are identical. As this is not exactly the case in reality, a second sag characteristic is introduced, namely the PN-factor. The PN-factor is equal to the pre-fault voltage (= 1 pu) if the system's positive and negative sequence impedance are the same. Under this assumption, the sag is characterised with one phasor. Thus far, unbalanced faults which are symmetrical with regard to the reference phase (phase a) is considered. The symmetrical phase is defined as the phase which is different from the other phases for an unbalanced fault. In practice, sags can occur in any of the phases. Table 6.1 provides expressions for all combinations of type C and D dips. A full theoretical derivation can be obtained in [32].

Table 6.1: Symmetrical component classification.

Sag in Phases	**Sag Type**	**Characteristic Voltage** (Vch)	**PN Factor** (F)
BC	C_a	$V_{ch} = \underline{V}_1 - \underline{V}_2$	$F = \underline{V}_1 + \underline{V}_2$
CA	C_b	$V_{ch} = \underline{V}_1 - a^2\underline{V}_2$	$F = \underline{V}_1 + a^2\underline{V}_2$
AB	C_c	$V_{ch} = \underline{V}_1 - a\underline{V}_2$	$F = \underline{V}_1 + a\underline{V}_2$
A	D_a	$V_{ch} = \underline{V}_1 + \underline{V}_2$	$F = \underline{V}_1 - \underline{V}_2$
B	D_b	$V_{ch} = \underline{V}_1 + a^2\underline{V}_2$	$F = \underline{V}_1 - a^2\underline{V}_2$
C	D_c	$V_{ch} = \underline{V}_1 + a^2\underline{V}_2$	$F = \underline{V}_1 - a^2\underline{V}_2$

Challenges for Online Implementation

Although the methods proposed by Bollen and Zhang offer tremendous potential for off-line sag analysis, there is no documented online application of the method to characterise sags. Traditionally, the implementation of their methods in a power quality recorder would require significant processing. To do this would require that the time-domain instantaneous voltages should first be converted to phasors. This would require the application of the DFT or another suitable algorithm. Next, the symmetrical component transformation is applied to obtain the positive, negative and zero sequence components. Finally, the characteristic voltage and the PN factor must be determined. This poses a problem for online implementation.

6.1.2 Online Method of Sag Characterisation

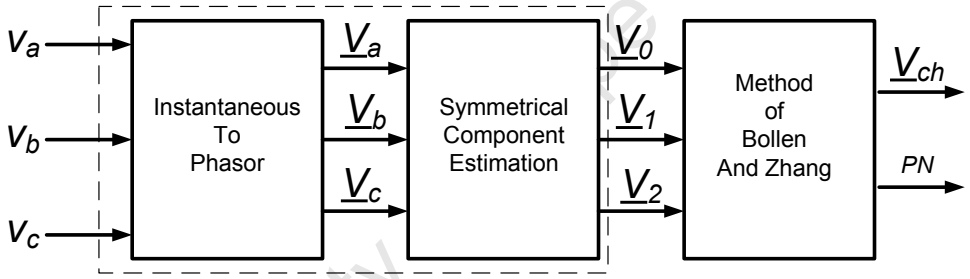

Figure 6-3: System overview of the proposed online method.

The proposed online characterisation method is shown in Figure 6-3. The first module converts the instantaneous three-phase voltages into phasors. The symmetrical components is then extracted in module 2. This has been implemented and extensively tested in chapter FIVE. The real-time symmetrical components are then passed to a module which completes the characterisation according to the method of Bollen and Zhang. An online procedure for online implementation is as follows:

1. Convert the three instantaneous voltages into phasors using the algorithm.
2. Obtain positive, negative and zero-sequence components of voltages.
3. Identify the phases in which sag occurs.

4. Obtain the corresponding sag type from Table 6.1.

5. Calculate the characteristic voltage based on sag type.

6. Determine the PN factor based on the sag type.

6.1.3 Simulation Results

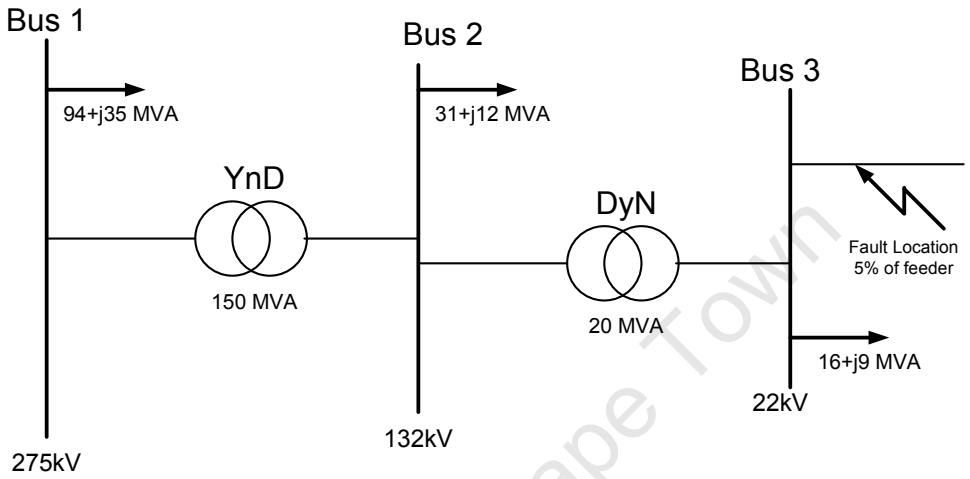

Figure 6-4: Single-line diagram of the system under study.

The Alternative Transients Program (ATP) was used to model an actual utility transmission power system and to generate fault data. This was used to prepare the data file containing voltage and current samples under different fault conditions. This data was used in MATLAB to evaluate the performance of the new method. Since the actual values of the symmetrical components are not known, the proposed technique is bench-marked against the DFT. The results are reported and discussed in this section. Figure 6-4 shows a single-line diagram of the utility three-phase system. The system is composed of three buses. A 275 kV transmission system feeds distribution voltages of 132 kV and 22 kV. The three-phase short circuit capacity at the 275 kV

Table 6.2: Transformer impedance's.

Transformer	Z_0 (pu)	Z_1 (pu)	Z_2 (pu)
$275/132kV$	0.07135	0.1536	0.1536
$132/22kV$	0.48150	0.5915	0.5915

bus is 1400 MVA. The system has two different transformers, a YnD and DyN. This is used later in the chapter to discuss the effects of propagation across transformers. The loads were modelled as constant power loads. For the studies, the fault is placed on a feeder close up to bus 3 from t = 0.4 s. Table 6.2 shows the transformer per unit data (on a 100 MVA base). The following cases were simulated:

- Three-phase fault.
- Line-ground fault.
- Line-line fault (results in Appendix B).
- Line-line-ground fault (results in Appendix B).

Three-phase fault

Figures 6-5(a) and 6-5(b) show the three phase voltages and currents at bus 3 for a three-phase fault. The tracked voltage amplitude is shown in Figure 6-5(c). The estimated phase is shown in Figure 6-5(d). From this, the instantaneous three-phase voltages are converted into positive, negative and zero sequence time-domain phasors. The characteristic voltage is then extracted as shown in Figure 6-6(a). The characteristic voltage is also determined using the Fourier method as shown in Figure 6-6(b). The characteristic angle is shown in Figure 6-6(c).

Single Line-Ground Fault

Bus 3 voltages and currents for a line-ground fault are shown in Figures 6-7(a) and 6-7(b) respectively. Figure 6-7(c) shows the tracked voltage amplitudes. The characteristic voltage is extracted using the DFT and the algorithm. This is shown in figures 6-8(c) and 6-8(d) respectively. The PN factor is shown in Figure 6-9(b). Results indicate that the steady-state error of the characteristic voltage from the proposed technique is within 0.8% from that of the DFT. Results for the line-line and line-line-ground fault are included in Appendix 2a and 2b respectively.

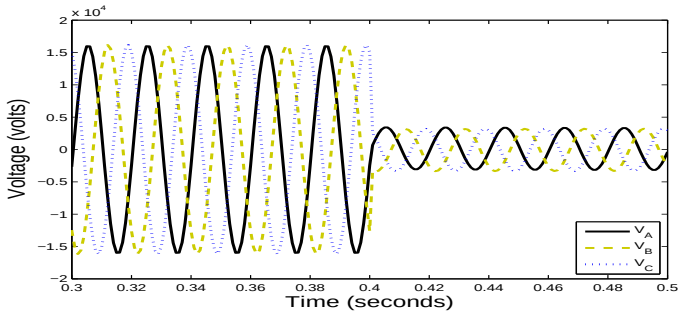

(a) Three-phase voltages.

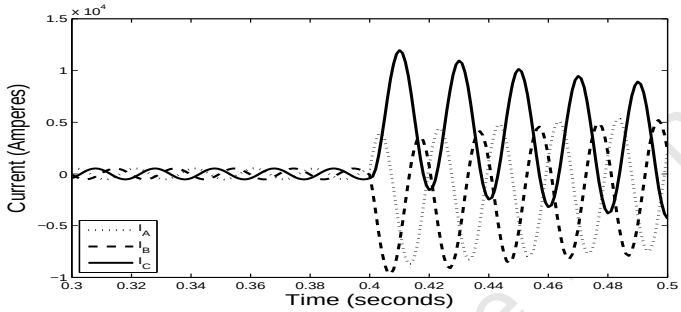

(b) Three phase fault currents.

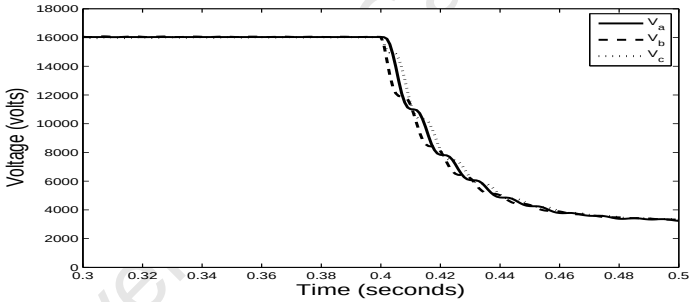

(c) Tracked voltage amplitude.

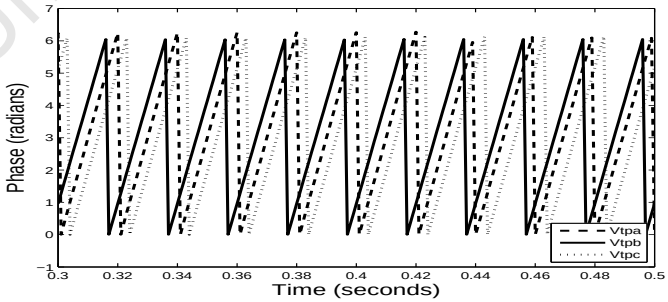

(d) Tracked phase.

Figure 6-5: Bus 3 parameters for a three-phase fault at bus 3.

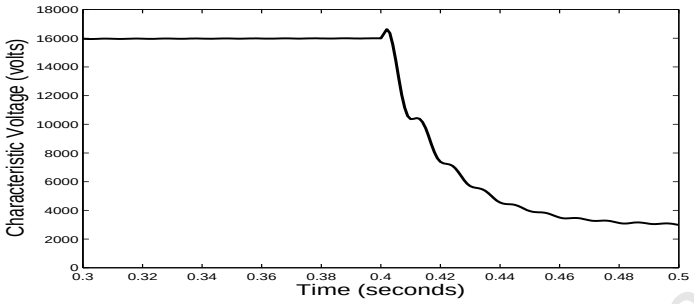

(a) Characteristic voltage - algorithm.

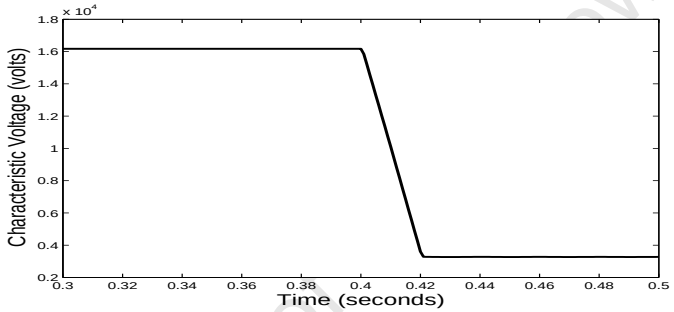

(b) Characteristic voltage - Fourier.

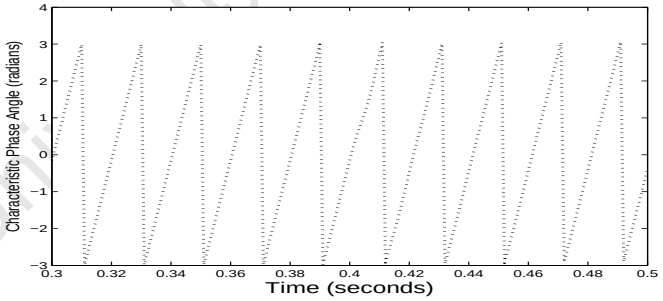

(c) Characteristic angle.

Figure 6-6: Bus 3 parameters for a three phase fault at bus 3.

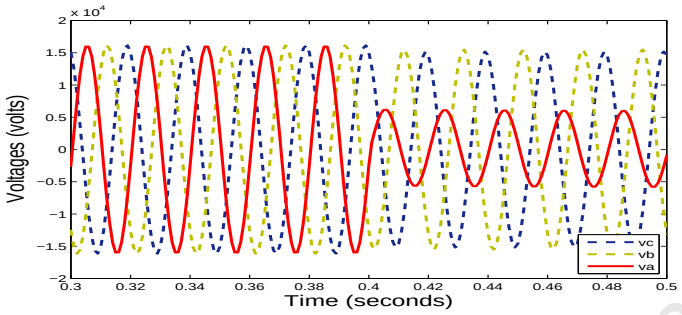

(a) Three phase voltages.

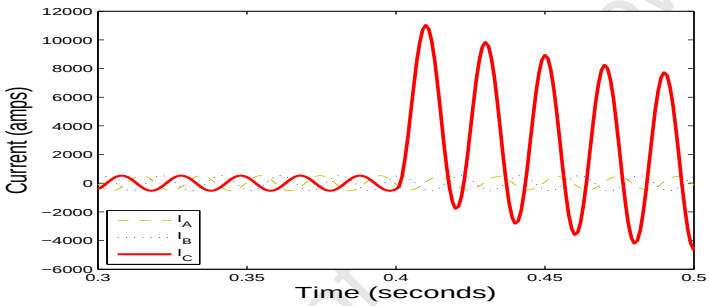

(b) Bus 3 currents.

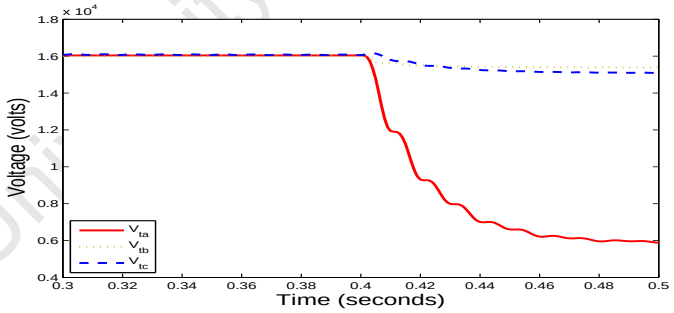

(c) Bus 3 tracked voltage amplitude.

Figure 6-7: Bus 3 parameters for a line-ground fault at bus 3.

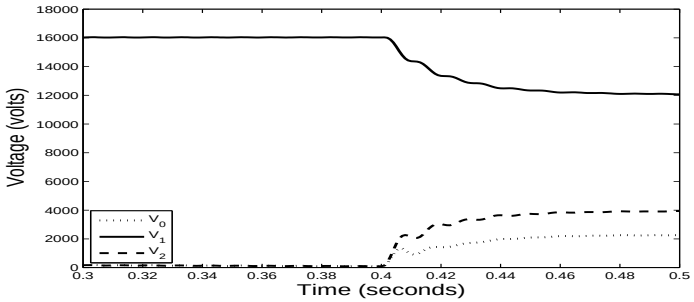

(a) Symmetrical components - algorithm.

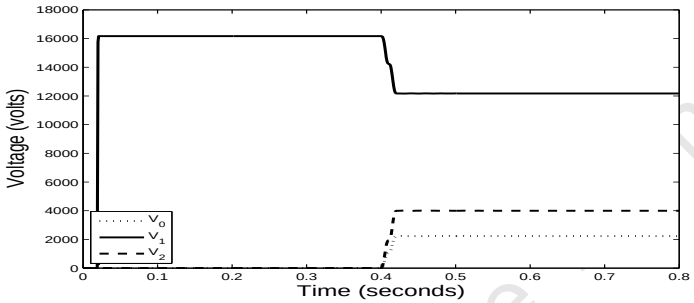

(b) Symmetrical components - Fourier.

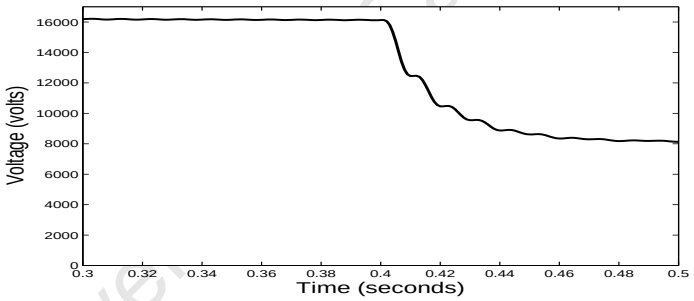

(c) Characteristic voltage - algorithm.

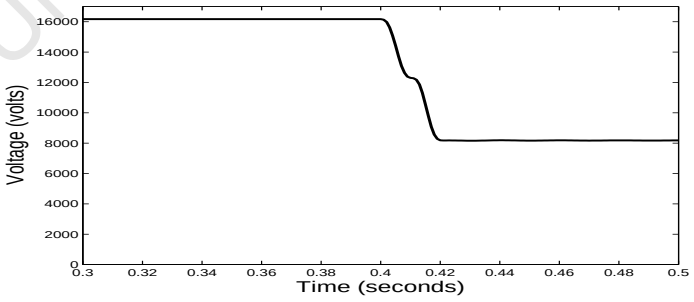

(d) Characteristic voltage - Fourier.

Figure 6-8: Bus 3 parameters for a line-ground fault at bus 3.

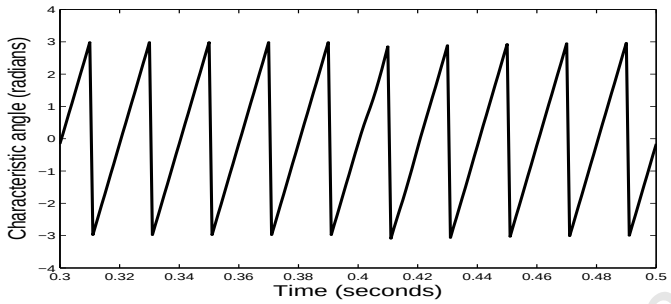

(a) Determining the characteristic angle using the algorithm.

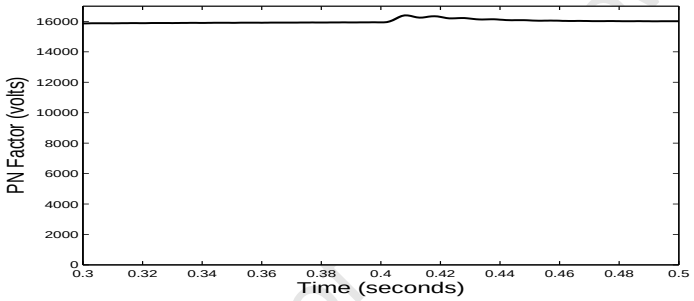

(b) Determining the PN factor using the algorithm.

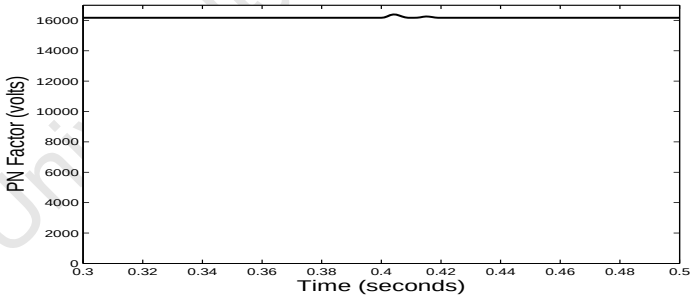

(c) Determining the PN factor using Fourier.

Figure 6-9: Bus 3 parameters for a line-ground fault at bus 3.

6.1.4 Sag Propagation Through Transformers

Transformers can be manufactured with many different winding connections. As a sag propagates through a transformer, the phasors relation of the voltage sag at the secondary side of the transformer can change from that of the primary. This depends on the transformer configuration and is known as sag propagation. This could result in a sag classification type change. This section demonstrates through the case study the effects of voltage propagation through time-domain tracking of the characteristic voltage. Figures 6-10(a) to 6-10(c) show the algorithm-tracked voltages at buses 1, 2 and 3 respectively for a three-phase fault. The tracked characteristic voltages are shown in Figure 6-10(d). The results show that a three-phase fault is not affected by propagation through transformers. The results from the line-ground study are shown in Figure 6-11. The actual fault type is D_a. The tracked voltages at bus 2 as shown in Figure 6-11(b), indicate a line-line fault (type C_c). This clearly demonstrates the effects of propagation across the transformer. A method to solve this is to use a combination of a transformer matrix and a symmetry changer [32].

6.2 Single Event Sag Indices

For sags, indices of interest include [62]:

- Sag magnitude and duration
- Phase angle jump
- Loss of voltage
- Sag energy
- Sag severity

The work on voltage sags in standard setting organisations has recently concentrated on the representation of voltage sags. A power quality measurement standard, IEC 61000-4-30 [63], defines power quality measurement methods. Basic voltage sag characteristics for measured voltage sag waveform's are available.

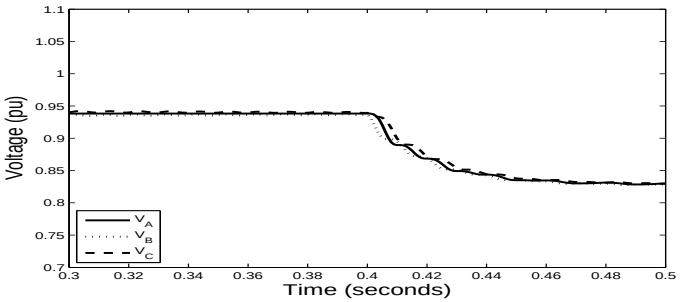

(a) Tracked voltages at bus 1 for a three phase fault.

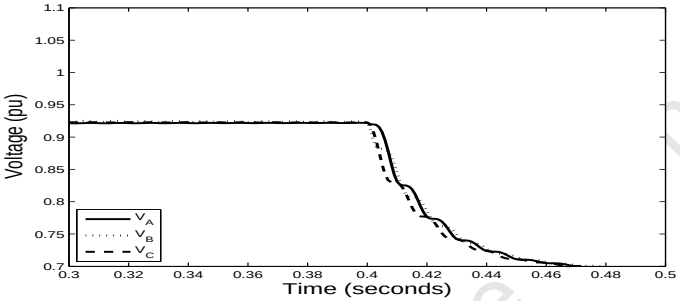

(b) Tracked voltages at bus 2 for a three phase fault.

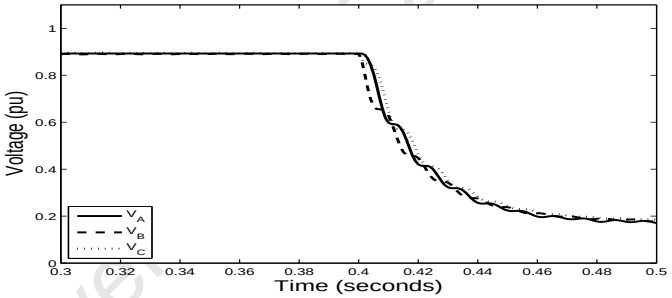

(c) Tracked voltages at bus 3 for a three phase fault.

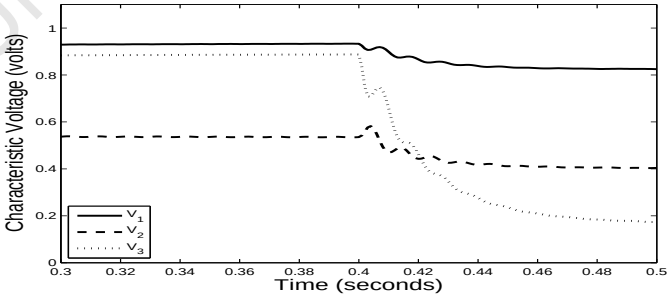

(d) Characteristic voltages at buses 1-3 for a three phase fault.

Figure 6-10: Bus 3 parameters for a three phase fault at bus 3.

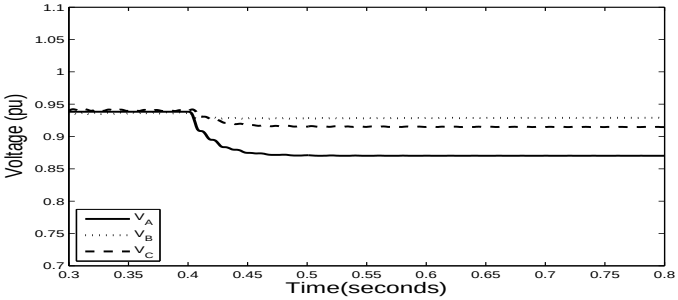

(a) Tracked voltages at bus 1 for a line-ground fault.

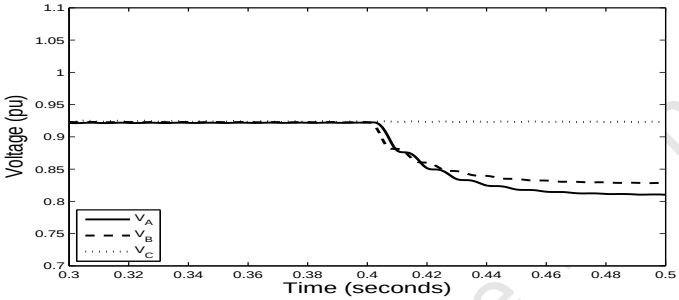

(b) Tracked voltages at bus 2 for a line-ground fault.

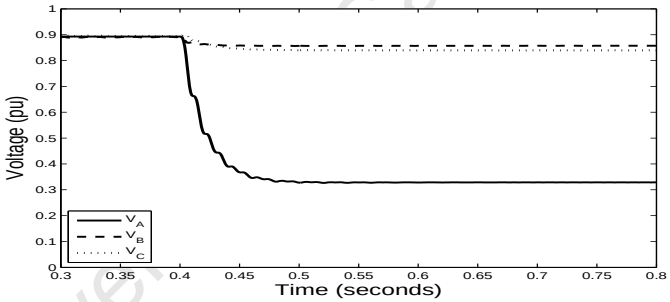

(c) Tracked voltages at bus 3 for a line-ground fault.

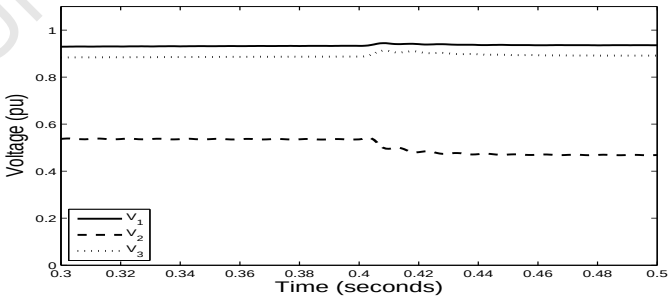

(d) Characteristic voltages at buses 1-3 for a line-ground fault.

Figure 6-11: Bus 3 parameters for a line-ground fault at bus 3.

The IEEE working group P1564, is responsible for defining voltage sag indices [64]. The aim of voltage sag indices is to describe the performance of a power system through a limited number of parameters. This description is by nature a statistical one, with averages and distributions over time and space. The first step in obtaining any voltage sag indices is to obtain sampled voltage waveform's, typically for the three phases. The sampling has to take place with a certain sampling frequency and resolution. To give a value to the performance of a power system as far as voltage sags are concerned, a five step procedure is proposed by the IEEE P1564:

1. Obtain sampled voltages with a certain sampling rate and resolution.
2. Calculate event characteristics as a function of time from the sampled voltages.
3. Calculate single event indices from the event characteristics.
4. Calculate site indices from single event indices of all events measured during a certain time period.
5. Calculate system indices from site indices for all sites within the system.

Suppose that the pre-sag amplitude of the input voltage signal is $v_{psag}(t)$, where V_{nom} is the amplitude and ϕ_a the phase angle.

$$v_{psag}(t) = V_{nom} \sin(\omega t - \phi_a) \tag{6.6}$$

During the sag, a sinusoidal signal $v_s(t)$ in phase with the input voltage $v(t)$ exists so that

$$v_s(t) = V_{sag}(t) \sin(\omega t - \phi_b(t)) \tag{6.7}$$

where $V_{sag}(t)$ and $\phi_b(t)$ represent the time varying amplitude and the phase angle during the sag. The sag can be assumed to commence at time t_1 and clear at t_2.

6.2.1 The Data Set

The Eskom power quality database is composed of digitally sampled voltage and current waveform's taken from power quality monitors and fault recorders.

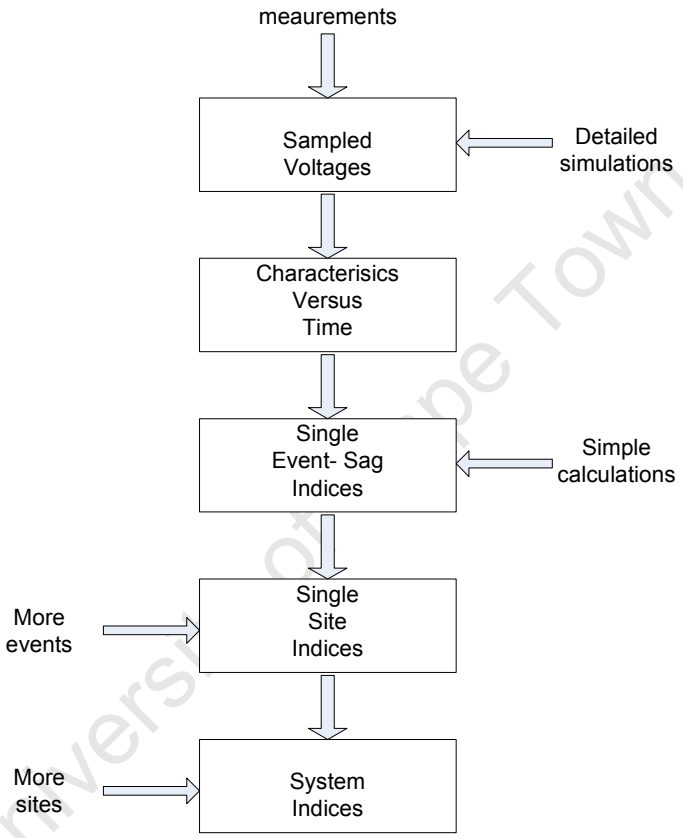

Figure 6-12: The general framework for obtaining voltage sag indices [62].

The algorithms are specifically designed to use this database, but it could be easily modified to accommodate other sampled database collections. Since the data is sampled, there is a limit to the resolution of parameters that can be computed. For example, the phase angle cannot be accurate to more than about 1.4° per increment.

6.2.2 Windowing

Historically, the analysis of voltage sags has focused on characteristics that can be computed from the RMS value of the normally sinusoidal voltage waveform. Many of the computations rely on a "window"function to make the calculation. A time series can be created in which the interval between the time series computations is the same interval of the sampling interval of the monitoring instrument. This approach is sometimes referred to as a sliding window RMS calculation. In practice, most commercially available power quality monitoring instruments do not create RMS time series measurements using the sliding window approach. This is because the processing time required is too excessive for real time. An error of up to one cycle can occur from the RMS computation due to the averaging that occurs [60].

6.2.3 Pre-Event Waveform

The pre-event waveform represents the instantaneous data prior to the disturbance that results in the sag. This data is typically stored in a buffer for analysis. The extrapolation of the pre-event data across the entire data set, synchronised with instantaneous event information, can assist in characterising the sag.

6.2.4 Sag Waveform

The typical amplitude-duration characteristics of a sag is shown in Figure 6-13. The RMS method is the most common method used to determine sag magnitude and duration. The sag magnitude is the lowest value of the voltage magnitude versus time, which is obtained from the recording.

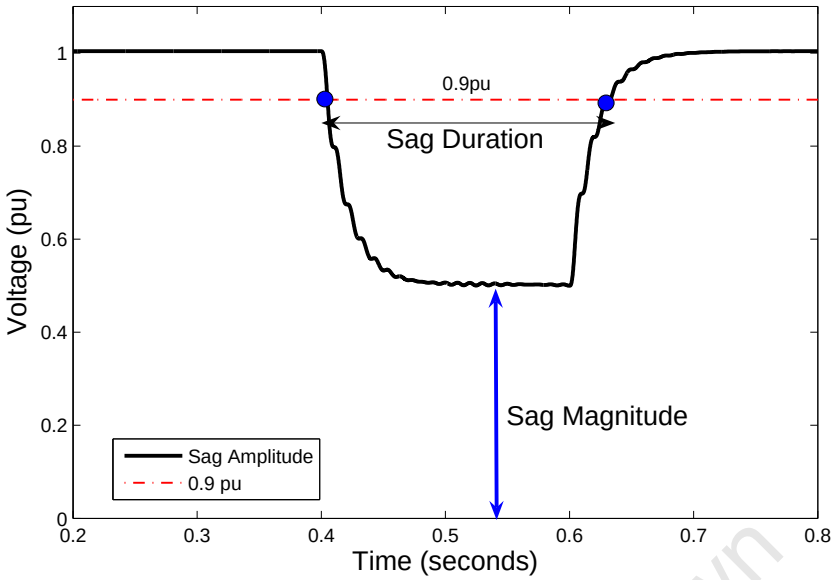

Figure 6-13: Amplitude duration characteristics of a typical sag.

The duration of a voltage sag is the time measured from the moment the RMS voltage drops below 0.9 pu of nominal voltage to when it rises above 0.9 pu of nominal voltage.

6.2.5 Phase-Angle Jump

A short circuit in a power system not only causes a drop in voltage magnitude, but also a change in the phase angle of the voltage. This sudden change in phase-angle is called the phase-angle jump. The phase-angle jump is visible in a time-domain plot of the sag as a shift in voltage zero-crossing occurs between the pre-event and the during-event voltage. Figure 6-14 shows a one-line diagram of a typical balanced fault. It is assumed that the three-phase fault occurred at a location F, where Z_a is the equivalent impedance of the transformer and lines from the fault position F, and Z_b is the equivalent impedance between the fault point and the load. Z_L is the impedance of the static load. The voltage V_f in the pre-fault position is given by

$$V_f = \frac{Z_b + Z_L}{Z_a + Z_b + Z_L} V_s \tag{6.8}$$

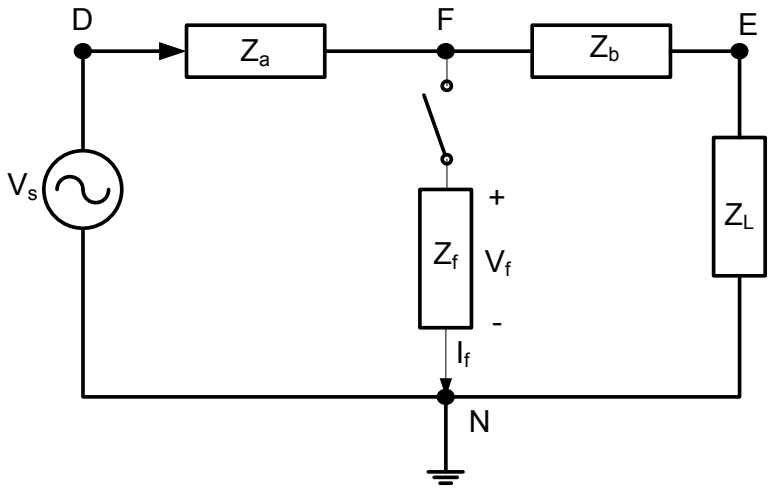

Figure 6-14: Circuit diagram for balanced fault [65].

where V_s is the source voltage. For a line fault between point F and the neutral (or ground), the voltage at point F becomes

$$V_f = \frac{Z_f || Z_{bL}}{Z_a + Z_f || Z_{bL}} V_s \tag{6.9}$$

where Z_f is the fault impedance, which is assumed to be a pure resistance (R_f), and $Z_f||Z_{bL}$ represents the equivalent impedance of Z_f in parallel with $Z_{bl} = Z_b + Z_L$. Applying equation (6.8) to (6.9), the fault voltage results in

$$V_f = \frac{G - jB}{G + G_f - jB} V_F \tag{6.10}$$

To obtain the phase-angle jump from the measured voltage wave-shape, the phase-angle of the voltage during the event must be compared with the phase-angle of the voltage before the event. The phase-angle of the voltage can be obtained from the voltage zero-crossings or from the argument of the fundamental component of the voltage. The IEEE P1564 project group [64] is implementing recommendations on how to extract phase angle information. Phase-angle changes have a great influence on electronic equipment and should therefore be taken into account when identifying and characterising the sag phenomenon.

The definition currently used in the IEEE P1564 project group reads as follows:

$$\psi(t) = \arg\left\{\frac{\overline{V}(t)}{\overline{V}(0)\exp\{j2\pi f_0 t\}}\right\} \tag{6.11}$$

ψ is the phase angle as a function of time, $\overline{V}(t)$ the complex fundamental voltage as a function of time and f_0 the synchronous frequency. The phase-angle jump according to (6.11) is the angular deviation from a synchronous sine-wave as a function of time. In terms of (6.7), this can be represented as

$$PhaseAngleJump = (\phi_a(t) - \phi_b(t)) \tag{6.12}$$

6.2.6 Sag Energy

Sags cause a reduction in energy transfer to load equipment. The ability of equipment to function as specified can be compromised depending on the amount of energy lost. The computation of sag energy has received a lot of attention by the IEEE P1564 project group on voltage sag indices. Voltage sag energy is defined as [62].

$$E_{VS} = \int_o^\tau \left[1 - \left\{\frac{V_{sag}(t)}{V_{nom}}\right\}^2\right] dt \tag{6.13}$$

There has been debate as to whether the nominal or pre-sag voltage should be used for the calculation. For simplicity, it will be assumed that the two voltages are the same. In practice, this is not necessarily true.

6.2.7 Loss of Voltage

In terms of (6.7), the loss of voltage LV is defined as the integral of the voltage drop during the event [62].

$$L_V = \int_{t_1}^{t_2} \{1 - V_{sag}(t)\} dt \tag{6.14}$$

where $V_{sag}(t)$ is the time varying amplitude during the sag event. For this index, it is essential that the voltage magnitude is expressed in pu. In order to complete the

definition, the start and end points of the summation have to be defined. Once again, the choice of reference value poses a problem [62]. This can be either the nominal voltage or the pre-sag voltage.

6.2.8 Structure of the Proposed Method

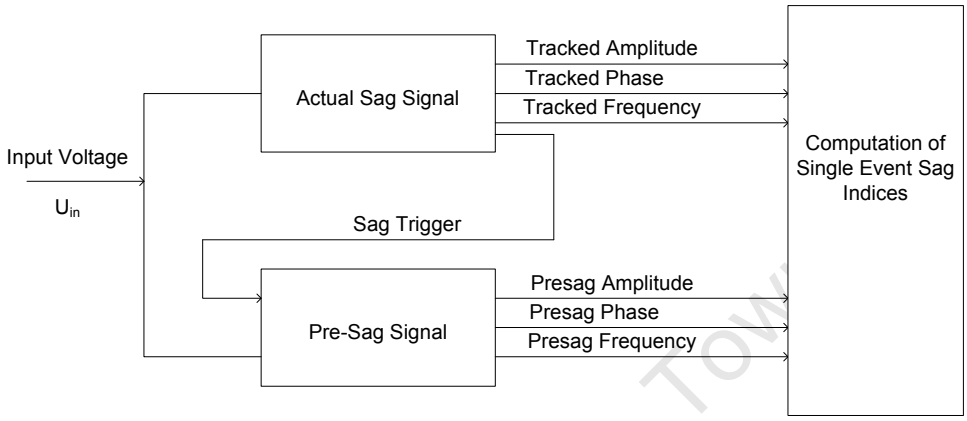

Figure 6-15: Overview of the proposed method.

The overall online method for determining single event sag indices is shown in Figure 6-15. The input is the instantaneous voltage waveform that is captured at a substation or customer site. This approach can also be used for post-sag analysis where instantaneous data is available from loggers. The outputs are the sag indices of interest. Utilising the algorithm, the actual sag block tracks the real-time amplitude and phase angle of the input signal $u(t)$. The pre-sag block stores a moving cycle of the pre-sag voltage in a buffer. Once the amplitude of the characteristic voltage is reduced to below 0.9 pu, the event is detected and a signal is received. The output form the pre-sag block includes a 1 pu voltage amplitude and the pre-sag phase-angle. From this, the sag indices are calculated using (6.12) - (6.14).

6.2.9 Field Results

The system described in Section 6.2.8 was tested using field data. Data from the Eskom power quality database was tested on the proposed system. A single line-ground fault was caused by a bird on the overhead line. The fault starts at approximately $t =$

0.409 s and is cleared at time $t = 1.67$ s. Figure 6-16 shows the three-phase voltages before, during and after the fault. The signal sampling rate is 2.5 kHz. The system frequency is 50 Hz. The positive and negative sequence components are extracted using the method proposed in chapter FIVE. This is shown in Figure 6-17. The type of sag is determined from the tracked amplitudes. For this study, the fault occurred on phase B. The characteristic equation used from Table 6.1 is $V_{ch} = \underline{V}_1 + a^2\underline{V}_2$.

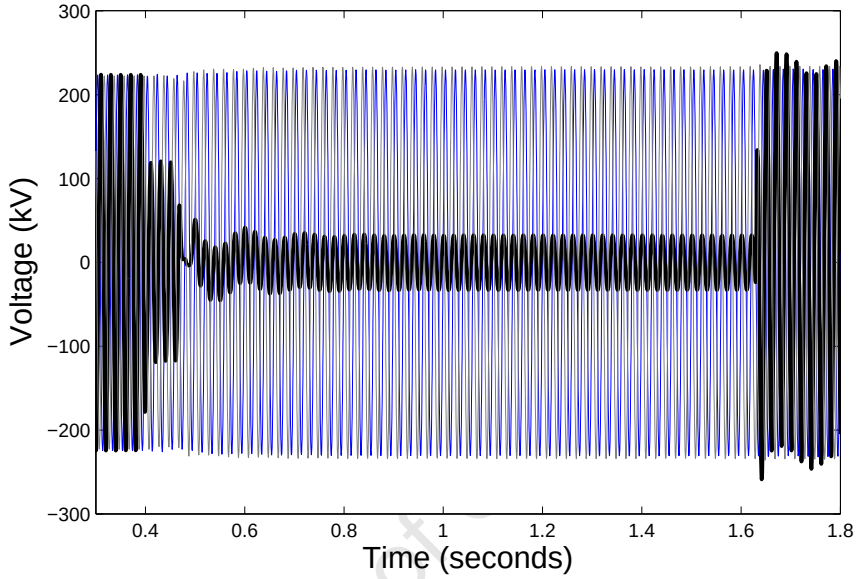

Figure 6-16: Input waveforms.

Sag Magnitude and Duration

The amplitudes of the characteristic voltage and sag trigger are shown in Figure 6-18. The sag duration is the difference between the rising and falling edge of the sag trigger. One can refer to this as times t_1 and t_2. This is used as the integration interval to determine some of the sag indices. For the case study, the minimum characteristic voltage is 0.242 pu. The duration of the sag trigger is t_2-$t_1 = 1.26$ s.

Phase-Angle Shift

Transmission system faults generally do not have large phase-angle jumps. This is as a result of the smaller X/R ratio. Distribution networks have a larger X/R ratio

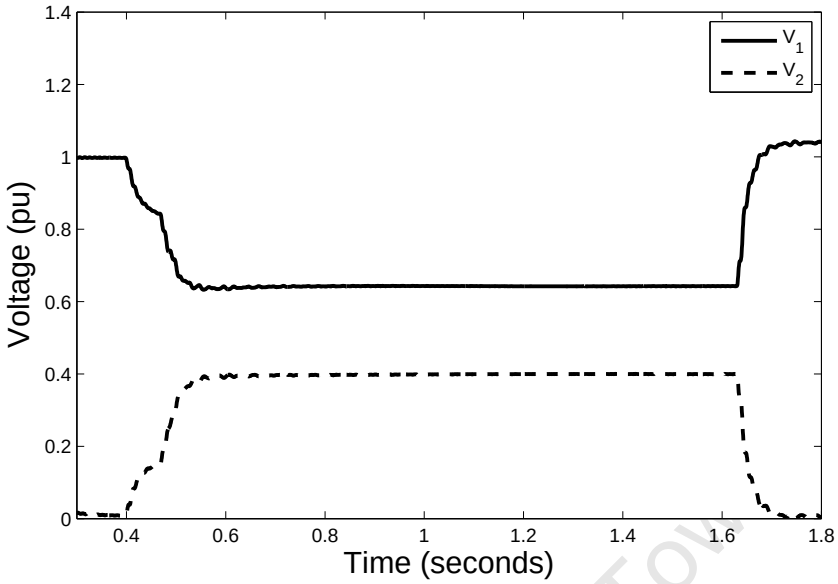

Figure 6-17: Extracted positive and negative sequence signals.

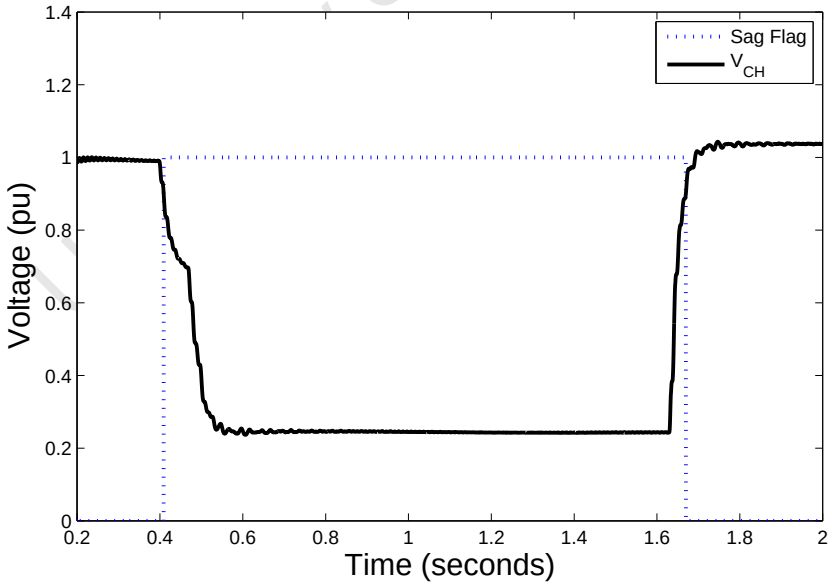

Figure 6-18: Extracted characteristic voltage and sag trigger.

and as a result the larger phase-angle jump associated with faults. There are other factors such as the fault resistance that need to be considered. For this study, the phase angle jump is determined from the difference between the phase angle of the tracked sine and pre-sag sine. The tracked phase-angle is shown in Figure 6-19. The extracted fundamental component of the three phase voltages is shown in Figure 6-20.

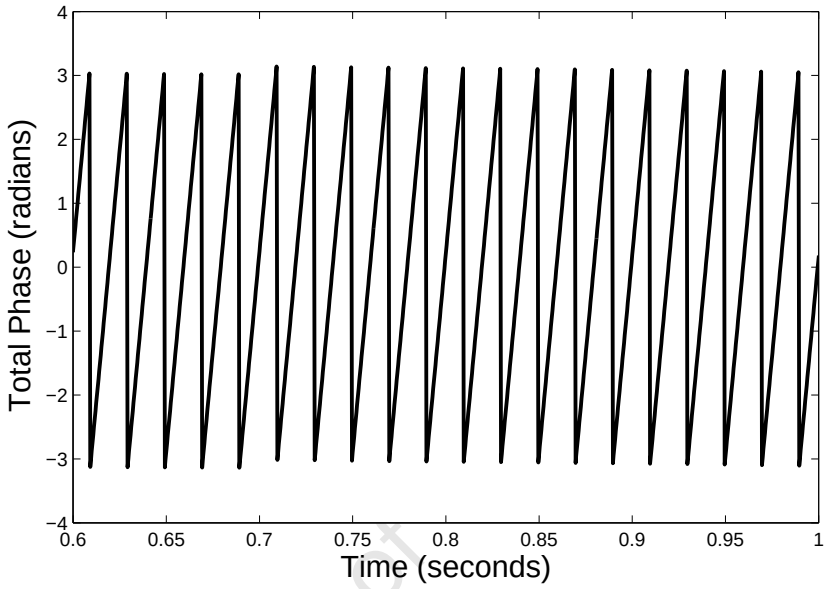

Figure 6-19: Tracked phase angle of faulted phase.

Sag Energy

Equation (6.13) can be modified as follows

$$E_{vs} = \frac{T_s \times N}{\tau} \times \sum_{t_1}^{t_2} \frac{\left(1 - V\left[n\right]\right)^2}{N} = \frac{T_s}{\tau} \times \sum_{t_1}^{t_2} \left(1 - V\left[n\right]\right)^2 \tag{6.15}$$

where $V[n]$ represents the time varying amplitude in pu, T_s the sampling time, τ the fundamental period (20 mSec for a 50 Hz system), t_1 and t_2 the sag start and end times and N the number of samples from t_1 to t_2 . In this study, $N = 3152$, $\tau = 0.02\ s$ and $T_s = 0.0004\ s$. From (6.15), the sag energy is calculated to be 32.99 pu.

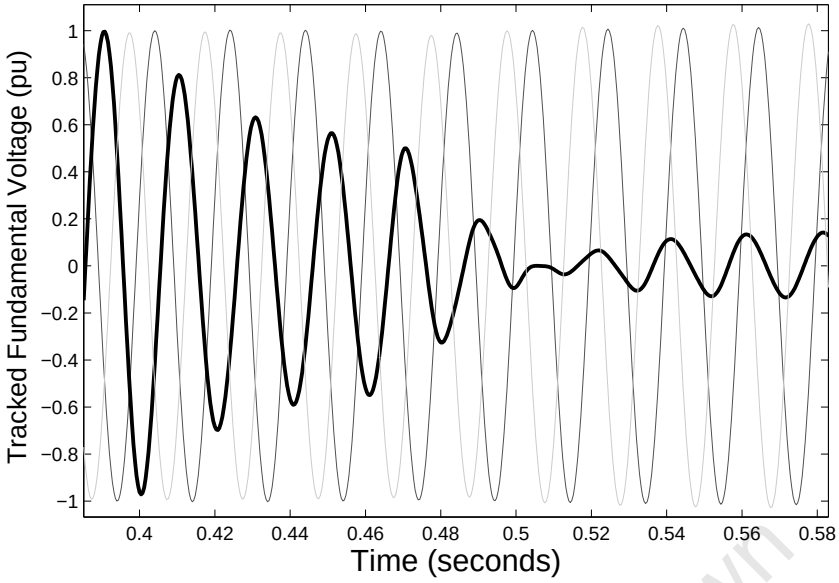

Figure 6-20: Extracted fundamental component of the three-phase voltages.

Lost Volt Seconds

In discrete form, the loss of voltage index can be determined as

$$L_V = \frac{T_s}{\tau} \times \sum_{t_1}^{t_2} (1 - V[n]) \tag{6.16}$$

The loss of voltage is the integral of the remaining voltage from time t_1 until t_2. From (6.16), the loss of voltage is calculated to be 44.76 pu.

6.3 Concluding Remarks

This chapter has presented an online method for characterising voltage sag using the method of Bollen and Zhang. By using the method, it is possible to extract the characteristic voltage and the PN factor in real-time. The proposed method can be implemented in power quality recorders to reduce processing power. The system is also capable of extracting single-event sag indices. Conventional methods such as the RMS only provide magnitude information. The proposed system is able to offer amplitude and phase information for reduced processing power. This additional

information can improve the general understanding of the impacts of sag on industrial processes. Utility engineers can use this data to create a disturbance profile at the customer location. This will provide improved correlation between sag characteristics and customer equipment response.

Chapter 7

Distributed Generation Synchronisation and Protection

Renewable energy as a resource is a reliable alternative to fossil fuels for power generation. The Distributed Power Generation Systems (DPGS) which is based on renewable energy resources is used extensively worldwide. Standards dictate that the power quality at the point of grid integration must be within prescribed limits. As a consequent improved control DPGS methods are continuously under study. The DPGS use current and voltage source converters or phase controlled rectifiers to synchronise with the ac line supply. The firing angle unit of a thyristor valve depends on the voltage zero crossing as a reference. The voltage zero crossing must be accurately detected for each half period of the grid voltage. A more demanding application is the grid connection of a forced commuted Voltage Source Converter (VSC) when vector current control is used. The synchronisation method must be updated not just at voltage zero crossings, but continuously under the whole period. The synchronisation algorithms used must be able to perform under conditions of noise, disturbances and frequency deviations. Failure to provide accurate synchronisation can be problematic. This can result in poor performance and instability [66].

The classical method of synchronisation is an analogue PLL. In recent years, control systems of converters are implemented in signal processors. The software solution to

the PLL results in a flexible and cost effective solution. For real-time control, processing time is critical. There is also a demand for fast and accurate algorithms [67]. This chapter gives an overview of the control structures of the DPGS. Synchronisation methods are of particular focus. The proposed nonlinear algorithm is applied and compared against the conventional reference frame controller. It is practically applied to protect wind energy systems. The impacts of noise, frequency deviations and disturbances are discussed. The basis of this chapter is formed by the core building blocks developed in chapters THREE and FOUR.

7.1 DPGS Structure [66]

A general structure for distributed systems is illustrated in Figure 7-1. [66] presents an overview of DPGS structures and a thorough evaluation of the control strategies. The input power is transformed into electricity by means of a power conversion unit. The configuration of the power conversion unit is closely related to the input power nature. The electricity that is produced can be delivered to local loads or to the utility network, depending on where the generation system is connected. An important part of the distributed system is its control. The control tasks can be divided into two major parts.

- Input-side controller - the main aim is to extract the maximum power from the input source. The protection of the input-side converter is important.
- Grid-side controller, which has the following tasks:
  - Control of active power generated to the grid;
  - control of reactive power transfer between the DPGS and the grid;
  - control of dc-link voltage;
  - ensure a high quality of the injected power and
  - grid synchronisation.

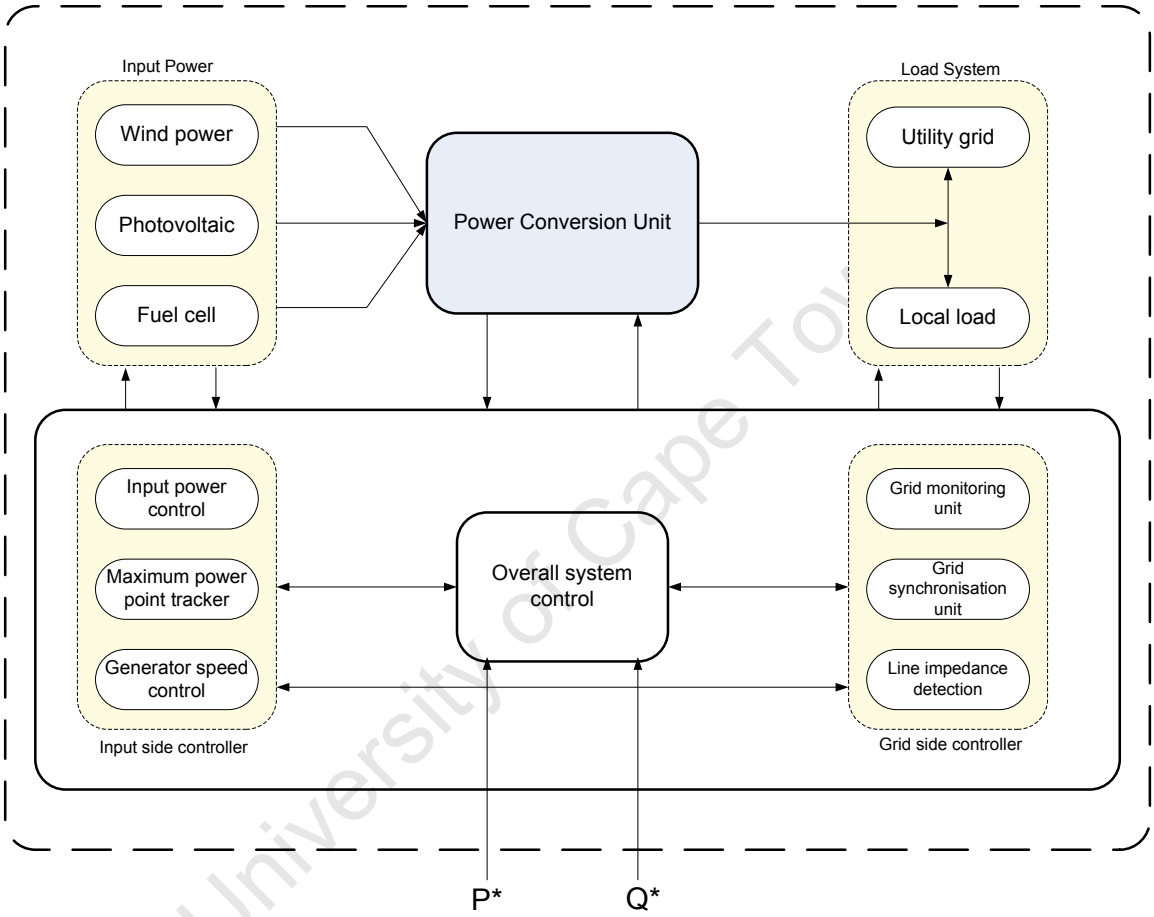

Figure 7-1: General structure for a distributed power system having more than 1 power sources [66].

Additionally, ancillary services such as voltage and frequency regulation, voltage harmonic compensation or active filtering may be requested by the grid operator.
The power conversion unit can have different hardware structures that are closely related to the nature of the input power.

7.2 Control Structure of a DGPS System [66]

The control strategy applied to the grid-side converter consists mainly of two cascaded loops. There is usually a fast internal current loop. This is used to regulate the grid current. The external voltage loop controls the dc-link voltage. The current loop is responsible for power quality issues and current protection. Harmonic compensation and dynamics are important properties of the current controller. The dc-link voltage controller is designed for balancing the power flow in the system. The design of this controller aims for system stability by means of employing slow dynamics. In some literature, the control of the grid-side controller is based on a dc-link voltage loop cascaded with an inner power loop instead of a current loop. In this way, the current that is injected into the utility network is indirectly controlled.

7.2.1 Synchronous Reference Frame

Synchronous reference frame control, also called $dq0$ control, uses a reference frame transformation module, e.g. $abc \rightarrow dq$ to transform the grid current and voltage waveform's into a reference frame that rotates synchronously with the grid voltage. The control variables become dc values. Filtering and controlling are easily achieved. In the $dq0$ structure, the dc-link voltage is controlled as per the required power output. Its output is the reference for the active current controller. The reference for the reactive current is usually set to zero. This is when reactive power control is needed. When the reactive power has to be controlled, a reactive power reference must be imposed on the system. The $dq0$ control structure is normally associated with Proportional Integral (PI) controllers. This is because it behaves satisfactory when regulating dc variables. The matrix transfer function of the controller in dq

coordinates can be written as

$$G_{PI}^{(dq)}(s) = \begin{bmatrix} K_p + \frac{K_i}{s} & 0 \\ 0 & K_p + \frac{K_i}{s} \end{bmatrix} \tag{7.1}$$

where K_p is the proportional gain and K_i the integral gain of the controller. For unity power factor, the controlled current has to be in phase with the grid voltage. The phase angle used by the $abc \rightarrow dq$ transformation module has to be extracted from the grid voltages. The grid voltage is filtered using the arc-tangent function to extract the phase angle.

7.2.2 Stationary Reference Frame Control

Another way to structure the control loops is to use an implementation in stationary reference frame. In this case, the grid currents are transformed into stationary reference frames using the $abc \rightarrow \alpha\beta$ module. Although the control variables are sinusoidal there is a known drawback of the PI controller in failing to remove the steady-state error when controlling sinusoidal waveform's. Employment of other controller types is necessary. The Proportional Resonant (PR) controller has gained popularity in the last decade for the regulation of grid-tied systems. In the PR case, the controller matrix in the stationary reference frame is given by

$$G_{PR}^{(\alpha\beta)}(s) = \begin{bmatrix} K_p + \frac{K_i s}{s^2+\omega^2} & 0 \\ 0 & \frac{K_i s}{s^2+\omega^2} \end{bmatrix} \tag{7.2}$$

where ω is the resonance frequency of the controller, K_p the proportional gain, and K_i the integral gain of the controller. A characteristic of this controller is that it achieves a very high gain close to resonance frequency. This eliminates the steady-state error between the controlled signal and its reference. The width of the frequency band around the resonance point depends on the integral time constant K_i. A low K_i value leads to a very narrow band. A high K_i value leads to a wider band.

7.2.3 Natural Frame Control

The aim of *abc* control is to have an individual controller for each grid current. The different ways to connect the three-phase systems, are e.g. delta and star with or without isolated neutral. The different ways that can be used to control the three-phase systems need to be considered when designing the controller. In the situation of isolated neutral systems, the phases interact with one another. As a result only two controllers are necessary, since the third current is given by Kirchhoff's current law. Three independent controllers are possible by considering the controller design. This is usually the case for hysteresis and dead-beat control. The *abc* control structure is preferred since nonlinear controllers like the hysteresis or the dead beat have a high dynamic performance. The performance of these controllers is proportional to the sampling frequency. The rapid development of digital systems such as digital signal processors or field-programmable gate array is an advantage for such an implementation. Typically, the output of the dc-link voltage controller sets the active current reference. The phase angle of the grid voltages is usually determined using a PLL system. From this, the three current references are created. Each of them is compared with the corresponding measured current. The error is input into the controller. If hysteresis or dead-beat controllers are employed in the current loop, a modulator is not required. The output of these controllers are the switching states of the power converter. Natural frame controllers include:

- PI controllers,
- PR controllers,
- hysteresis controllers and
- dead-beat controllers.

7.2.4 Evaluation of Control Structures

The necessity of voltage feed-forward and cross-coupling terms is a major drawback of the synchronous reference frame control structure. The phase angle of the grid

voltage is required in this implementation. For control structures with PR controllers implemented in stationary reference frame, the complexity of the control is lower than that of the structure implemented in dq frame. The phase angle information is also not required. The filtered grid voltages can be used as a template for the reference current waveform. For control structure implemented in a natural frame, the complexity of the control can be high if an adaptive band hysteresis controller is used for current regulation. A simpler control scheme can be achieved by implementing a dead-beat controller. With this control structure, independent control of each phase can be achieved if three single-phase PLL's are used to generate the current reference.

7.3 Control Strategy Under Grid Faults

The interconnection of a large amount of distributed power generation poses a problem for system stability. Consequently, more stringent demands for interconnection must be met. Synchronisation is of particular concern. The DPGS must be able to ride through short grid disturbances such as voltage and frequency deviations. Grid faults can be classified as either symmetrical or asymmetrical. Control variables can be adversely affected by disturbances. This has a negative influence on the current reference generation. Disturbances compromise the ride-through capability of the DPGS. Typical control strategies include:

- Unity power factor control strategy,
- positive sequence control,
- constant active power control, and
- constant reactive power control.

7.4 Reference Signal Generation for Synchronisation

For implementation with zero reactive power compensation, the injected current has to be synchronised with the grid voltage. Synchronisation algorithms play an important role in the performance of the DPGS, especially under disturbances. The synchronisation algorithm mainly outputs the phase of the grid voltage vector. This is used to synchronise the control variables e.g. synchronising the grid currents with the grid voltages using different transformation modules like $abc \rightarrow dq0$. Different methods to extract the phase angle have been developed and presented in [67].

7.4.1 Zero-Crossing Method

Out of all the techniques, the zero-crossing method has the simplest implementation. However, poor performance has been reported in literature [68], [69].

7.4.2 Filtering of Grid Voltages

The filtering of the grid voltages in different reference frames such as dq or $\alpha\beta$ is possible. The filtering technique encounters difficulty when trying to extract the phase angle when grid variations or faults occur in the utility network. A delay is introduced with the processed signal, which is unacceptable as proper filter design is a necessity.

7.4.3 PLL Technique

As discussed in chapter FOUR, the three-phase PLL technique is a state-of-the-art method used to extract the phase angle of the grid voltages. The three-phase PLL is implemented in a dq synchronous reference frame. The phase angle is obtained from the integration of the grid frequency. This is fed back into the dq transformation module to transform back into the synchronous rotating reference frame. This algorithm has an improved rejection capability of grid harmonics, notches and other

disturbances. Its performance offers an improvement over conventional techniques in the presence of grid unbalance.

7.4.4 Structure of the Proposed Technique

The structure of the proposed method for reference signal generation in current controllers is shown in Figure 7-2.

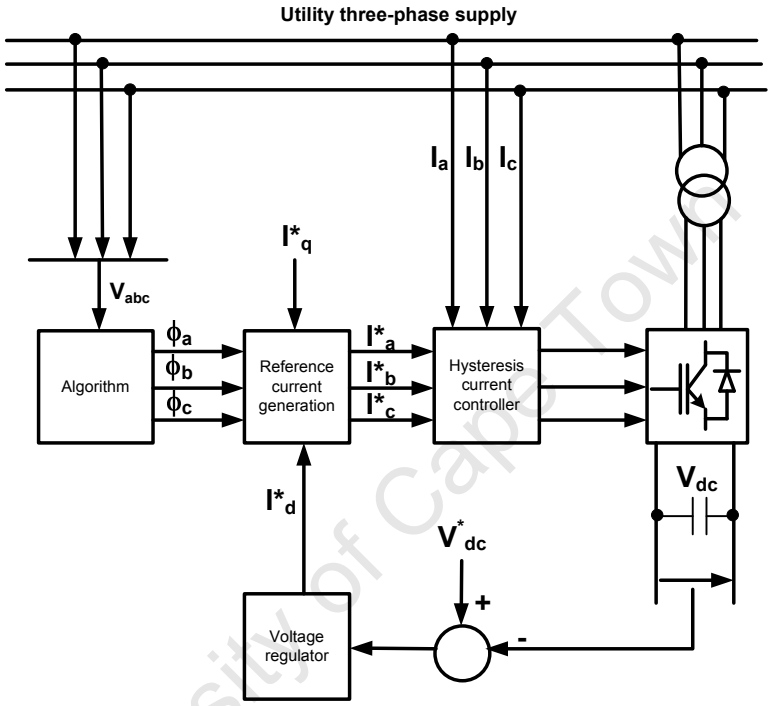

Figure 7-2: Structure of proposed reference frame generation technique.

Conventional methods produce a single phase angle for reference signal generation. The proposed technique estimates the phase angle for each of the three phases. This has a distinct advantage under unbalanced conditions as will be demonstrated in the next sections.

7.4.5 Performance

The effectiveness of the proposed method in reducing the phase error under unbalanced grid conditions and frequency deviations is demonstrated through simulations.

It is compared against conventional methods to generate a synchronisation reference signal.

Frequency Deviations

Grid code demands that the DPGS operate under system frequency deviations. The input signal undergoes a step change in frequency from time $t = 0.5\,\text{s}$ to $1\,\text{s}$. The behaviour of the PLL when the grid frequency is stepped to 3 Hz from the nominal is shown in Figures 7-3 and 7-4. Reference signal generation using the proposed technique is shown in Figures 7-5 and 7-6. The simulations demonstrate that the PLL is unable to generate a stable reference signal for a controller.

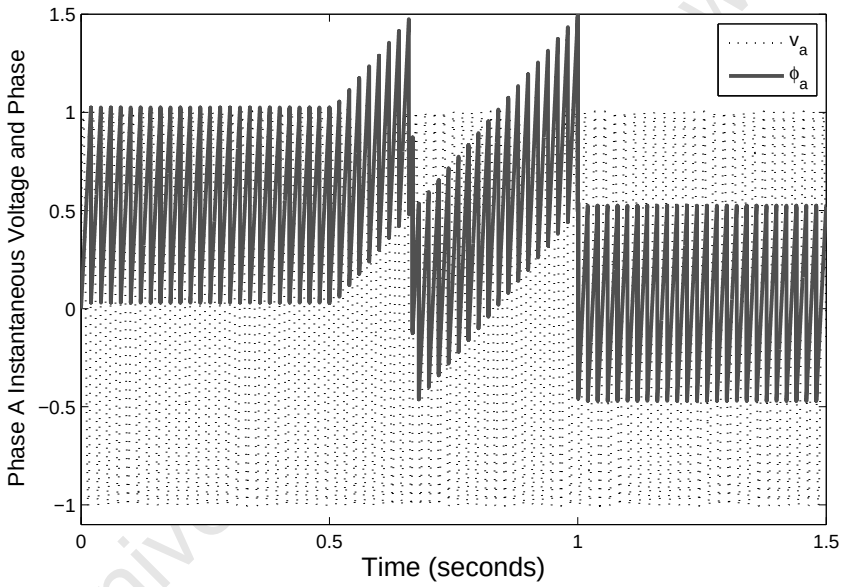

Figure 7-3: Reference signal generation using a PLL under a 3 Hz step change in frequency.

Single Line-Ground Fault

Unbalanced faults are common on the power ground. The single line-ground fault is the most common type of unbalanced fault. The DPGS has to ride through sudden changes in amplitude/phase as is common from unbalanced faults.

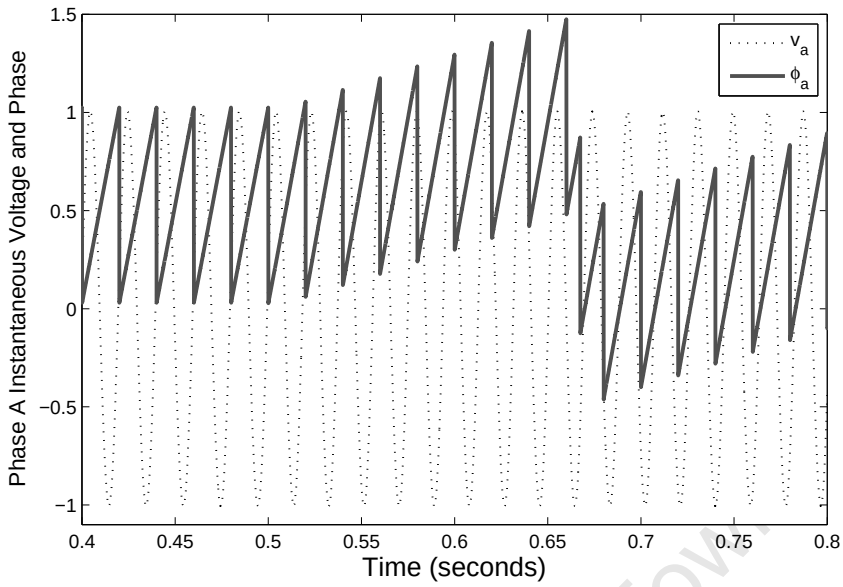

Figure 7-4: Close-up reference of the signal generation using the PLL under a 3 Hz step change in frequency.

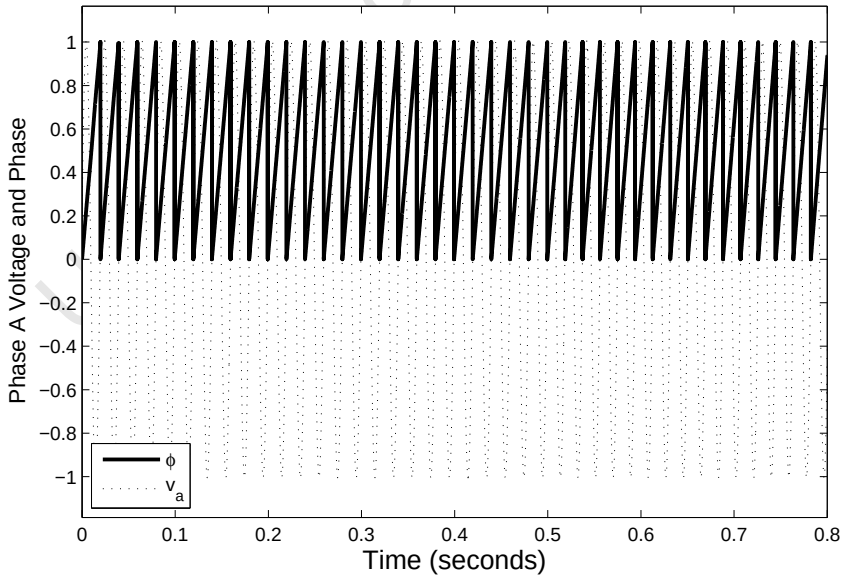

Figure 7-5: Reference signal generation using the nonlinear algorithm under a 3 Hz step change in frequency using the algorithm.

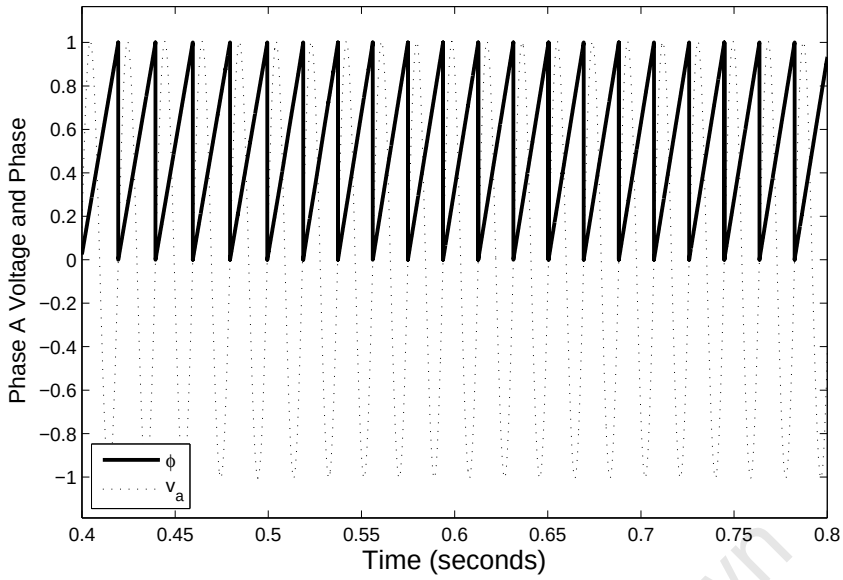

Figure 7-6: Close-up reference signal generation using algorithm under a 3 Hz step change in frequency.

A typical line-ground fault is shown in Figure 7-7, where the input signal undergoes a 50% reduction in voltage and a 30° step in phase simultaneously from time $t = 0.4$ s until $t = 1$ s. The synchronisation method used must be able to rapidly and accurately converge to the new parameters. A comparison of the phase angle estimation with the $dq0$ and algorithm is shown in Figure 7-8. Although the $dq0$ has a faster dynamic response, its steady state error is large. This makes it unsuitable for use in the controller. The maximum steady-state error from the proposed technique is 0.5%. Convergence is reached within two cycles of the nominal voltage. Figures 7-9 and 7-10 show the reference signal generation using the $dq0$ method and the proposed technique respectively.

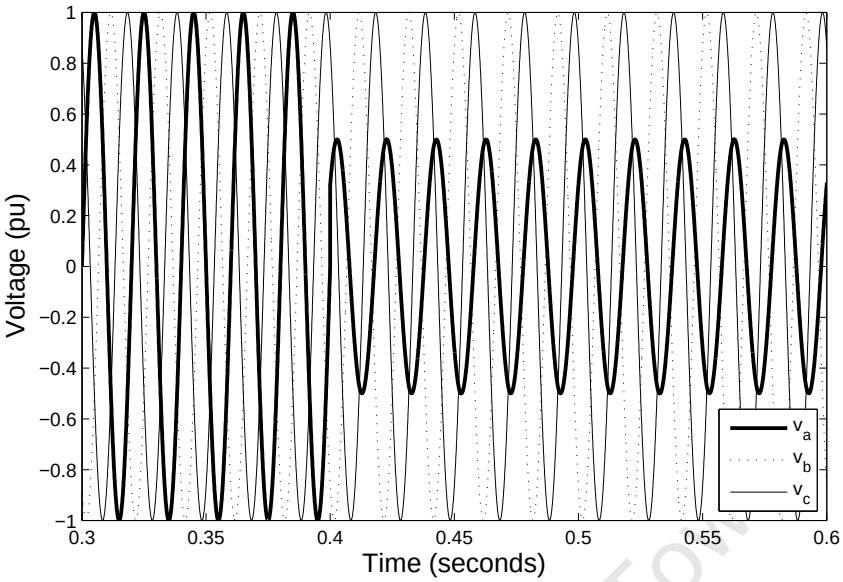

Figure 7-7: Single-phase sag with phase angle jump.

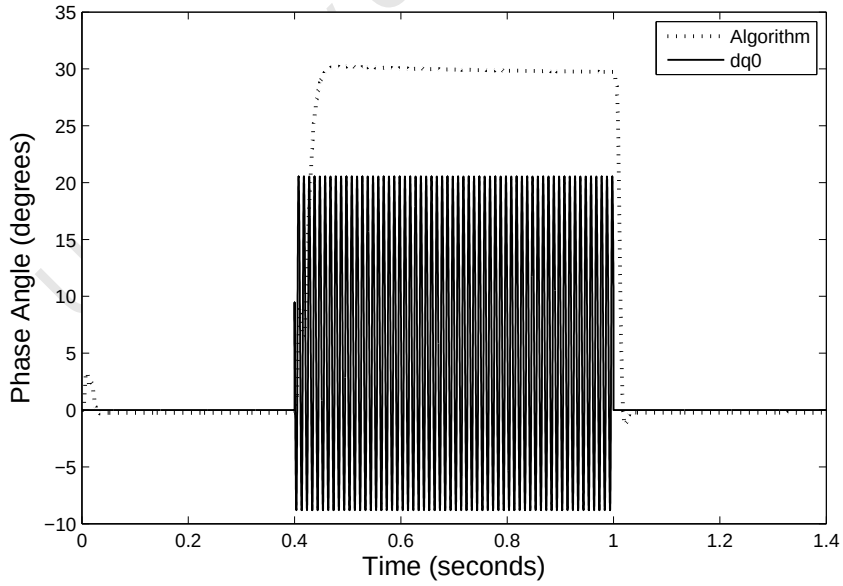

Figure 7-8: Phase angle estimation comparing nonlinear algorithm and $dq0$.

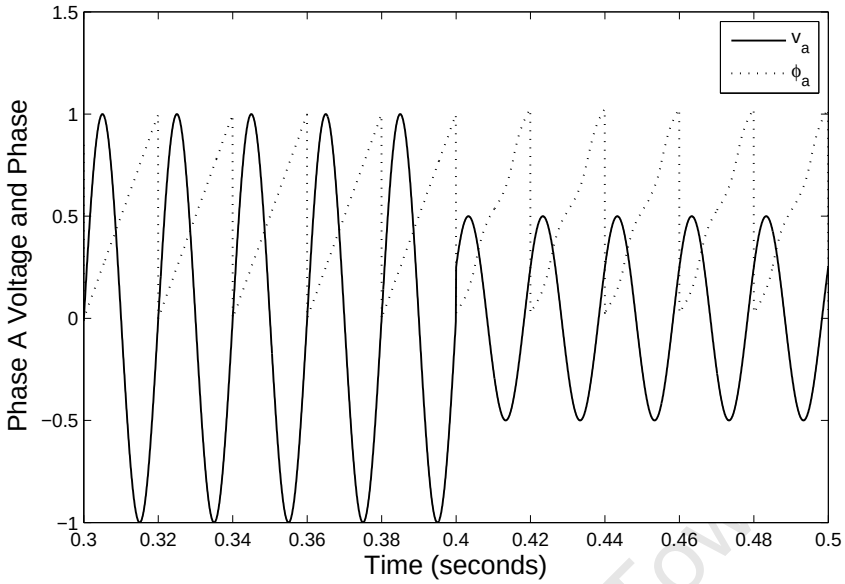

Figure 7-9: Close up of the reference angle generation using the $dq0$ method.

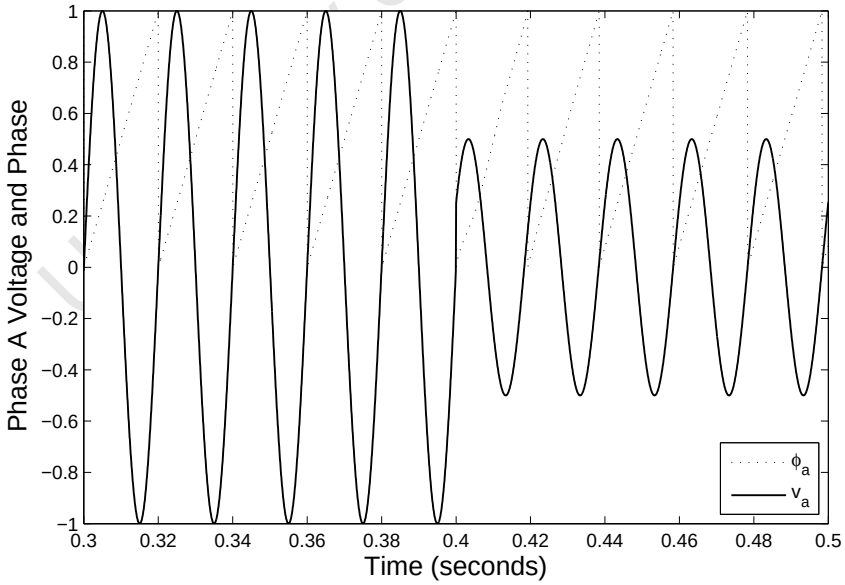

Figure 7-10: Close up of the reference angle generation using the nonlinear algorithm.

Modulated Phase

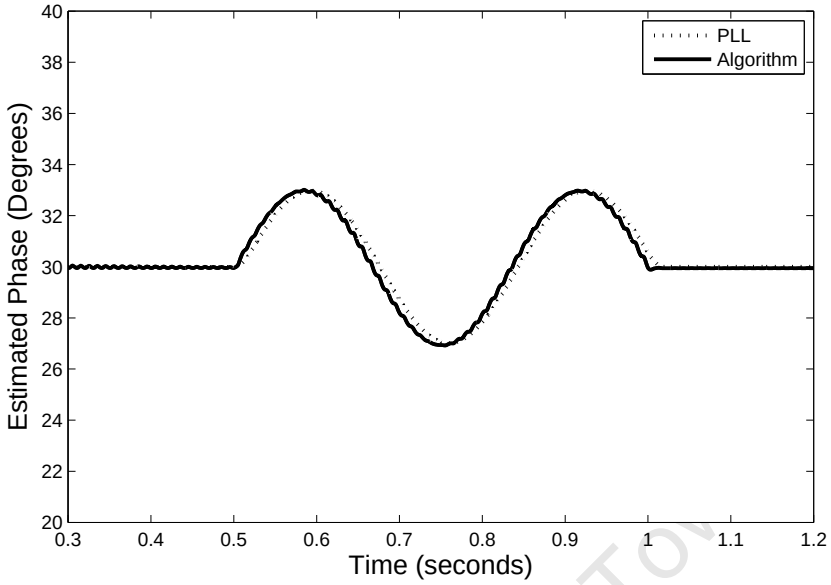

Figure 7-11: Phase tracking of a modulated input signal using the PLL and the nonlinear algorithm.

Figure 7-11 shows a comparison of the PLL and the nonlinear algorithm for a phase modulated input signal. The amplitude and frequency of the modulated signal is 3° and 3 Hz respectively. From the figure, it can be seen that the proposed technique is able to track the modulated phase at 1/2 cycle (10 ms) quicker than the PLL.

7.5 Application to Protect the Doubly-Fed Induction Generator

As a renewable energy resource, wind energy conversion systems have received tremendous growth due to economics and environmental concerns related to fossil fuels. This has prompted the design and implementation of many wind energy conversion systems across the globe. The preferred topology that is used for wind generators in the megawatt range is the Doubly Fed Induction Generator (DFIG). The advantages of this topology include high efficiency, good controllability, a wide range of speed

operation and most importantly, a reduction in the cost of the power electronic converters as compared to stator-controlled systems [70]. These generators are designed to support the grid by delivering rated power over a large speed range. The power flow is controlled by bi-directional power electronic converters that attempt to keep the output voltage constant. Problems occur when the grid experiences a disturbance (in particular sag). This makes the power electronics of the DFIG vulnerable to failure. Failure of the system during a sag can introduce instability problems on the power network. It is therefore important that the wind energy conversion system is controlled in such a manner so as to protect the components from failure. Although fault mitigation techniques exist, the deciding factor that could prevent catastrophic failure is the time required to detect the sag. It is therefore imperative to incorporate a mitigation strategy based on sag detection into the control system of a doubly-fed induction generator for rapid response protection.

7.5.1 Description of the Overall System

For variable speed generation, the wound rotor induction generator has proven to be extremely alluring since the converters are located in the rotor circuit, thus reducing the rating and cost of the converter requirements since they need only handle the rotor power. Figure 7-12 represents a schematic representation of the vector control of a typical DFIG system. The Field Orientated Control (FOC) of the machine is achieved via the rotor-side converter. This allows for independent control of the torque and rotor excitation of the machine. The supply-side converter is responsible for maintaining a constant dc-link voltage, as well as control over the power factor [70], [71]. Rotor control of the induction machine is achieved in the synchronously rotating *dq* reference frame. The D-axis is aligned with the stator-flux vector position, which sets the Q-axis stator-flux component to zero. In this way, a decoupled control between the electrical torque and the magnetic field is obtained [72], [73].

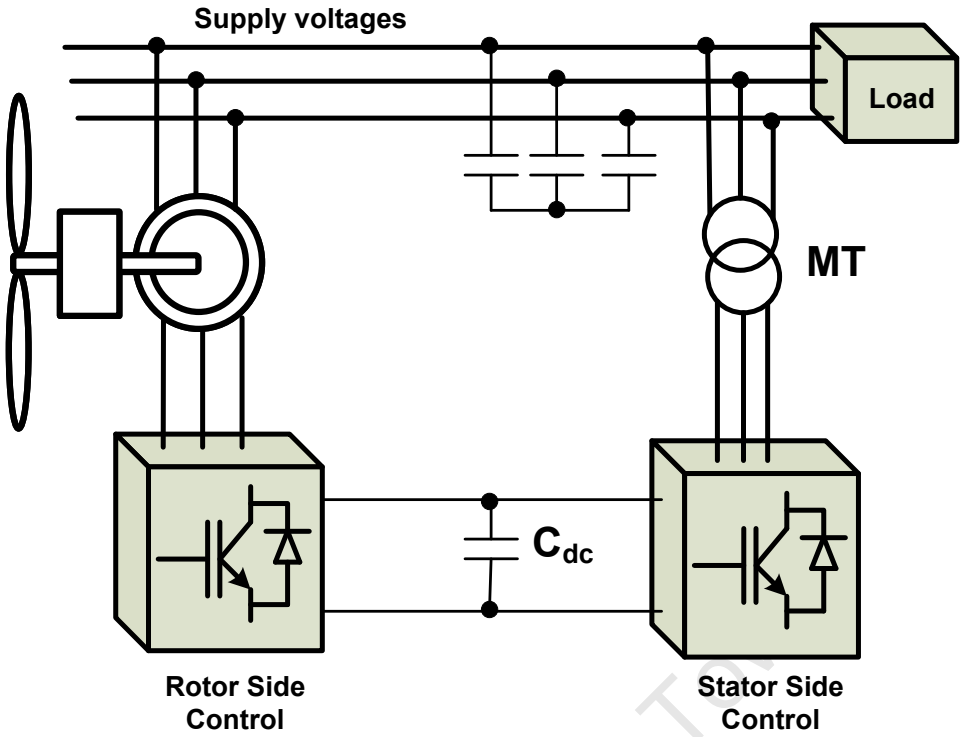

Figure 7-12: Schematic representation of the vector control system.

7.5.2 Stator Side Control

The supply-side converter is used to keep the dc-link voltage constant, regardless of the rotor power direction. A vector control approach is used, whereby independent control of active and reactive power is achieved. The synchronous reference frame is orientated along the supply voltage vector. i_{De} is used to establish the dc-link voltage and i_{Qe} is used to regulate the reactive power. Figure 7-13 illustrates the schematic representation of the vector control for the supply-side converter.

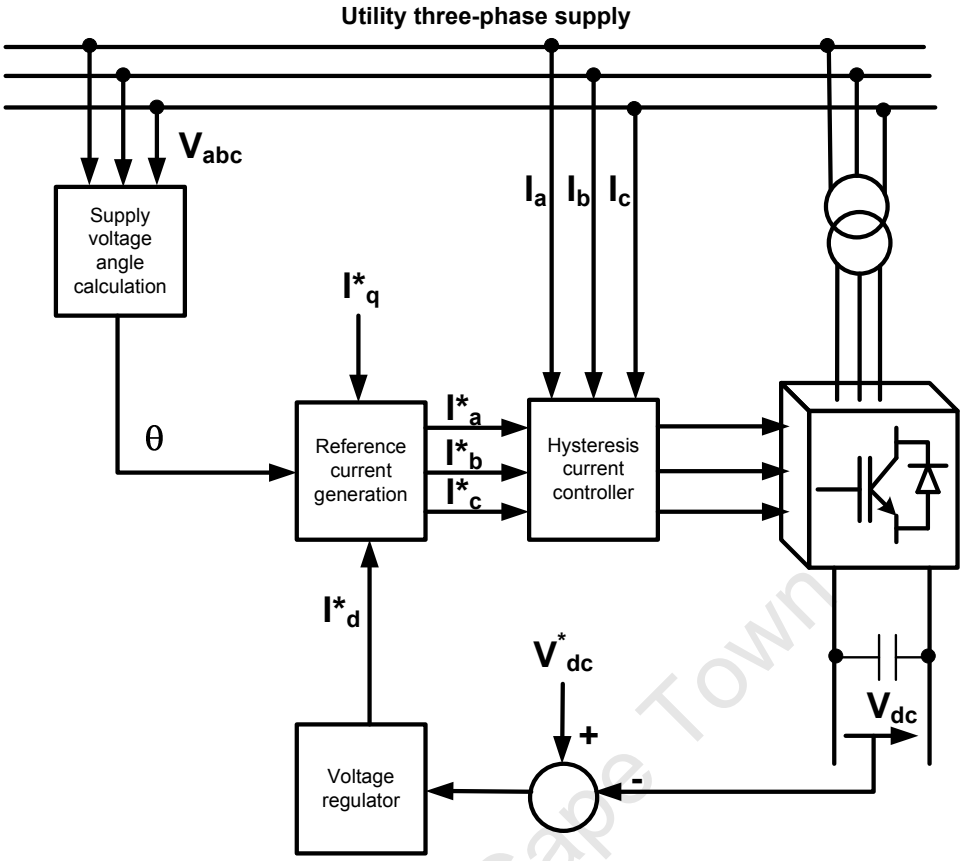

Figure 7-13: Schematic representation of a control system for the supply-side converter

7.5.3 The Threat of Sags

Voltage sag at the terminals of an induction motor can produce transient currents and transient torques. This is well documented in [74] and [75]. Reference [74] discusses the threat of sags on the converter of the DFIG. In [75], a technique is proposed for ride through where a set of resistors is connected to the rotor circuits. A thyristor is used to control the firing of a discharge resistor that is connected in parallel with the rotor circuit. No experimental results were shown for this proposed solution. The results show the machine operating under rated conditions at 25% above synchronous speed without any mechanisms to detect and compensate for voltage sags. Figure 7-14 shows the grid voltage whereby a sag in voltage of 0.5 pu. is experienced at 0.5 s and lasts for 100 ms. Figure 7-15 shows the rise in stator currents as a result of the voltage sag [76].

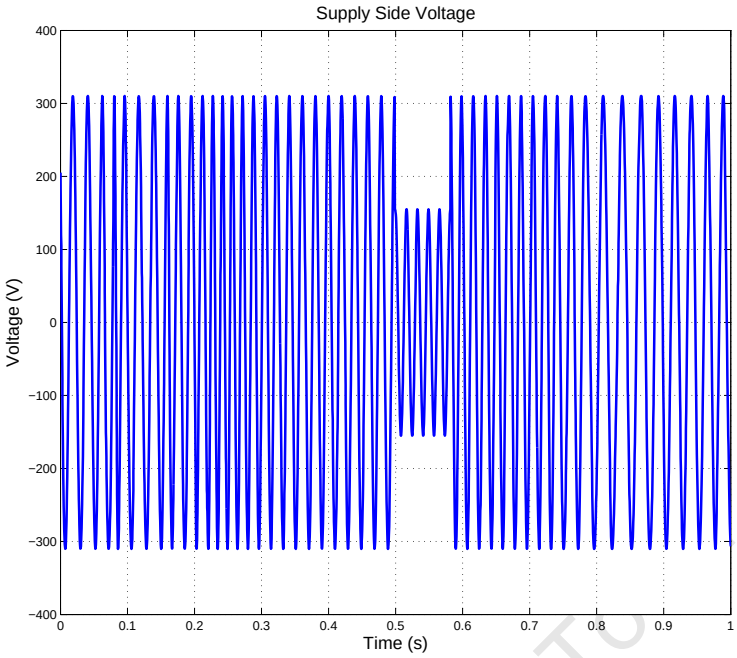

Figure 7-14: System supply voltage under sag conditions.

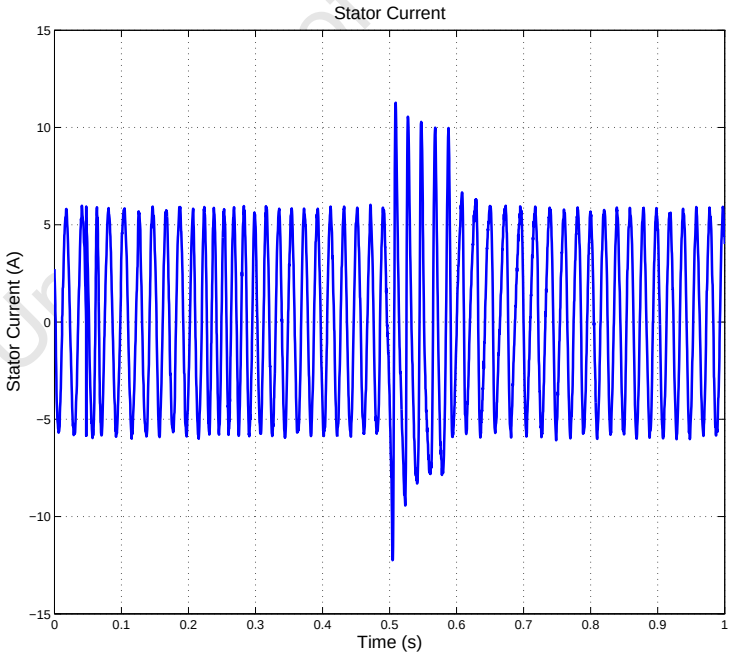

Figure 7-15: Stator current with no mitigation implemented.

7.5.4 Proposed Mitigation Strategy

Figure 7-16 gives an overview of the proposed mitigation strategy. The stator voltage signals from the transducers are sent as input to the nonlinear algorithm. The output of the nonlinear algorithm is a trigger signal that represents sag inception and recovery. The trigger signal is sent to a driver for rapidly switching the discharge resistor R_d on for the sag duration. This is achieved by opening all the power switches and transferring the excess energy into the discharge resistor, R_d. This limits the excess currents. The response of the filter during the sag is determined by the time constant of the discharge resistor and dc link capacitance.

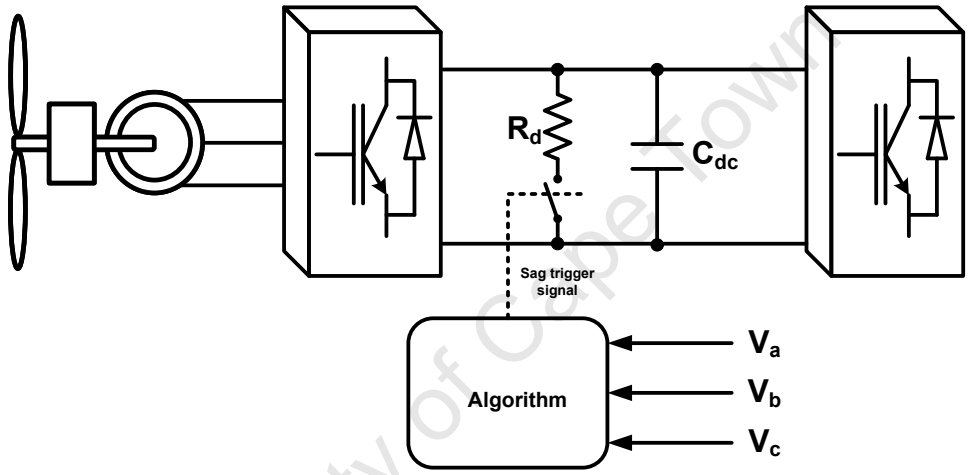

Figure 7-16: Overview of proposed ride through strategy.

7.5.5 Experimental Test System

The Wound Rotor Induction Machine (WRIM) used is a 2.2 kW, 3-phase, 380 V, 50 Hz, 4-pole machine. Two hysteresis current controlled converters are placed in the rotor circuit, which provides the supply and rotor-side control. Extra resistors and chokes are added to the supply-side converter, which are located between the 3-phase variac and the supply-side converter. The extra resistors and inductors added onto the supply-side converter are, R = 0.1 Ω and L = 20 mH. The dc-link voltage is maintained at 300 V and the supply-side 3-phase voltage is set to 100 V (i.e. output of the variac). The DC drive used to emulate the wind turbine consists of a 2.2 kW

dc machine, which is torque controlled by an ac/dc thyristor converter. A dSPACE, DS1104 controller card is used to perform the computational and control tasks for both converters. The converters used are standard 100 A commercial IGBT inverters. The inverters are switched at a maximum frequency of 5 kHz during the simulated and experimental tests, due to the computational constraints of the controller card. However, this switching frequency employed in the prototype confirms that the control techniques can be extended to higher power levels.

7.5.6 Experimental Results

A trigger signal is generated when a sag of below 90% of the rated voltage is detected. This is maintained until the voltage is recovered to its nominal, at which point the output goes low. It is evident from the figure that the detection and trigger happens almost instantaneously. This proves to be extremely valuable as the necessary steps may now be taken to prevent over-currents and over-voltages from occurring in the system. In [77], it was shown that the biggest influence on detection time is point on wave. Sags that occur close to the zero crossing have the fastest detection time. For sags with a point of wave of 90°, the detection time is marginally slower (5 ms in the worst case). The key of the proposed mitigation strategy is to provide a rapid discharge path for the excess currents during the sag. The rating of the discharge resistor is not critical. It should be rated to carry the maximum anticipated currents. The rapid response of the controller ensures that transients at the onset and recovery of the sag and recovery are contained.

7.5.7 Experimental Results Achieved with No Mitigation

Figures 7-17 and 7-18 show the experimental results obtained with no mitigation applied. The supply voltage is reduced by 40% for a duration of 280 ms to simulate a field sag. The increase of current is a concern for the converter equipment.

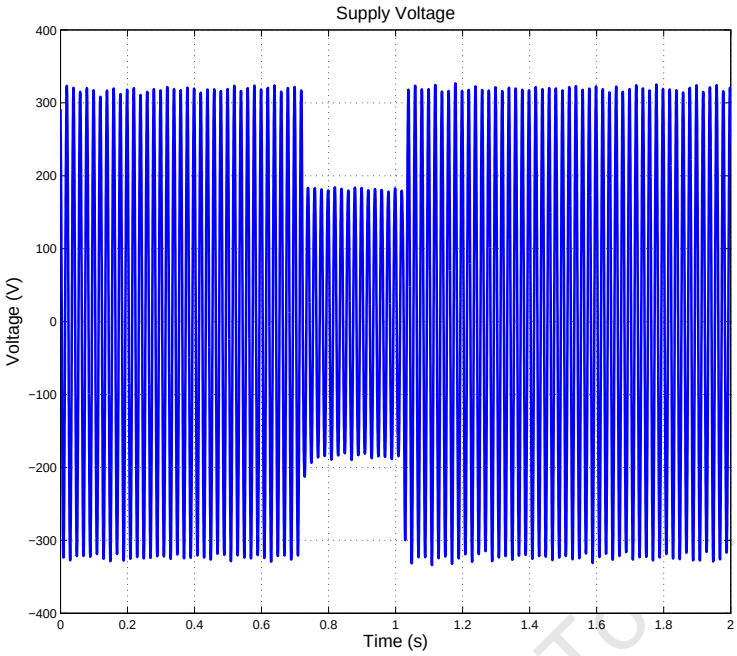

Figure 7-17: System supply voltage under sag conditions. [76].

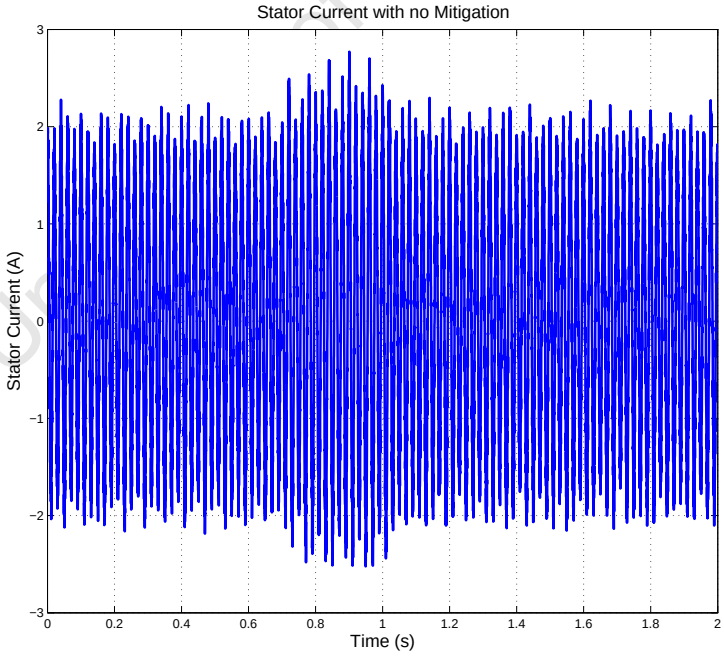

Figure 7-18: Stator current with no mitigation implemented. [76].

7.5.8 Experimental Results Achieved with the Proposed Mitigation Strategy

The system was experimentally tested using the proposed mitigation strategy. From Figure 7-20 it is clear that the stator current pose no danger to the power electronic converter. Further research must consider the mechanical torque of the turbine and ensure that the electrical torque is sufficient to provide control, especially during long duration sags. This could be done in combination with the pitch controller.

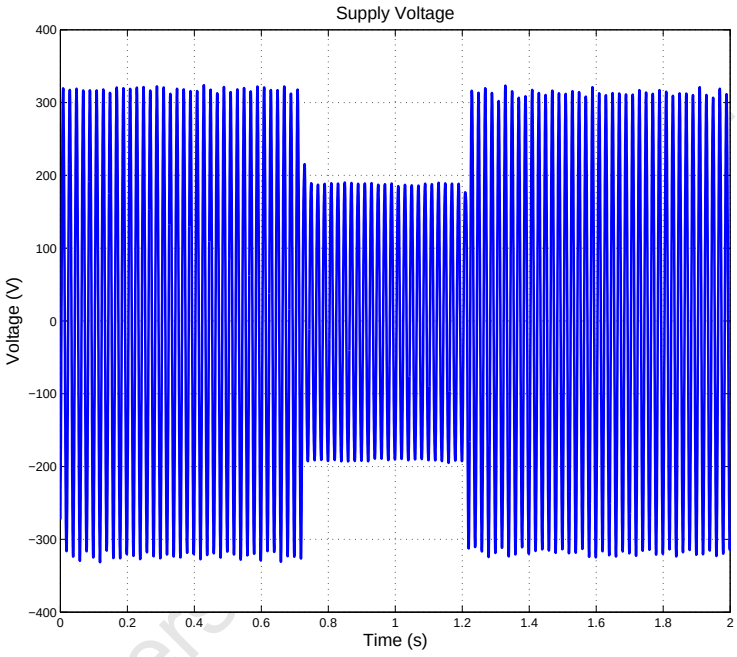

Figure 7-19: System supply voltage under sag conditions. [76].

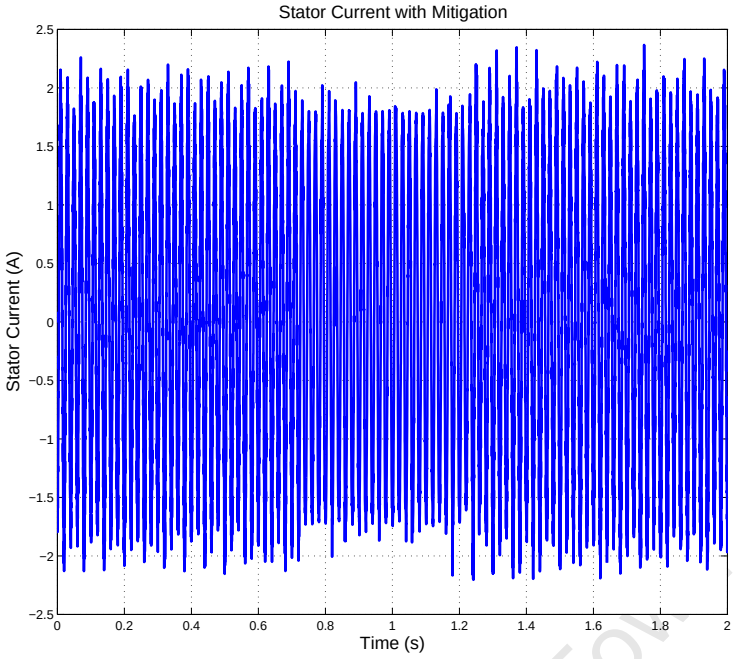

Figure 7-20: Stator current with proposed mitigation strategy implemented. [76].

7.6 Concluding Remarks

This chapter has discussed the control and protection of the DPGS. The control structures and strategies relevant to the DPGS were presented. An overview of grid synchronisation algorithms was given. Simulations were performed to evaluate the different methods used to generate a synchronisation reference signal. The proposed method was compared to the conventional PLL and $dq0$ methods. A frequency domain step response was used to validate the method. The method was further tested against grid faults (single line-ground) and a modulated phase. The results show improved performance of the proposed system as compared to the conventional methods whilst ensuring high system dynamics. The algorithm was further applied to the protection of a DGPS, in particular the DFIG. This chapter has shown that the algorithm can be effectively used as a control strategy to protect the DFIG under grid disturbances. Simulation and experimental results confirm the effectiveness of the solution.

Chapter 8

Summary and Conclusions

8.1 Work Presented

This thesis presented the application of a novel nonlinear adaptive algorithm to estimate amplitude, phase, frequency and symmetrical components. The motivation for the choice of applications was to ensure that the nonlinear adaptive algorithm's tracking ability is thoroughly tested under diverse power system conditions. It is also to ensure that the research questions posed in chapter ONE have been answered. The methods presented are applied to problems where shortcomings with conventional techniques were identified. A background of power quality and signal processing techniques is presented in chapter ONE. Chapter TWO presented a brief mathematical description of the proposed system. Issues of convergence and parameter settings were discussed.

In chapter THREE, the nonlinear adaptive algorithm was applied to the detection of sags/swells. The motivation for this was to test the amplitude tracking ability of the nonlinear filter. A comparison was made of the nonlinear adaptive algorithm against existing methods and its performance was evaluated in terms of amplitude variations, robustness and noise immunity, differing sag gradients and point-on-wave. The results show that the magnitude of the sag/swell does influence detection time. A detection time of 1 ms can be achieved for sags $\leq 30\%$ and swells $\geq 160\%$. Simula-

tions showed that the filter is able to track sags/swells more effectively than existing methods in the presence of noise. For a noise level of $\sigma^2 = 0.1$, it was found that the PV and RMS methods can produce errors of up to 16.5% and 3.8% respectively. The proposed method was able to contain the error to within 0.95%. The filter was able to effectively track sags/swells occurring at different point on waves. It was found that sags/swells occurring at close to 90° have can respond by up to 3 ms slower than sags occurring at the zero crossing.

Chapter FOUR presented a new method of phase and frequency estimation. The nonlinear adaptive filter was shown to be able to estimate step changes of up to 20 Hz in frequency to within 0.02% accuracy and 1 cycle. A comparison was made to the PLL. The PLL can only accommodate step changes of up to 5 Hz. There is also an error of 0.02% and a delay of up to six cycles using the PLL. In the presence of harmonics and noise (measured up to 22% THD and 7 db noise), the nonlinear filter was able to estimate the amplitude to within 0.3% and the frequency to within 0.1%. A modulated frequency of up to 3 Hz to within 0.01% of the steady state error and a 10 ms delay were tracked. This is an improvement of 100 ms when compared to the PLL. The DFT and nonlinear filter are both able to estimate step changes in phase to within 2%. However, the nonlinear filter showed a 15 ms improvement in response time over the DFT. For three-phase systems, commonly used methods such as the DFT and $dq0$ suffer in the presence of unbalance. Errors of up to 100% were recorded with the $dq0$ method. The three-phase PLL compares favourably to the nonlinear filter in terms of performance. Errors of 15% and 11% were recorded by the PLL and the nonlinear filter respectively. When combined, the results and discussions of chapters THREE and FOUR answer research question one.

A mathematical model of dynamic symmetrical component estimation is derived in chapter FIVE. For step changes in amplitude, it was found that the DFT and the nonlinear filter yield symmetrical components with the same accuracy. The nonlinear filter offers an improvement in terms of response time of up to 5 ms. For step

changes in phase, the steady state error from both the DFT and the nonlinear filter is approximately 0.5%. A response time difference of up to 10 ms can be achieved by employing the nonlinear adaptive filter. It was found that for noise levels of $\sigma^2 > 0.03$, the influence of noise impacts the DFT significantly. The proposed method is able to offer improved accuracy. Consequently, research question two was answered in chapter FIVE.

The application of the core building blocks to sag analysis was presented in chapter SIX. An online method for characterising voltage sag using the method of Bollen and Zhang was presented. The system is further capable of extracting single-event sag indices. Conventional methods such as the RMS only provide magnitude information. The proposed system is able to offer amplitude and phase information. The method has been successfully benchmarked against the DFT.

Chapter SEVEN investigated the control and protection of a DPGS. Simulations were performed to evaluate different methods of generating a synchronised reference signal. The proposed method was compared to the conventional PLL and $dq0$ methods. A frequency domain step response was used to validate the method. The method was further tested against grid faults (single line-ground) and a modulated phase. The results show improved performance of the proposed system as compared to the conventional methods, whilst ensuring high system dynamics. The filter is further applied to the protection of a DGPS, in particular the DFIG. It has been shown that the detection strategy of chapter ONE can be applied to protect the DFIG under grid disturbances. Simulation and experimental results confirm the effectiveness of the solution. Research questions three to five have been answered in chapters SIX and SEVEN.

This thesis has demonstrated that the presence of harmonics, noise and disturbances do not adversely affect the filter's performance. The performance of the nonlinear filter has been thoroughly evaluated through a detailed consideration of research

questions six to nine listed in chapter ONE. The presentation and performance of the filter has demonstrated its superiority over existing methods. The results and discussions presented throughout the thesis demonstrate that the objectives of the thesis have been met.

8.2 Proposed Future Research

A summary of some research areas identified as potential areas of application is provided in this section. Essentially, potential applications will include any power system application that requires amplitude, phase or frequency estimation. Examples of such problems include:

- **Generator voltage control**: The Automatic Voltage Regulator (AVR) in a synchronous machine regulates the terminal voltage while supplying power to the system. Conventionally, a diode bridge or thyristor rectifier is used to convert the sensed terminal voltage from ac to dc. The dc voltage is compared to the dc set point in the AVR to generate an error signal. The nonlinear algorithm can be applied to track the terminal voltage of a synchronous machine for step changes in load. This can then be compared to the conventional method of sensing the terminal voltage using a diode bridge rectifier.

- **Custom power applications**: Custom power devices such as the STATCOM require an instantaneously estimated voltage and phase for control of the injection voltage or current. Techniques that are available to continuously control the output voltage waveform include the instantaneous reactive power theory. However, existing methods pose problems under conditions of unbalance, noise and harmonics. Hence adaptive filtering is more suitable. The nonlinear algorithm can be used to track the amplitude and phase in real-time. These signals can be sent through to the control loop for improved dynamic response.

- **Noise reduction for zero crossing applications**: Zero-crossings of sinusoidal signals are used for component synchronisation, especially in many ap-

plications in power electronics. Events such as capacitor switching and fault can result in multiple zero crossings on the ac waveform. A method that can only extract the fundamental component of a noisy signal can improve the response of control equipment that rely on zero crossings. Other techniques include predictive Finite Impulse Response (FIR) filters and bandpass filters with negative phase delay at a specific frequency. The algorithm can be used to instantaneously estimate the zero-crossing of the fundamental component of a multi-component signal.

- **Simplification for transient analysis**: The continuous discrete wavelet transform is a useful tool for characterising transient events. However, processing requirements are a concern for real-time implementation. A reduction in processing time can be achieved if the fundamental component is extracted from the input signal. The remaining signal can be processed using wavelets. The processing performance can be further investigated with different event types.

Bibliography

[1] "Data file format for power quality data interchange," IEEE P1159 Task Force 3 - Monitoring Electric Power Quality, 2002, accessed 24 April 2006. [Online]. Available: http://grouper.ieee.org/groups/1159/2/testwave.html

[2] J. Arilaga, N. R. Watson, and S. Chen, *Power System Quality Assessment.* England: Wiley, 2001.

[3] M. F. McGranaghan, R. C. Dugan, H. W. Beaty, and S. Santoso, *Electric Power Systems Quality.* McGraw Hill, 2002.

[4] *IEEE Standard Dictionary of Electrical and Electronics Terms*, IEEE Standard 100 Std., 1996.

[5] P. Kundur, *Power System Stability and Control.* New York: McGraw Hill, 1994.

[6] T. Lin and A. Domijan, "Real-time measurement of power disturbances: Part 1. survey and a novel complex filter approach," *Electric Power Systems Research*, vol. 76, no. 12, pp. 1027–1032, Aug. 2006.

[7] ——, "Real-time measurement of power disturbances: Part 2. implementation and evaluation of the novel complex filter/recursive algorithm," *Electric Power Systems Research*, vol. 76, no. 12, pp. 1033–1039, Aug. 2006.

[8] T. Sidhu and M. Sachdev, "An iterative technique for fast and accurate estimation of power system frequency," *IEEE Trans. Power Delivery*, vol. 13, no. 1, pp. 109–115, Jan. 1998.

[9] J. Delao, H. Altuve, and I. Diaz, "A new digital filter for phasor computation-part 1: theory," *IEEE Trans. Power Syst.*, vol. 15, no. 1, pp. 1026–1031, Apr. 2000.

[10] J. Delao, "New family of digital filters for phasor computation," *IEEE Trans. Power Delivery*, vol. 15, no. 1, pp. 86–91, Apr. 2000.

[11] P. Pillay and A. Battacharjee, "Application of wavelets to model short-term power system disturbances," *IEEE Trans. Power Syst.*, vol. 11, no. 4, pp. 2031–2037, Nov. 1996.

[12] S. Santoso and P. Hoffman, "Power quality assessment via wavelet transform analysis," *IEEE Trans. Power Delivery*, vol. 11, no. 2, pp. 924–930, Apr. 1996.

[13] D. Karras, "Improved defect detection using support vector machines and wavelet feature extraction based on vector quantization and svd techniques," in *Neural Networks, 2003. Proceedings of the International Joint Conference on*, 2003.

[14] Z. Luo and Z. Shi, "On electronic equipment fault diagnosis using least squares wavelet support vector machines," in *Intelligent Control and Automation, 2006. WCICA 2006. The Sixth World Congress on*, 2006.

[15] N. Ruiz, M. Rosa, F. Lopez, D. Martinez, and R. Mata, "New algorithm for searching minimum bit rate wavelet representations with application to multiresolution-based perceptual audio coding," in *Pattern Recognition, 2000. Proceedings. 15th International Conference on*, 2000.

[16] Z. Wenhui, L. Lili, Y. Xiuqing, and G. Weikang, "Wavelet transform based new methods for voltage flicker signal and harmonic detection," in *Power Electronics and Drive Systems, 2003. PEDS 2003. The Fifth International Conference on*, 2003.

[17] S. Sadkhan, N. Abdulmuhsen, and N. Al-Tahan, "A proposed analog speech scrambler based on parallel structure of wavelet transforms," in *Radio Science Conference, 2007. NRSC 2007. National*, 2007.

[18] H. Zheng-you, C. Xiaoqing, and L. Guoming, "Wavelet entropy measure definition and its application for transmission line fault detection and identification; (part *i*: Definition and methodology)," in *Power System Technology, 2006. PowerCon 2006. International Conference on*, 2006.

[19] B. Akin, U. Orguner, and A. Ersak, "A comparative study on kalman filtering techniques designed for state estimation of industrial ac drive systems," in *Mechatronics, 2004. ICM '04. Proceedings of the IEEE International Conference on*, 2004.

[20] M. K. Ghartemani and M. R. Iravani, "A nonlinear adaptive filter for online signal analysis in power systems: Applications," *IEEE Trans. Power Delivery*, vol. 17, no. 2, pp. 617–622, Apr. 2002.

[21] A. Ziarani and A. Konrad, "A nonlinear adaptive method of elimination of power line interference in *ecg* signals," *IEEE Trans. Biomed. Eng.*, vol. 496, no. 6, pp. 540–547, Jun. 2002.

[22] R. Stockwell, L. Mansinha, and R. Lowe, "Localization of the complex spectrum: the s transform," *IEEE Trans. Signal Processing*, vol. 44, no. 4, pp. 998–1001, Apr. 1996.

[23] O. Poisson, P. Rioual, and M. Meunier, "New signal processing tools applied to power quality analysis," *IEEE Trans. Power Delivery*, vol. 14, no. 2, pp. 561–566, Nov. 1999.

[24] V. Terz and D. Markovic, "Symmetrical components estimation through non-recursive newton type numeric algorithm," *IEEE Trans. Power Delivery*, vol. 18, no. 2, pp. 359–363, Nov. 2003.

[25] M. Bettayeb and U. Qidwai, "Recursive estimation of power system harmonics," *Electric Power Systems Research*, vol. 47, no. 2, pp. 143–152, 1998.

[26] A. Girgis, W. Chang, and E. Makram, "A digital recursive method for on line tracking of power system harmonics," *IEEE Trans. Power Delivery*, vol. 6, no. 3, pp. 1153–1160, Nov. 1991.

[27] L. Lai, W. Chan, C. Tse, and A. So, "Real-time frequency and harmonic evaluation using artificial neural networks," *IEEE Trans. Power Delivery*, vol. 49, no. 1, pp. 52–57, Apr. 1999.

[28] P. Dash, P. Jena, and M. Salama, "An adaptive linear combiner for on-line tracking of power system harmonics," *IEEE Trans. Power Syst.*, vol. 11, no. 3, pp. 1730–1735, Apr. 1996.

[29] D. McNamara, J. Majo, and A. Ziarani, "Power line interference elimination on telephone loops," in *Instrumentation and Measurement Technology Conference, 2005. IMTC 2005. Proceedings of the IEEE*, 2005.

[30] A. K. Ziarani and A. Konrad, "A method of extraction of non-stationery sinusoids," *Elsevier Science - Journal of Signal Processing*, vol. 84, no. 8, pp. 1323–1346, Apr. 2004.

[31] P. Pillay, A. K. Ziarani, and H. Douglas, "Broken rotor bar detection in induction machines with transient operating speeds," *IEEE Trans. Energy Conversion*, vol. 20, no. 1, pp. 135–141, Mar. 2005.

[32] M. H. J. Bollen and L. D. Zhang, "Characteristic of voltage dips (sags) in power systems," *IEEE Trans. Power Delivery*, vol. 36, no. 2, pp. 827–832, Apr. 2000.

[33] A. Ziarani, "Extraction of non-stationary sinusoids," Ph.D. dissertation, University of Toronto, Toronto, Canada, 2002.

[34] B. M. Weedy and B. J. Cory, *Electric Power Systems*. New York: Wiley, 1998.

[35] M. H. J. Bollen, *Understanding Power Quality Problems*. New York: IEEE Press, 1999.

[36] B. P. Roberts, "Energy storage applications for large scale power protection systems," in *Proc. IEEE Transmission and Distribution Conference and Exposition*, 2001, pp. 1157–1160.

[37] P. Wang, N. Jenkins, and M. H. J. Bollen, "Experimental investigation of voltage sag mitigation by an advanced static var compensator," *IEEE Trans. Power Delivery*, vol. 13, pp. 1461–1467, Oct. 1998.

[38] J. C. Gomez and G. N. Campetelli, "Voltage sag mitigation by current limiting fuses," in *Proc. IEEE Industry Applications Conference*, 2000, pp. 3202–3207.

[39] N. S. Tunaboylu, J. E. R. Collins, and P. R. Chaney, "Voltage disturbance evaluation using the missing voltage technique," in *Proc. IEEE International Conference on Harmonics and Quality of Power*, 1998, pp. 577–582.

[40] X. Xiangning, X. Yonghai, and L. Lianguang, "Simulation and analysis of voltage sag mitigation using active series voltage injection," in *Proc. IEEE International Conference on Power System Technology*, 2000, pp. 1317–1322.

[41] A. C. Parsons, W. M. Grady, and E. J. Powers, "A wavelet-based procedure for automatically determining the beginning and end of transmission system voltage sags," in *Proc. IEEE PES Winter Meeting*, 1999, pp. 1310–1315.

[42] M. H. J. Bollen, "Voltage sag analysis," IEEE Tutorial Course, Oct. 1999, TP139-0.

[43] H. S. Song and K. Nam, "Instantaneous phase-angle estimation algorithm under unbalanced voltage-sag conditions," in *Proc. Inst Elect. Eng.*, 2000, pp. 409–415.

[44] M. Wang and Y. Sun, "A practical, precise method for frequency tracking and phasor estimation," *IEEE Trans. Power Delivery*, vol. 19, no. 4, pp. 1547–1552, Apr. 2004.

[45] M. K. Ghartemani, "A novel three-phase magnitude-phase-locked loop system," *IEEE Trans. Circuits Syst. I*, vol. 53, no. 8, pp. 1792–1802, Aug. 2006.

[46] *Electromagnetic compatibility (EMC) - Assessment of emission limits for distorting loads in MV and HV power systems*, IEC Standard 61000-3-6 Std., 1996.

[47] C. Fortescue, "Method of symmetrical coordinates applied to the solution of polyphase networks," *Trans. AIEE*, vol. 37, no. 2, pp. 1027–1140, Nov. 1918.

[48] M. Karimi-Ghartemani and H. Karimi, "Processing of symmetrical components in the time domain," *IEEE Trans. Power Syst.*, vol. 22, no. 2, pp. 572–579, May 2007.

[49] A. M. Stankovic, H. Lev-Ari, and M. M. Perisic, "Analysis and implementation of model-based linear estimation of dynamic phasors," *IEEE Trans. Power Syst.*, vol. 15, no. 2, pp. 1062–1068, Aug. 2000.

[50] A. M. Stankovic and T. Aydin, "Analysis of asymmetrical faults in power systems using dynamic phasors," *IEEE Trans. Power Syst.*, vol. 19, no. 2, pp. 1903–1910, Nov. 2004.

[51] R. A. Flores, I. Y. H. Gu, and M. H. J. Bollen, "Positive and negative sequence estimation for unbalanced voltage dips," in *Proc. IEEE Power Eng. Soc. General Meeting*, vol. 4, Jul. 2003, pp. 2498–2502.

[52] G. Andria and L. Salvatore, "Inverter drive signal processing via dft and ekf," in *Proc. Inst Elect. Eng*, 1990, pp. 111–119.

[53] M. H. J. Bollen, "Algorithms for characterizing three-phase unbalanced dips," *IEEE Trans. Power Delivery*, vol. 18, no. 2, pp. 937–944, Jul. 2003.

[54] W. V. Lyon, *Transient Analysis of Alternating-Current Machinery.* New York: Wiley, 1954.

[55] G. C. Paap, "Symmetrical components in the time domain and their application to power network calculations," *IEEE Trans. Power Syst.*, vol. 15, no. 2, pp. 522–528, May 2000.

[56] A. Ghosh and A. Joshi, "A new approach to load balancing and power factor correction in power distribution systems," *IEEE Trans. Power Delivery*, vol. 15, no. 2, pp. 417–422, Jan. 2000.

[57] S. J. Lee, J. K. Kang, and S. K. Sul, "A new phase detecting method for power conversion systems considering distorted conditions in power systems," in *Proc. IEEE Industry Applications Conf., 34th IAS Annual Meeting*, 1999, pp. 2167–2172.

[58] M. R. Iravani and M. Karimi-Ghartemani, "Online estimation of steady state and instantaneous symmetrical components," in *Proc. Inst Elect. Eng*, 2003, pp. 616–622.

[59] S. Chen and G. Joos, "A novel dsp-based adaptive line synchronization system for three-phase utility interface power converters," in *Proc. IEEE Power Electronics Specialist Conf.*, 2001, pp. 528–532.

[60] R. Collins, "Waveform characteristics of voltage sags: definition and algorithm development," EPRI, Tech. Rep., July 1999.

[61] R. Leborne, "Voltage sags characterisation and estimation," Master's thesis, Chalmers University of Technology, Sweden, 2005.

[62] M. H. J. Bollen and D. D. Sabin, "International coordination for voltage sag indices," in *Proc. IEEE PES Transmission and Distribution Conference*, 2006, pp. 229–234.

[63] IEC, *Electromagnetic compatibility (EMC): Testing and measurement techniques - Power quality measurement methods*, Standard 61000-4-30 Std., 2003.

[64] "Voltage sag indices," IEEE PES and IAS Task Force *P*1564, 2004, accessed 01 February 2007. [Online]. Available: http://grouper.ieee.org/groups/sag/.

[65] J. C. Gomez, S. D. Kim, and M. M. Morcos, "Voltage-sag magnitude and phase jump due to short circuits in distribution systems with variable fault resistance,"

Taylor and Francis, Electric Power Components and Systems, vol. 33, no. 5, pp. 493–512, Nov. 2005.

[66] F. Blaaberg, R. Teodorescu, M. Liserre, and A. V. Timbus, "Overview of control and grid synchronization for distributed power generation systems," *IEEE Trans. Ind. Electron.*, vol. 53, no. 5, pp. 1398–1409, Oct. 2006.

[67] J. Svensson, "Synchronisation methods for grid connected voltage source converters," *Proc. IEE Gen. Transm. Distrib.*, vol. 148, no. 3, pp. 229–235, May 2001.

[68] O. Vainio and S. J. Ovaska, "Noise reduction in zero-crossing detection by predicitive digital filtering," *IEEE Trans. Ind. Electron.*, vol. 42, no. 1, pp. 58–62, Feb. 1995.

[69] ——, "Digital filtering for robust 50 hz zero crossing detectors," *IEEE Trans. Instrum. Meas.*, vol. 45, no. 2, pp. 426–430, Apr. 1996.

[70] R. Datta and V. T. Ranganathon, "Variable speed wind power generation using doubly fed wound rotor induction machine-comparison with alternative schemes," *IEEE Trans. Energy Conversion*, vol. 17, no. 3, pp. 414–421, Sep. 2002.

[71] P. Barendse and P. Pillay, "Matlab simulation of a doubly-fed induction generator ($dfig$) system in its application to wind energy generation," in *Proc. South African Universities Power Engineering Conference (SAUPEC'04)*, 2004, pp. 110–114.

[72] R. Pena, G. M. Asher, and J. C. Clare, "A doubly fed induction generator using back to back pwm converters supplying an isolated load from a variable speed wind turbine," in *Proc. IEE Inst. Elec. Eng. B*, 1996, pp. 231–241.

[73] C. S. Brune, "Experimental evaluation of variable speed, doubly-fed wind-power generation system," *IEEE Trans. Ind. Applicat.*, vol. 30, no. 3, pp. 648–655, May 1994.

[74] J. M. van Coller and S. Q. Davies, "The threat that voltage dips impose on wind power generation," in *Proc. CIGRE 5th Southern African Regional Conference*, 2005, pp. 242–248.

[75] J. Morren and S. W. H. de Haan, "Ride-through of wind turbines with doubly-fed induction generator during a voltage dip," *IEEE Trans. Energy Conversion*, vol. 20, no. 2, pp. 435–441, Jun. 2005.

[76] R. Naidoo, P. Barendse, H. Douglas, and P. Pillay, "A new algorithm for improved dip/sag detection with application to improved performance of wind turbine generators," in *Proc. IEEE IAS Annual Meeting*, 2006, pp. 118–123.

[77] R. Naidoo and P. Pillay, "A new method of voltage sag and swell detection," *IEEE Trans. Power Delivery*, vol. 22, no. 2, pp. 1056–1063, Apr. 2007.

Appendix A

Publications

A.1 Journal Articles

1. Naidoo R.M and Pillay P, A new method of voltage sag and swell detection, IEEE Transactions on Power Delivery, Apr 2007, Vol 22, No. 2.

2. Naidoo R.M and Pillay P, An online method to characterise sags, to submit, IEEE Transactions on Power Delivery.

3. Naidoo R.M, Barendse P and Pillay P, A strategy for wind turbine sag mitigation through rapid sag detection, under revision for submission to Elsevier.

A.2 Conferences

1. R. Naidoo and P.Pillay, A nonlinear adaptive filter for improved power system operation and protection, IEEE Power Engineering Society General Meeting, Denver, Colorado, June 2004.

2. R. Naidoo, P.Pillay, A new algorithm for voltage sag analysis and mitigation, IEEE Power Engineering Society General Meeting, San Francisco, California, June, 2005.

3. R. Naidoo, P. Barendse, H. Douglas and P. Pillay, A new algorithm for improved dip/sag detection with application to improved performance of wind turbine generators, IEEE Industry Application Society Annual Meeting, Tampa, Florida, October, 2006.

4. R. Naidoo and P. Pillay, An online method to determine single-event sag indices, IEEE PES Africa, Johannesburg, South Africa, July, 2007.

Appendix B

Sag Classification

B.1 Results: Line-Line Fault at Bus 3

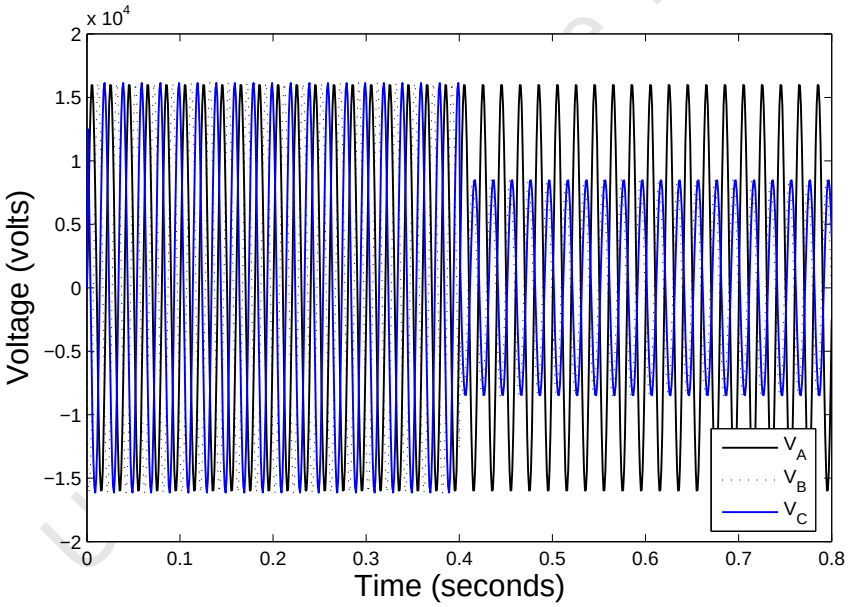

Figure B-1: Bus 3 voltages.

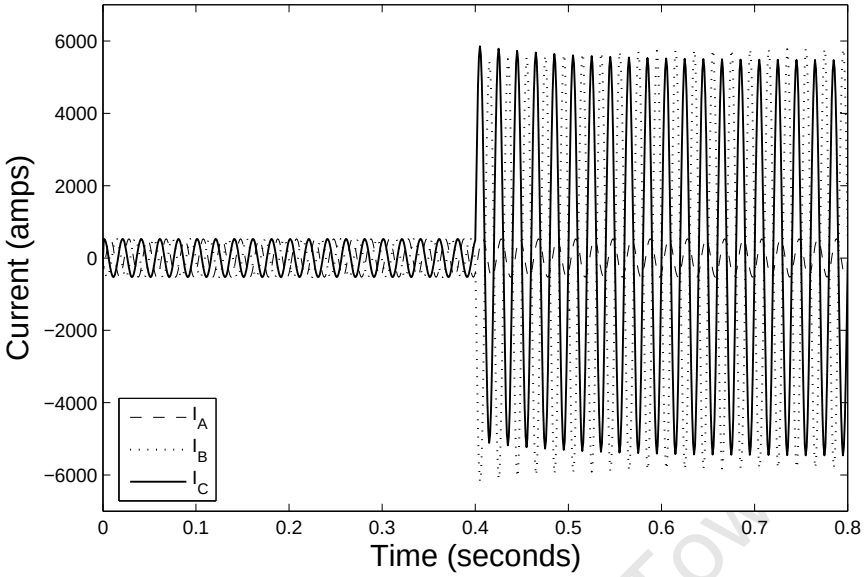

Figure B-2: Bus 3 currents.

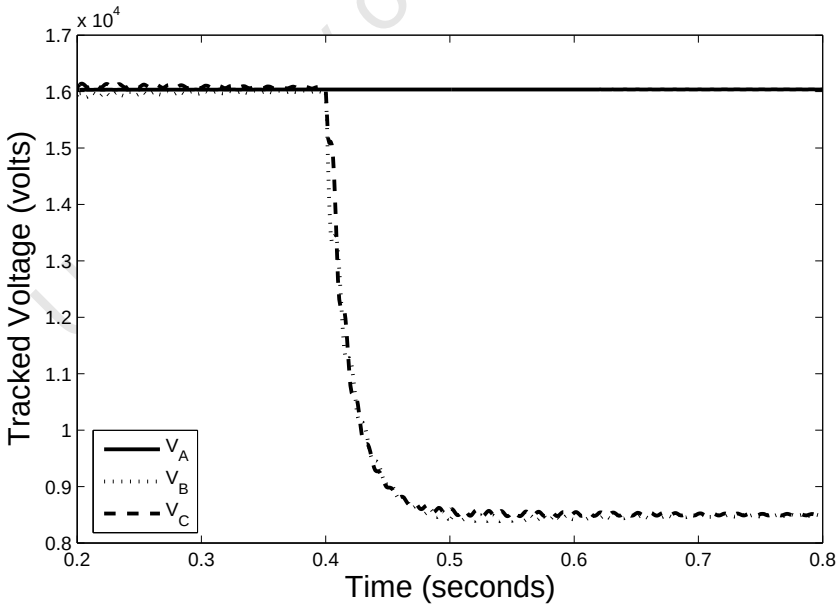

Figure B-3: Bus 3 tracked voltages (algorithm).

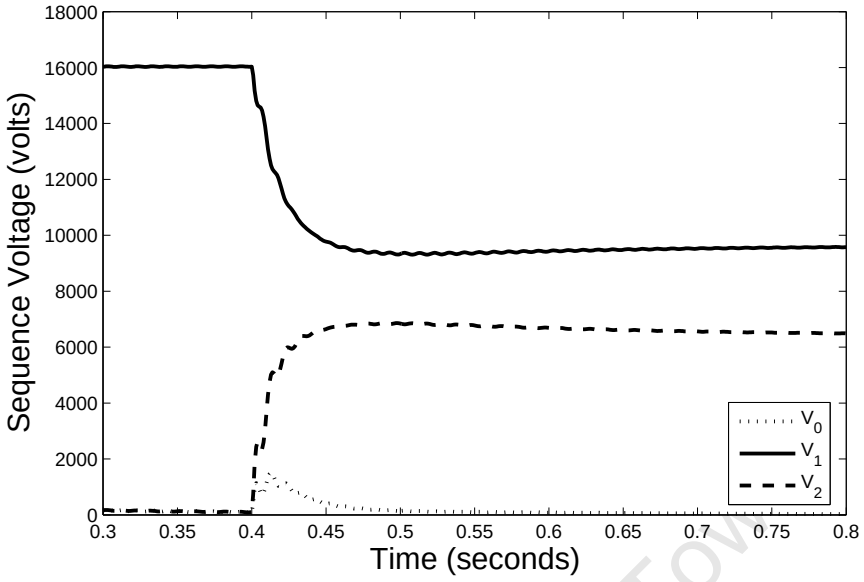

Figure B-4: Bus 3 estimated sequence voltages (algorithm).

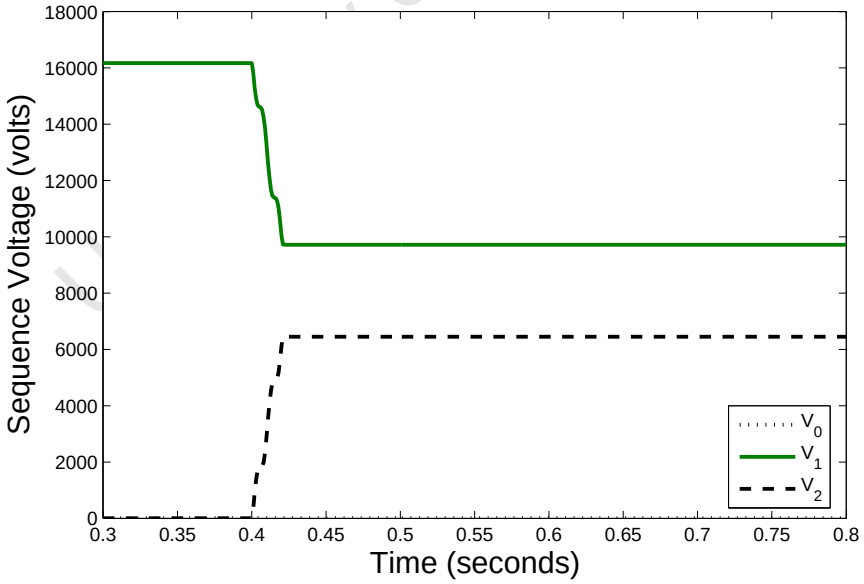

Figure B-5: Bus 3 estimated sequence voltages (algorithm).

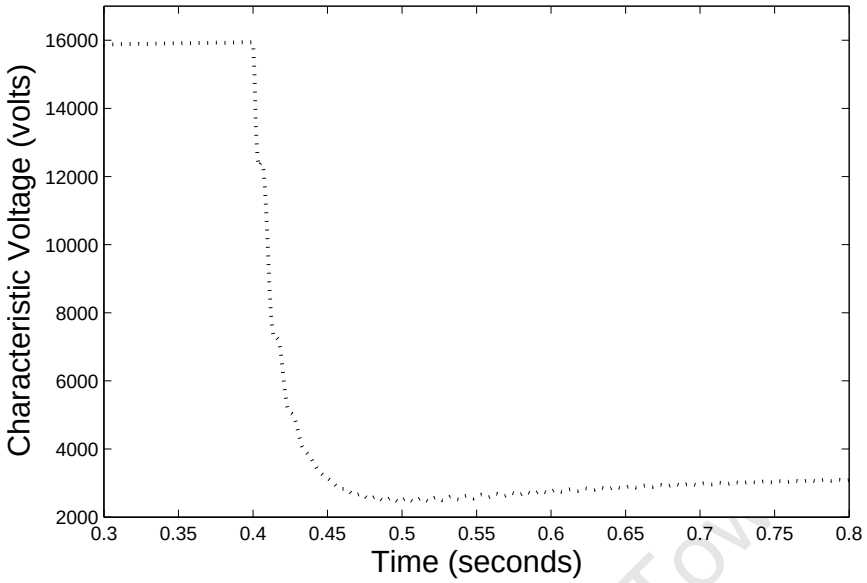

Figure B-6: Bus 3 estimated characteristic voltage (algorithm).

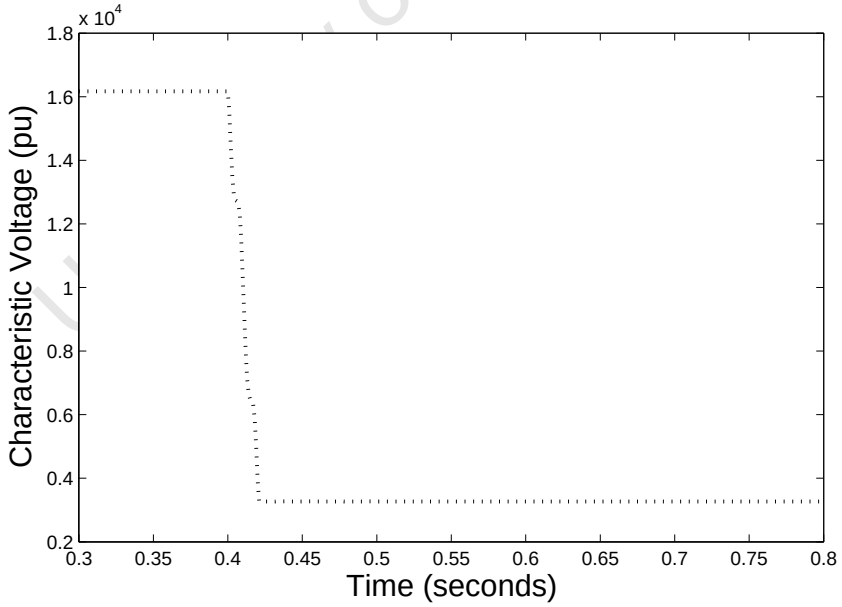

Figure B-7: Bus 3 estimated characteristic voltage (Fourier).

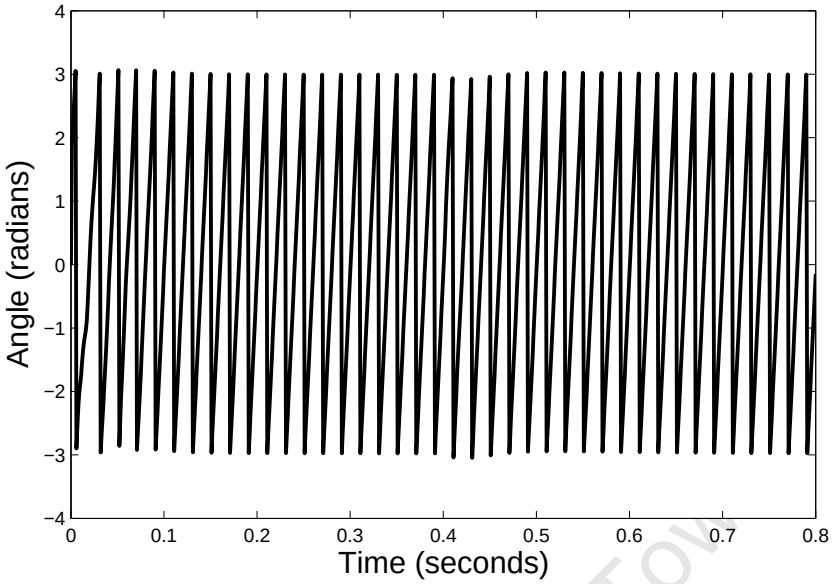

Figure B-8: Bus 3 estimated characteristic angle (algorithm).

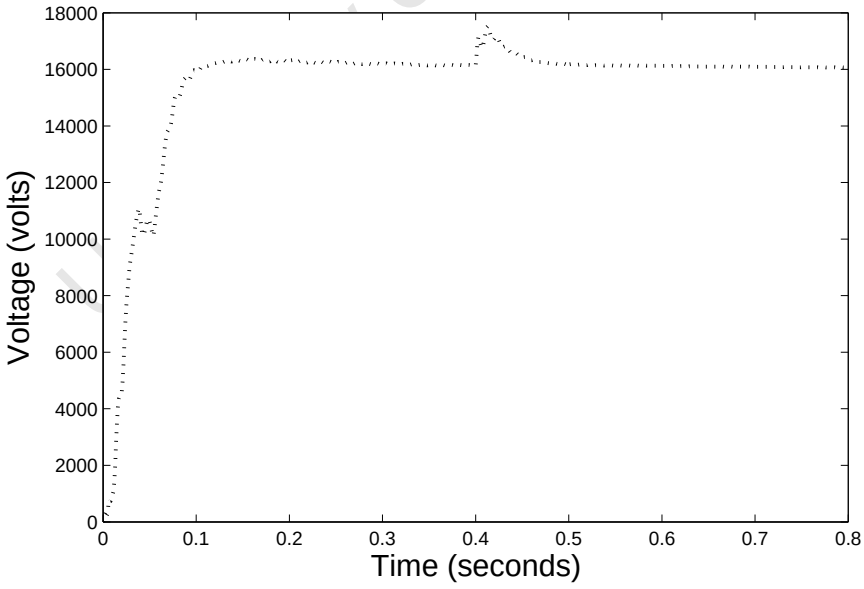

Figure B-9: Bus 3 estimated PN Factor (algorithm).

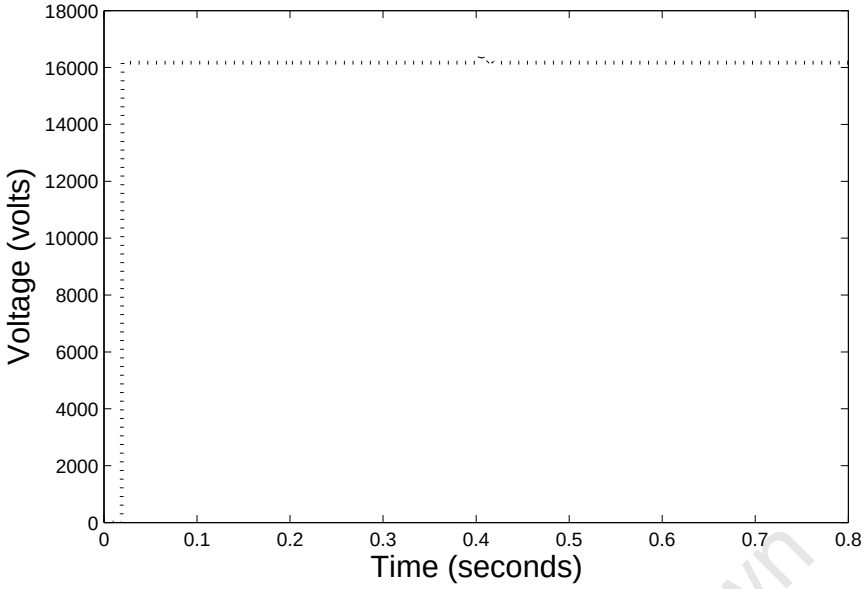

Figure B-10: Bus 3 estimated PN Factor (Fourier).

B.2 Results: Line-Line-Ground Fault at Bus 3

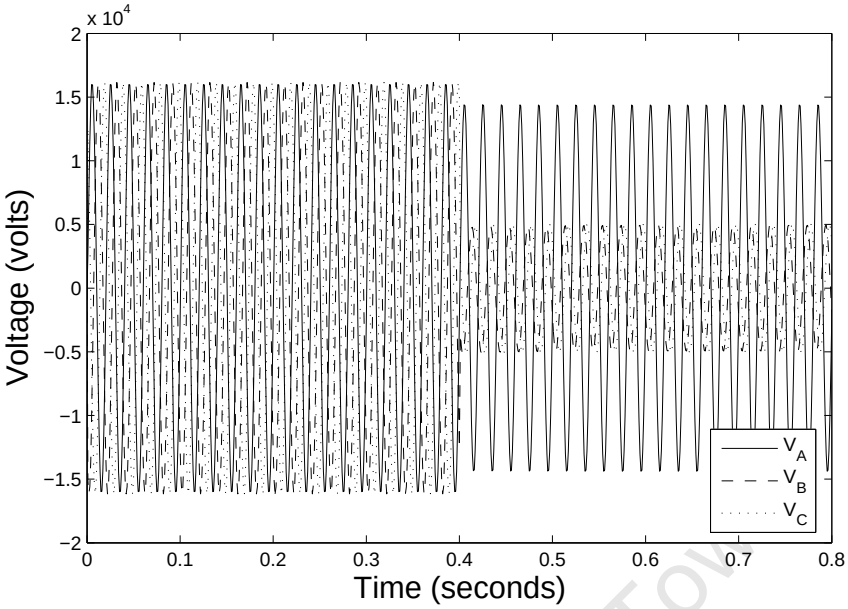

Figure B-11: Bus 3 voltages.

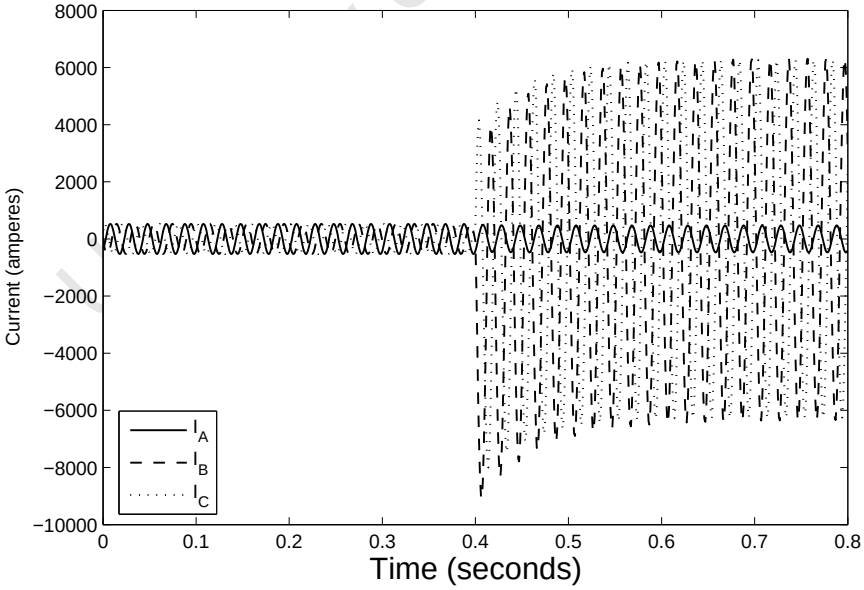

Figure B-12: Bus 3 currents.

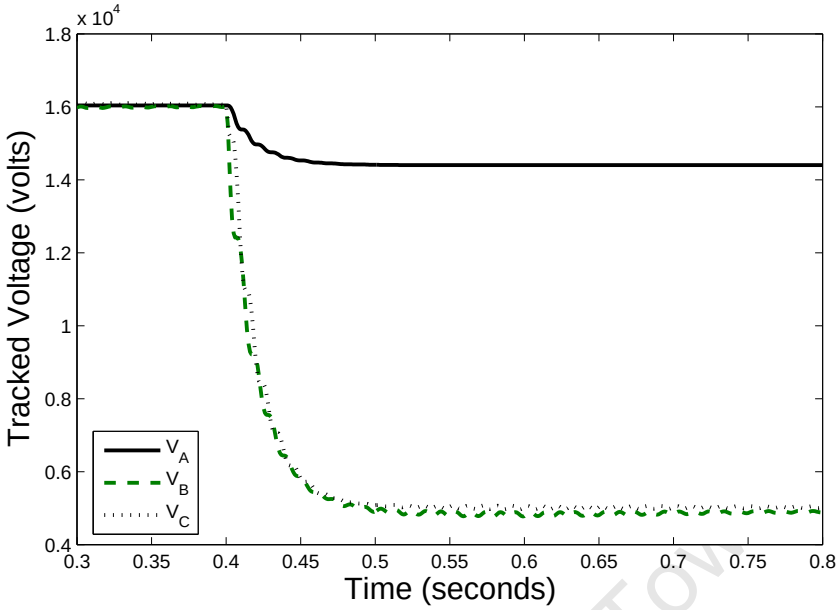

Figure B-13: Bus 3 tracked voltages (algorithm).

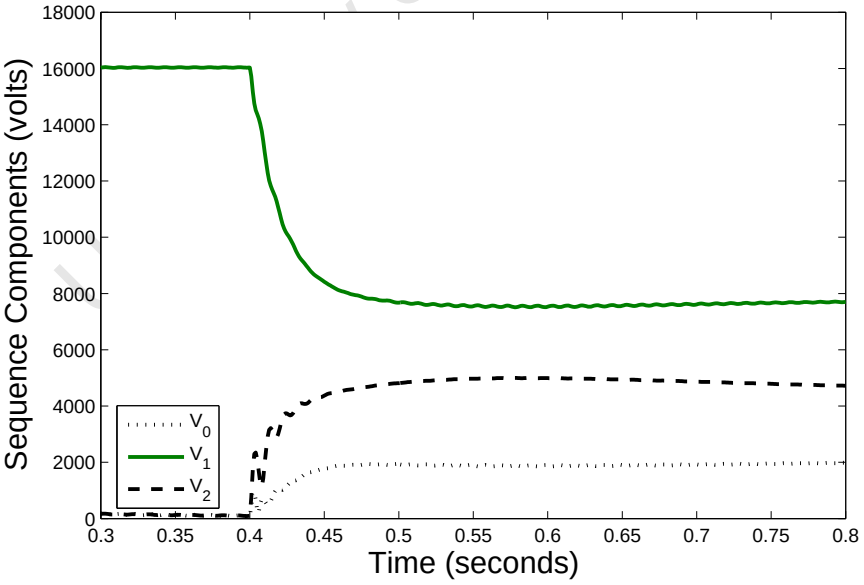

Figure B-14: Bus 3 estimated sequence voltages (algorithm).

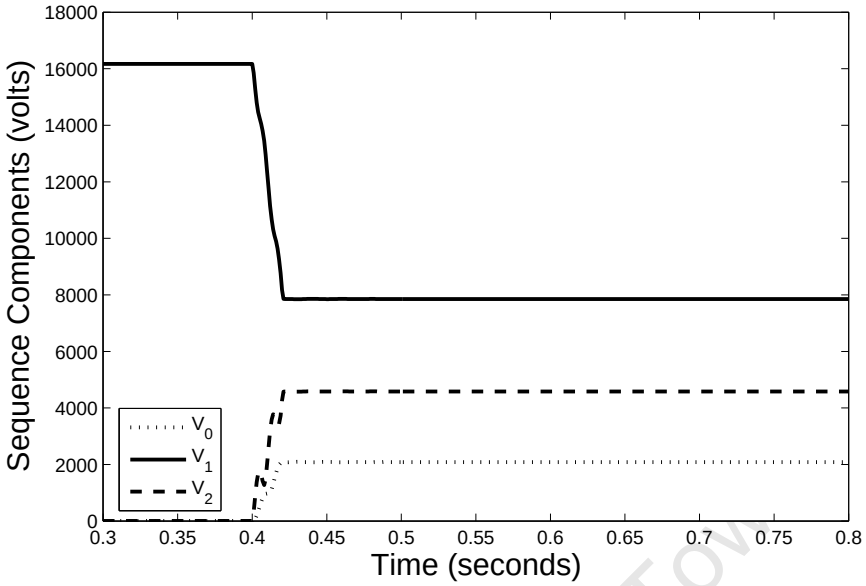

Figure B-15: Bus 3 estimated sequence voltages (algorithm).

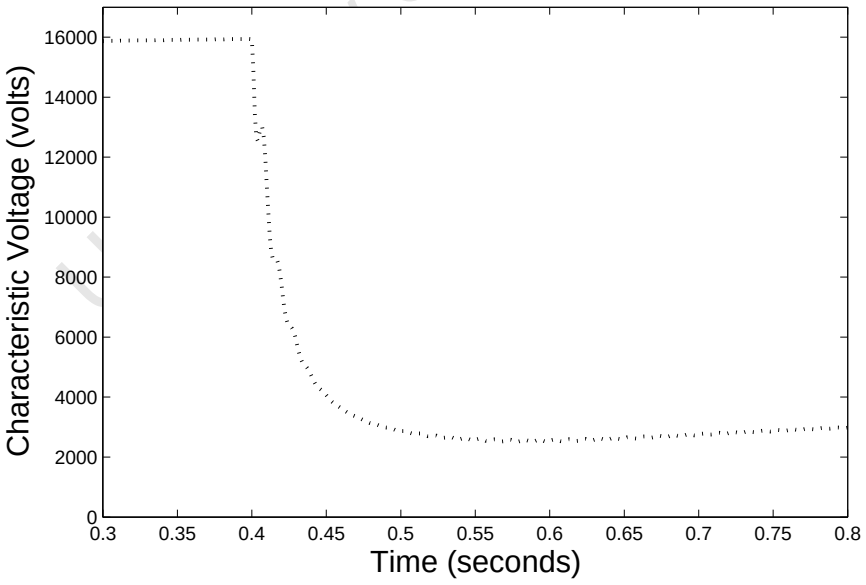

Figure B-16: Bus 3 estimated characteristic voltage (algorithm).

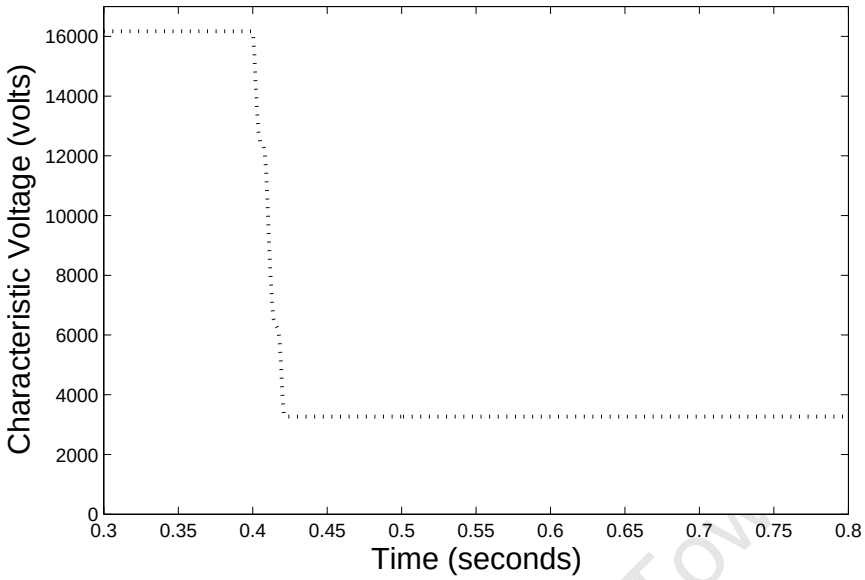

Figure B-17: Bus 3 estimated characteristic voltage (Fourier).

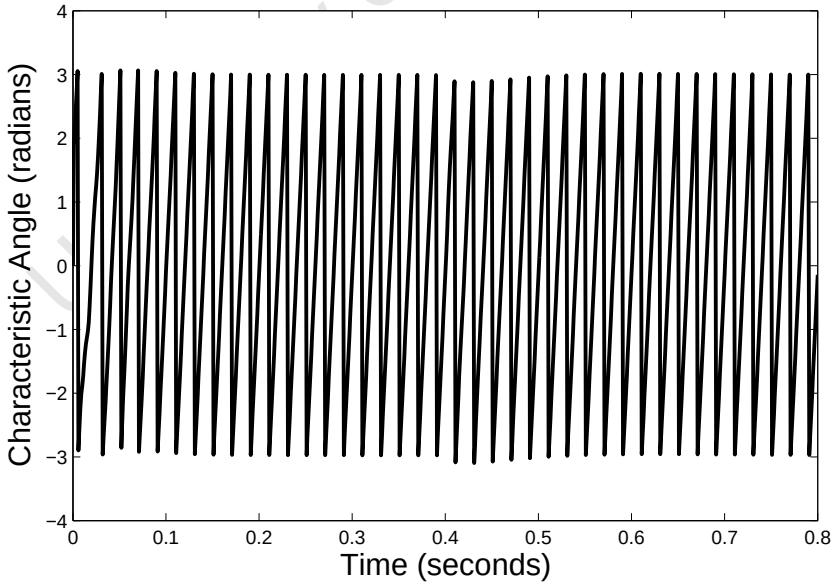

Figure B-18: Bus 3 estimated characteristic angle (algorithm).